UNIVERSITÉ CATHOLIQUE DE LOUVAIN

INSTITUTE OF CONDENSED MATTER AND NANOSCIENCES

(IMCN)

Laboratory of Crystal Engineering

Prof. Tom Leyssens

Dr. Koen Robysens

Towards multi-component pharmaceutical solid forms through crystal engineering

Thèse présentée en vue de l'obtention du grade

de docteur en Sciences par

Fucheng Leng

Louvain-la-Neuve

October 2022

Jury Members

Prof. Grepioni F.

University of Bologna

Prof. Gaigneaux E..

Université catholique de Louvain

Dr. Shemchuk O.

Université catholique de Louvain

Prof. Wouters J.

Université de Namur

Dr. Robeyns K. (Promotor)

Université catholique de Louvain

Prof. Leyssens T. (Promotor)

Université catholique de Louvain

Acknowledgements

About five years ago, I was stuck in an existential crisis. I didn't know where to go, what to do and why should I do. The only thing I knew is the life that was in front of me was not what I wanted. But in China everything is so fast, there is no time for me to think about all these problems. So I started to think about finding a quiet place to halt, to meet different people, to experience a different world, and, of course, to earn a PhD degree. So, on a sunny day four years ago, I boarded a plane to Belgium, which was my first ever experience in another country.

I must say that my stay in Belgium exceeded by far my expectation. Indeed, the reduced work pressure and adequate spare time offered me the opportunity to slow down, to read books and think about everything. The distinctly different cultural environment also gave me a new perspective on everything. The techniques I learned in science gave me the confidence and capability to accept my current job. I would like to express my appreciation to everybody who has helped me and supported me in the past four years.

First of all, I would like to express my gratitude to my two supervisors, Tom and Koen. Tom, thanks for giving me a chance to start a wonderful journey here. Apart from that, you gave me full freedom to explore the area I am interested in. Working in your lab is the best working experience I could image. Koen, you became my supervisor accidentally, but in the last four years, you performed as the best tutor I met. Thanks for your patience and unreserved teaching in crystallography. And thanks for your kind help in my life. I believe we will still be good friends in the future.

Secondly, I want to thank my colleagues those who are still in the lab as well as those who already left. Due to the language problem, I know in fact I am not so active in lab maintenance. It is you make the lab runs well every day. Apart from that, as a foreigner, I did not know how to speak French. I met countless strange problems, without your help, I don't think I could solve any of them. And finally, a special thanks to Oleksii, not only for the tremendously in the preparation of my papers but also for all the inspiring scientific discussions we had.

Thirdly, I want to say thanks to all the people who helped me with my experimental work: Pascal for his help with TGA and DSC measurement, Nikolay and François for helping me measure PXRD profiles.

Last but not least, I must express my gratitude to my family. I know none of you will try to read my thesis, especially as it is written in English. I know in fact you can't understand why I gave up some 'good choices' and chose to leave you for four years, but you still trusted and supported me unconditionally, and respected every decision I made. For this I could say nothing but thanks.

List of Publications

1. Song L, **Leng F**, Robeyns K, et al. Quaternary phase diagrams as a tool for ionic cocrystallization: the case of a solid solution between a racemic and enantiopure ionic cocrystal[J]. *CrystEngComm*, **2020**, 22(14): 2537-2542.
2. **Leng F**, Robeyns K, Leyssens T. Urea as a Cocrystal Former—Study of 3 Urea Based Pharmaceutical Cocrystals[J]. *Pharmaceutics*, **2021**, 13(5): 671.
3. **Leng F**, Robeyns K, Leyssens T, et al. Combining Racetams with a Sweetener through Complexation[J]. *Crystal Growth & Design*, **2022**, 22(5): 3016-3023.
4. **Leng F**, Shemchuk O, Robeyns K, et al. Complexation: An Interesting Pathway for Combining Two APIs at the Solid State[J]. *Pharmaceutics*, **2022**, 14(9): 1960.

Abstract

Combining APIs with specific molecules in a single crystal form shows potential during the development of new drug solid forms. Compared to the physical mixture, combination through crystallization can not only lead to improved manufacture processes and also allows improving the physical properties of APIs. Traditional crystal engineering methods like cocrystallization and salt formation have been widely studied in the context of multi-component systems. In this work, we explored some novel crystal engineering methodologies leading to multi-component systems.

Our first attempt relies upon the use of an organic linker to combine two drugs. We focused on the use of urea as a bridge, but this technique did not lead to the desired results. Based on this result, we decided to turn to a different type of interaction, using complexation as a tool. Doing so, we were able to show sweeteners and racetams, pyridine containing drugs and carboxylic acid containing drugs, were successfully combined. Finally, we investigate an interesting system consisting of a solid solution involving the drugs piracetam and S-oxiracetam and a third coformer gallic acid. Solid solutions allow fine-tuning of the amount of piracetam vs S-oxiracetam.

In the first part, we start with a binary cocrystal screen between urea and various drugs leading to the successful identification and characterization of three binary cocrystals: urea-catechin, urea-ellagic acid and urea-3-hydroxyl-2-naphtholic acid. Interestingly, the stability of catechin towards humidity or high temperatures is improved upon cocrystallization with urea. Moreover, the solubility of ellagic acid is improved through this cocrystallization approach. However, subsequent attempts to obtain the ternary cocrystal met complete failure.

In the second part, we focus on combining molecules through complexation. Racetams, a series of normally bitter drugs, cannot be combined in a binary cocrystal with the popular sweetener saccharin through either salt or cocrystal formation. We here successfully show how such a feature can be obtained using zinc saccharinate rather than saccharin. Following this approach, a series of carboxylic acid containing drugs were transformed to their zinc salts and successfully combined with a series of pyridine containing drugs.

In the final part, we focus on a particular system. Various proportions of piracetam and S-oxiracetam, are successfully combined using a third conformer, gallic acid,

through formation of a solid solution. Apart from this, the phase diagram of such system is also constructed, which demonstrated the solubility behavior of this cocrystal solid solution in solvent.

List of Abbreviations

AMI	3.4-diaminopyridine
API	Active Pharmaceutical Ingredient
ASP	Aspirin
CCDC	Cambridge Crystallographic Data Center
CAD	Carboxylic acid contained drug
DSC	Differential Scanning Calorimetry
DVS	Dynamic Vapor Sorption
FDA	Food and Drug Administration
FDC	Fixed-Dose Combination
FTIR	Fourier-Transform Infrared Spectroscopy
GA	Gallic Acid
GRAS	Generally Regarded As Safe
HPLC	High-performance liquid chromatography
HSM	Hot Stage Microscopy
IBU	Ibuprofen
INC	Isonicotinamide
INZ	Isoniazid
IUPAC	International Union of Pure and Applied Chemistry
LAG	Liquid Assisted Grinding
MN	Methyl Nicotinate
NC	Nicotinamide
Oxi	Oxiracetam
PABA	Para-aminobenzoic acid
PD	Pyridine Contained Drugs
Pir	Piracetam
PXRD	Powder X-ray diffraction
RH	Relative Humidity
RT	Room Temperature
SCXRD	Single Crystal X-ray diffraction
SEM	Scanning electron microscopy
SSNMR	Solid State Nuclear Magnetic Resonance
TGA	Thermogravimetric Analysis

UC	Urea catechin cocrystal
UE	Urea ellagic acid cocrystal
UH	Urea 3-hydroxyl-2-naphthoic acid cocrystal
UV-vis	Ultraviolet–Visible
VT-PXRD	Variable Temperature Powder X-ray Diffraction

Table of Contents

Chapter 1
1. General Introduction

1.1 crystal engineering

With the discovery and development of X-ray diffraction in the early days of the 20th century, crystallographers and chemists started to explore the relationship between molecules and crystal structure.[1-3] W.H. Bragg's and Lonsdale's work in predicting the benzene ring size through analysis of the unit cell can be regarded as pioneering work in this area.[4, 5] The first appearance of the term "crystal engineering" can be traced back to 1955, at a meeting of the American Physical Society in Mexico City. In this meeting, Ray Pepinsky stated: "crystallization of organic ions with metal-containing complex ions of suitable sizes, charges and solubilities results in structures with cells and symmetries determined chiefly by packing of complex ions. These cells and symmetries are to a good extent controllable: hence **crystals** with advantageous properties can be **engineered**."[6] For the first time, the three most important elements of crystal engineering: analysis, design and function were clarified. After more than half a century of development, crystal engineering has moved from the fringes into the mainstream of chemistry and is now widely applied in various areas including catalysis, food, pharmaceutical and agricultural industry, ….[7-9] At present, Crystal engineering is defined as the subject which aims at understanding intermolecular interactions of crystal packing and the use of such understanding in the design of new solids with desired physical and chemical properties.[2] Modern crystal engineering can be regarded as a hybrid of crystallography and chemistry, in which crystallography is used to deal with the problem of understanding while chemistry is used to design functional crystals.

1.2 pharmaceutical crystal engineering

The development of novel and effective APIs is a topic of concern both in academia and in industry.[10, 11] Most APIs are still administered in the solid state, under a crystalline form due to the convenience in manufacture like the rejection of impurities inherent to the crystallization process and the physicochemical stability that the crystalline solid state affords.[12] The problems that arise with the use of crystalline materials are usually related to poor solubility properties and the existence of more

than one crystalline form of an API.[10] In recent years, crystal engineering was applied in drug development and has been proven a powerful and feasible tool in physical property modulation of desired APIs. Through combination with a second component in the crystal structure, the physical properties of APIs could be significantly improved.[13] Pharmaceutical crystal engineering faces two notable restrictions: firstly, in the early stages of drug development, a molecule is chosen mainly based on its biological activity rather than usability in crystal engineering. This led to often complicated chemical structures, with difficult to predict structural arrangements. The second restriction is the limited library of assisting molecules. Indeed, normally only molecules included in the GRAS list can be used in pharmaceutical crystal engineering.[10]

Until now, countless pharmaceutical crystal engineering approaches have been designed based on chemical principles and experimental evidence. Crystal engineering is still evolving, which comes with continuous discussions and debates about the nomenclature and taxonomy of the crystal engineering product.[14, 15] A well-accepted classification of API solid forms was demonstrated and is shown in Figure 1.1, in which crystalline forms of APIs are divided into salts, cocrystals and hydrates/solvates.[16] Considering hydrates/solvate forms are mainly found and identified rather than designed and synthesized during drug solid forms research, these forms will not be discussed in this chapter.

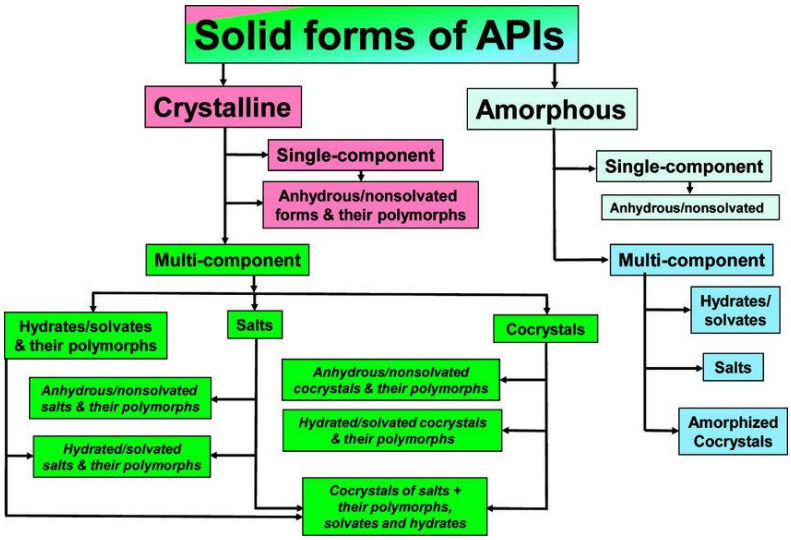

Figure 1.1 The diversity of solid forms that can exist for an API. Cited from Karagianni, A. et.al.

1.3 Salt formation

The IUPAC defined a salt as a "chemical compound consisting of an assembly of cations and anions".[11] As for the pharmaceutical area, the FDA suggested the following definition of salts : "Any of numerous compounds that result from replacement of part or all of the acid hydrogens of an acid by a metal or a radical acting as a metal: an ionic or electrovalent crystalline compound. Per the current regulatory scheme, different salt forms of the same active moiety are considered different active ingredients."[12] Salt formation is the most mature and widely-used crystal engineering method in the pharmaceutical area. It is estimated that 50% of all marketed drug molecules are administered as salts.[17, 18] In this part, only the classical simple salt form (lost) will be discussed here.

1.3.1 Design of salts

The first principle in salt design is that the API must be ionizable.[19] According to the definition of salts, two requirements must be fulfilled in the design:

1) the API should be ionizable, which means the presence of acidic or basic functional groups is a necessary requirement for the formation of salts.

2) the counterion used must be safe for human use, which limits the available counterions to a small library. [20]

In practice, not every combination between ionizable API and counterions is successful. Most of the APIs are either weakly acidic or weakly basic in nature. Based on experimental findings, when the pKa difference between an acid and base is larger than three, salt formation is expected (Figure 1.2).[17, 21] Under these circumstances, the salt will not break down into individual species under normal circumstance. For example, an aspirin-metformin drug-drug salt is designed based on the pKa difference between the imino group (pKa =13.8) of metformin and carboxylic acid group (pKa = 3.5) of aspirin (difference =10.5).[22] If the difference in pKa is below 3, proton transfer does not occur, and a so called co-crystal is obtained, which is discussed in detail further on in this manuscript.

A transition between these two cases occurs, leading to a zone (zone 2) known as the cocrystal-salt continuum.

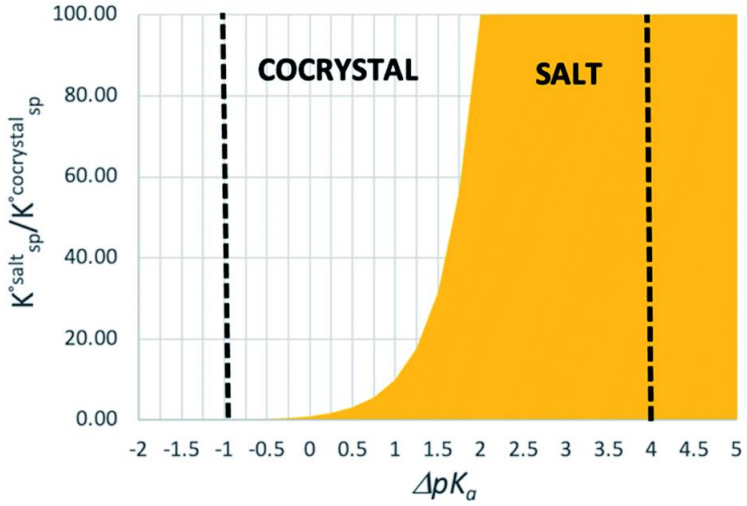

Figure 1.2 Diagram showing the regions where salt (yellow) and co-crystal (no fill) are favoured as a function of the ΔpKa of the acid–base pair and the relative solubility of the salt and the co-crystal, cited from A. J. Cruz-Cabeza et.al[23]

1.3.2 Preparation of salts

Traditionally, solution-based methods like cooling, anti-solvent addition, evaporation and slurry conversion are the mainstream processes used for salt preparation. As the solubility of most compounds drops with the decrease in temperature, cooling saturated solutions will lead to the precipitation of the salt. Similarly, adding an anti-solvent will also decrease the solubility of the salt, leading to its crystallization. Slurry conversion is another widely used technique in the manufacture of salts. In this method, a small amount of solvent is added to the physical mixture of the API and counterion forming compound giving a meta-stable suspension of both. As the salt is less soluble, it will nucleate at a given point, leading to its crystallization. The parent compounds dissolve further, and fully transform into the salt form.

Despite its advantages, solution-based methods also face the problem of extensive use of organic solvents and are often lengthy processes. Some recently developed techniques towards salts include spray-drying, freeze-drying, supercritical processes, mechanical neat grinding, liquid assisted grinding (LAG) and extrusion. The advantage and disadvantage of all these techniques are summarized in Table 1.1[19]. Notably, mechanochemical methods (neat grinding and LAG) have attracted increasing attention in recent years due to their extremely high efficiency and convenience in salt form screening. William Jones et.al. screened two drugs

trimethoprim and pyrimethamine with a series of pharmaceutically accepted carboxylic acids, in which neat grinding illustrates a 6/14 success rate and LAG gave a 100% success rate.[24] Besides, a mechanochemistry study between lamotrigine and a series of carboxylic acids resulted in 34 isostructural salt solvates. These pioneering works demonstrate the superiority of mechanochemistry in salt form screening.[25]

Table 1.1 advantages and disadvantages of salt preparation techniques, cited from S. H. Mithu. Et.al[19]

method	Advantage	Disadvantage
Solvent mediated methods (thermal, anti-solvent, evaporation, and slurry conversion)	• High purity • Wide range of drug-former pairs • Accurate process control	• Not easy to scale-up • Use of organic solvent
Spray drying	• High purity • Particle engineering • Easy to scale up • Small footprint • Fast processing • Wide range of drug-former pairs	• Use of organic solvent • Low yields(40−45%) • Limited number of studies on salt formation
Freeze-drying	• High purity • Suitable for thermolabile materials • Accurate process control • Relative high yield	• Time consuming • Not easy to scale-up • Costly • solvent residues • Limited number of studies
Supercritical fluid process	• High purity • suitable for thermolabile materials • Accurate process control • Use of low process temperature	• Time consuming • Limited number of studies • solvent residues

Mechanochemical neat grinding	• good purity salt • wide range of drug-former pairs • particle size reduction • Environmentally friendly, no solvents • Isolate polymorphs of same salt • Use different stoichiometric ratios	• Low yield • Scale-up issues • Time-consuming • Every time not in a reproducible manner
LAG	• High purity • Wide range of drug-former pairs • Broader range of synthesized salts • Particle size reduction • Fast processing • Isolate polymorphs of same salts • Use different stoichiometric ratios	• Use of solvent • Scale-up issues
Extrusion	• High purity • Continuous process • Easy to scale-up • small footprint • Environmentally friendly, no solvents • short residence time • In-line process monitoring • Wide range of drug-former pairs	• Only one polymorph of the same salt

1.3.3 Characterization of salts

There is no doubt that crystallographic methods including SCXRD and PXRD are the most powerful characterization techniques for the identification of new solid forms. SCXRD, allows identifying the exact position of each compound in the solid structure.[26] PXRD on the other hand offers a unique fingerprint pattern for every solid form, which is valuable in new solid form screens and quality control. Furthermore, when single crystals are not available, PXRD could also be used for crystal structure determination. Similarly, SSNMR can also offer complementary structural information of a unknown solid form, such as the number of independent molecules in the unit cell (Z′), the presence of disorder, hydrogen bonding properties, salt or cocrystal character, as well as the presence of either water or solvent molecules.[27, 28] For example, the structure of the salt lidocainium hydrogen succinate was determined from a laboratory PXRD pattern assisted by SSNMR data.[29] Spectroscopic techniques like FTIR and Raman are also applied in the characterization of salts. The interactions between drug and counterion can be detected by looking at the vibrational spectrum as the shape or position characteristic peaks change.[30] As for physical properties, characterization of thermal properties, dissolution behavior, hygroscopicity, can be determined. A comprehensive summary table has been presented in a previous report, which is shown below in Table 1.2.

Table 1.2. Physical properties that are normally considered for comparison of salt forms and parent compounds for oral dosage forms. Cited from Bastin, R. J. et.al[31]

Test	Suitable technique
dissociation constant and basic physico-chemical properties	potentiometry, solubility, UV spectroscopy
melting point	HSM, DSC
aqueous solubility	overnight equilibration at 25 °C; analysis by UV spectroscopy or HPLC
cosolvent solubility	overnight equilibration at 25 °C, analysis by UV spectroscopy or HPLC
common ion effect on solubility	overnight equilibration at 25 °C in suitable media and analysis by UV spectroscopy or HPLC

Hygroscopicity	use DVS apparatus or expose to various relative humidity values and measure weight gain after 1 week
intrinsic dissolution rate	use Wood's apparatus
crystal shape and appearance	SEM or optical microscopy
particle size	SEM and laser diffusion
polymorphism/pesudopolymorphism	recrystallizations, HSM, DSC, TGA
powder properties	bulk density measurement

1.3.4 Applications of salts

In general, salt formation can be interesting during the design and manufacture of a pharmaceutical solid dosage forms. Firstly, physical properties like solubility, bioavailability, hygroscopicity, mechanical properties and thermal stability can be modulated combining an API with various pharmaceutically acceptable counterions.[11, 32] Thus, a solid dosage form with acceptable physical properties in all aspects could be selected after careful comparison with the other salt form.[33, 34] For example, five salt forms, including a hydrochloride, a mesylate, a citrate, a tartrate, and a sulphate, have been found for a candidate drug RPR 127963. Detailed research found citrate and the tartrate bearing a relatively low solubility while the hydrochloride salt suffered from polymorphism, and the formation of hydrates. Thus, the mesylate and the sulphate salts were selected as candidate salt forms because of their considerable thermal stability, excellent aqueous solubility, and they were shown to be non-hygroscopic. Considering the sulphate salt had a better solubility behavior in cosolvents, which could give a better chance of achieving a higher dose in an injectable formulations, the sulphate salt was selected as the final choice of salt form.[31]

Secondly, salt formation can also be used to achieve desired multi-component crystal forms.[35] Drugs like quinine, venlafaxine, haloperidol, stanozolol, lamivudine, triamterene, and mirtazapine have been successfully combined with a widely-used sweetener saccharin, for masking their unpleasant taste.[36-40] Multi-drug combination has also demonstrated superiority compared to traditional mono-therapy approaches for the treatment of chronic and complex diseases like diabetes, cancer, and cardiovascular disorders.[41-43] Combining different drugs in a single solid form, could overcome potential issues observed with fixed-dose combinations, and at the same

time allow improving physicochemical properties and even bioactivity.[35] Hidehiro Uekusa et.al demonstrated a great example of drug-drug combination via salt formation combining the two antidiabetic drugs gliclazide and metformin. The salt not only showed improved solubility and dissolution rate characteristics with respect to those of gliclazide, but also solved the hygroscopicity issues of metformin.[44]

Last but not least, salt formation plays a very important role in chiral resolution and optimization of crystallization process. Crystallization is one of the most popular chiral resolution methods as it is a well-known, easily up-scalable, low-cost technique. As an example, formation of a diastereomeric salt with tartaric acid led to the resolution of the anti-obesity drug Lorcaserin.[45] Similar, the telaprevir bicyclic [3.3.0] proline intermediate is successfully resolved with the assistance of di-1,4-toluoyltartaric acid.[46] This area has been reviewed in detail by Renata Siedlecka.[47]

1.3.5 Limitations to the use of salts

The largest limitation of salt formation is that it can only be applied to ionizable drugs. Due to the requirement of the pKa difference mentioned before, only a limited series of counterions are available. Another issue worth considering is the influence of the common-ion effect. According to an investigation based on salts approved by the FDA from 2015 to 2019, hydrochloride salts and sodium salts are the most dominating salt forms for acidic and basic drugs respectively.[48] It is well known that the sodium cation and chloride anion are widely spread in the human body, which may lower the solubility and dissolution rate of these salts.[13, 49] Finally, although some works have revealed the physical-properties relationship among salts with similar structure, the prediction of salt structures and their physical properties is still under continuous development, which makes the identification and selection of optimized salt forms a trial-and-error process rather than one based on rational design.[13, 18]

1.4 Cocrystallization

Comparing to salt formation, cocrystallization is a relatively new field. After unremitting efforts from both academia and industry in the past decades, cocrystallization is now a well-accepted idea in pharmaceutical industry.[50, 51] There are now no less than eight commercially available pharmaceutical cocrystals on the market and more cocrystal products are currently undergoing clinical trials.[50] The common accepted definition of a cocrystal is as follows “cocrystals are solids that are crystalline single-phase materials composed of two or more different molecules compounds generally in a stoichiometric ratio which are neither solvates nor simple

salts".[51] Particularly, the pharmaceutical cocrystal must be composed of an API and a GRAS coformer.

Apart from classical cocrystals, a new-emerging cocrystal subclass, ionic cocrystals, started to attract increasing interest in recent years.[52] Generally, ionic cocrystals could be thought of as cocrystals between neutral compounds and salts. Different from common cocrystals in which molecules are combined with each other through hydrogen bonds. In ionic cocrystals, salt and neutral compound are combined with each other through coordination bonds. In another view, IUPAC defined a complex as a molecular entity formed by loose association involving two or more component molecular entities (ionic or uncharged), or the corresponding chemical species. Especially, complex is used as the simplified form of a coordination complex and commonly used to refer to compounds which are combined with each other through coordination bonds. Ionic cocrystals could be regarded as special complexes.

1.4.1 Design of cocrystals

Compatibility is the key principle of cocrystal design. Different from salts, the dominating interaction which combines two or more molecules in a cocrystal together is hydrogen bonding or coordination bonding instead of electrostatic forces.[13] Molecular recognition events are responsible for the self-assembly of cocrystals through noncovalent interactions with energetically favorable geometries. Synthons are the basic noncovalent intermolecular interactions that combine drug and coformer into a structure (Figure 1.3). Therefore, drugs can be selected to cocrystallize with a series of selected coformers through synthon analysis.[53] Etter and Donohue developed the following guidelines to predict hydrogen bond interactions that result in crystal formation: [54, 55]

(1) the hydrogen bonding in the crystal structure will include all acidic hydrogen atoms.

(2) all good hydrogen bond acceptors will participate in hydrogen bonding if there is an adequate supply of hydrogen bond donors.

(3) hydrogen bonds will preferentially form between the best proton donor and acceptor.

(4) intramolecular hydrogen bonds in a six-membered ring form in preference to intermolecular hydrogen bonds.

Due to the different interactions in ionic cocrystals, ionic cocrystal design follows different rules comparing to normal molecular cocrystals. Until now, it is still a less explored area compared to normal cocrystalization.[52] But knowledge from coordination chemistry informs us that metals normally possess some favored coordination mode.[56] It could be assumed that coordination mode analysis may be used in ionic cocrystal design like synthon analysis in classical cocrystals.

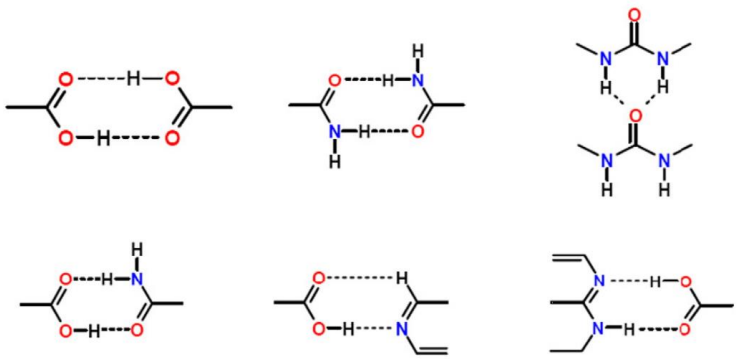

Figure 1.3 Common supramolecular synthons formed from carboxylic acids, amides, pyridines, and other aromatic nitrogens. Cited from Desiraju, G. R.[57]

1.4.2 Preparation of cocrystals

Like salt preparation, traditional solution-based methods (including solvent evaporation, anti-solvent addition, cooling crystallization, reaction cocrystallization, slurry conversion) and solid-based methods (including contact cocrystallization, neat grinding, LAG, melt crystallization) have been developed. It is worth noting that the solid based methodology is the most commonly used for cocrystal screening in the early stages of cocrystal research owing to its cheapness, high efficiency and convenience. On the contrary, the solution-based methods are often used in the later stages of research because their excellent performance in obtaining of high-quality crystals. Some other relatively new methods include supercritical crystallization, laser irradiation, spray-drying, resonant acoustic mixing which all demonstrate considerable potential.[58]

1.4.3 Characterization of cocrystals

Like salts, cocrystals are typically analyzed by crystallographic methods including SCXRD and PXRD.[26] Furthermore, spectroscopic characterization includes infrared spectroscopy, Terahertz spectroscopy, Raman spectroscopy and SSNMR. Methods used to characterize the physical properties of salts are also used for cocrystals (thermal analysis, stability experiments and solubility measurements). Recently, a new method (X-ray photoelectron spectroscopy) was introduced to distinguish salts from cocrystal, through analysis of XPS N 1s binding energies.[59]

1.4.4 Application of cocrystals

Cocrystals are used in the same context as salts. For those molecules that are not easily ionizable, cocrystallization is a promising way to improve solubility and hence bio-availability. Indeed, it has been shown that sometimes cocrystal solubilities can exceed drug solubilities by orders of magnitude. For example, a danazol vanillin cocrystal performed 370 times better in terms of solubility compared to the original API.[60, 61] Some recent contributions showed other possibilities in applying cocrystals (eg. for physical property improvement).[50] Cocrystals have shown great potential to solve solid stability problems under high relative humidity . William Jones proved the cocrystal between oxalic acid and caffeine, a well-known model pharmaceutical compound unstable under high humidity, to be stable even at 98% relative humidity for several days.[62] Physical property improvement also includes formulation properties such as API tabletability. Paracetamol is characterized by three polymorphs. The most stable form, polymorph I, has issues in tablet formation because of its poor compressibility induced by the lack of a layered structure. Thus, a large amount of binder must be added during the process. With the help of a crystal engineering strategy, a layered cocrystal with high tensile strength has been obtained.[63] Changquan Calvin Sun's work on the caffeine-methyl gallate system also showed how compaction properties of powders could be largely improved by introducing flat slip planes in the structure through the formation of cocrystals.[64]

Cocrystallization is also an excellent choice to achieve multi-component crystals.[50, 61] For instance, oxcarbazepine, spironolactone, and carbamazepine were successfully cocrystallized with saccharin, obtaining sweet drugs with improved solubility.[65-67] Besides, dozens of drug-drug cocrystals have been reported,[68, 69] some of them (e.g. meloxicam-aspirin, piracetam–lithium chloride, curcumin–pyrogallol) exhibiting superior solubility profiles compared to one or both parent compounds.[70-72] The

cocrystal between monosodium sacubitril and disodium valsartan, which has been marketed by Novartis under the name Entresto for the treatment of chronic heart failure, shows improved bioavailability compared to valsartan.[73]

Aside from the physical property improvement, the cocrystallization process is also a very powerful tool for purification and optical resolution. Allan S. Myerson et al. showed ibuprofen could be separated easily in the ibuprofen-ketoprofen model system, when 4,4'-bipydine was chosen as the coformer.[74] As for chiral resolution, our group has developed a series of methods to resolve compounds through cocrystallization. Interestingly, two racemic compounds (etiracetam and mandelic acid) were separated simultaneously in high enantiopurity through a single preferential cocrystallization process, which is impossible for chiral resolution through salt formation.[75]

1.4.5 Limitation to cocrystallization

The largest limitation of cocrystallization is its fairly low success rate. Indeed, common screens between a drug and a series of commonly used coformers will normally lead to about 10% success rate. [76, 77] Even with the guidance of synthon design, the success rate is still not very high.[78] Apart from that, a recent review talked about the challenges in cocrystal engineering of pharmaceutical solids including industrial scale-up of cocrystal production, inflexible dosing regimen of drug-drug cocrystals, cocrystal dissociation in the solid state, cocrystal dissociation and transformation in solution and cocrystal-excipient interaction (Figure 1.4).

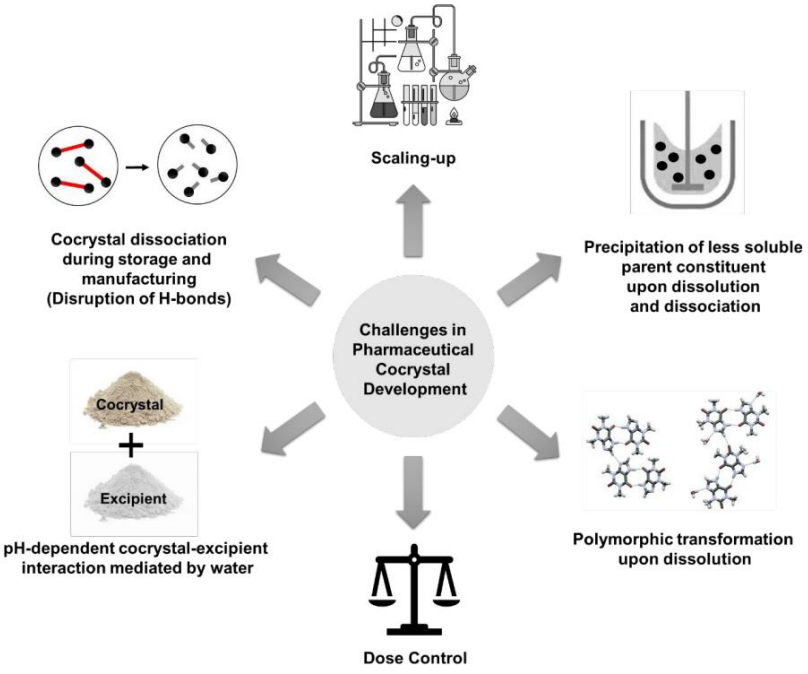

Figure 1.4 a schematic diagram depicting the challenges of pharmaceutical cocrystal product development. Cited from Wong, S. N. et.al[79]

1.5 solid solutions

Solid solutions are a less explored area in API solid form design, which is why it is not included in most solid form classification systems. We here, however, successfully design some innovative solid forms through the use of a solid solution. The basic background of solid solutions is presented here.

The term 'solid solutions' was first introduced by Van't Hoff in the 1890s.[80] In its literal sense, a solid solution is a solid phase with similar behavior to the liquid solution in which the ratio of two or more components can vary freely without the generation of new phase. The L defined a solid solution as "a crystal containing a second constituent which fits into and is distributed in the lattice of the host crystal" and does not recommend the use of solid solution for amorphous materials. The freely changed ratio of different compounds in a solid solution endows the physical properties of the solid phase with continuous adjustability.[81]

1.5.1 Design of solid solutions

Similarity is the key principle of solid solution design. Indeed, resemblance is always thought as a necessary condition for solid solution formation.[82, 83] Solid solution formation is driven by entropy increase due to homogeneous mixing of two or more substances. Traditionally, solid solution formation is expected only when identical crystals are mixed because the enthalpy will not change after alloying due to the breaking or formation of hydrogen/coordination bonds. However, some recent works have questioned this law. For example, although dihydrogen citrate salts of sodium and lithium are isomorphous, their solid-state solubility is only about 10%.[84] In contrast, phenazine and acridine demonstrate 80% solubility despite the fact that they crystallize into different crystal structures.[85]

Another criterion for solubility is based on atomic/molecular sizes and shapes. Hume-Rothery postulated three rules in solid solution design in his research about metal alloys and ceramics. Two metals will form a substitutional solid solution if:

1) their crystal structures are the same

2) difference of atomic size between the two is not more than 15%

3) their valences are the same.[82]

4) their electronegativies are similar[86]

This statement was also broken by Matteo Lusi, who developed a solid solution between monohydrate lithium isoorotate and monohydrate sodium isoorotate (the radius difference between sodium and lithium is about 25%).[84]

Although these exceptions exist, these two laws are still worth referencing. At present, solid solutions are normally designed between small molecules that differ in a terminal groups such as methyl or hydrogen and chlorine, or between chloro- and bromo-substituted versions of the same molecule.[87] For molecules with larger differences, introduction of a third compound is a potential option to solid solution formation. An excellent example is presented by Kazuki Sada et al. With the assistance of a 1-naphthylmethylamine ion, different aliphatic carboxylic acids could be alloyed as long as the multiple pairs of carboxylates sum to the same length in every layer.[88]

1.5.2 preparation of solid solutions

The synthesis of solid solutions is little explored. Until now, several methods including melting, sublimation, grinding, slow evaporation, cooling from solution, spray-drying, partial substitution through photo- or thermal treatment have been developed. For thermally stable compounds, the most traditional method, melting has played an important role even from the early ages of civilization in the smelting of bronze.[82] It is worth noting that the product obtained from cooling of a molten solution is not homogenous. Based on the phase diagram, solids that crystalize out first contain higher melting components while later crystals will be richer in the low melting ones (Figure 1.5). Solution-based methods like cooling or evaporation are dominating in preparation of large single crystals, which is extremely important in proving the formation of solid solutions. Similar to the melting method, the product obtained from traditional solution-based methods is also not homogenous when the starting materials have very distinct solubilities. Those crystals that crystalize out first, are richer in the low solubility component while those crystals that form at a later stage will be richer in the high solubility component. D. E. Braun's work showed, unexpected molecules like water may be included in the product and further interfere with the preparation of a solid solution.[89] In contrast to solution-based methods, grinding can be used as an alternative. Grinding allows avoiding most of the above-mentioned issues and affords high purity end-products. Furthermore, this method scales easily. The ratio of the two components in the solid solution can, in principle, be tuned simply by changing the feed ratio of the starting materials during the grinding procedure. Its simplicity, rapidity, ease of upscaling and environmental friendliness make grinding a popular method in solid solution synthesis. [82]

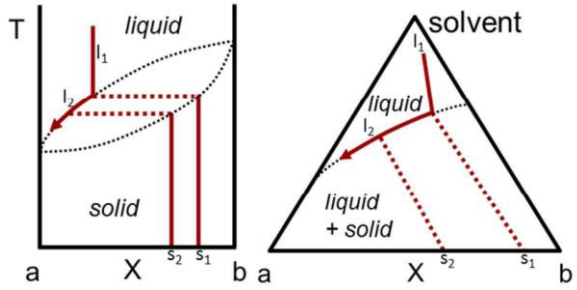

Figure 1.5. Phase diagrams showing the relationship between liquid and solids upon cooling of a binary system (left) and solvent evaporation of ternary system (right). Cited from M.Lusi[82]

1.5.3 characterization of solid solutions

SCXRD is definitely the most straightforward and convincing evidence for solid solution characterization. When the data quality is good enough, both compounds can be located in the electron density. Besides, a gradual change in space group or enantiomeric excess may be observed in some specific systems. These parameters can furthermore be used to evidence solid solution formation.[90] Last but not least, according to Vegard's rule, the lattice parameter of a solid solution of two constituents is approximately a weighted mean of the two constituents' lattice parameters at the same temperature.[91] The change of cell parameters could also be a good evidence of solid solution formation.

PXRD could confirm whether the powder product (normally obtained from grinding) is a physical mixture or solid solution. As mentioned before, the alloying of two compounds could lead to the change of unit cell parameters, which is shown through the shift of certain peaks. With the change in composition, the peaks of a solid solution will shift while physical mixtures give identical peaks apart from the change of intensity.[92] Moreover, Pawley, Le Bail and Rietveld refinement can help to determine the unit cell dimensions of the bulk product at a particular composition whereas the analysis of the diffraction peak profile can give an indication on how homogeneous the product is.[93]

Beyond the crystallographic methods, techniques like DSC, SSNMR, or even DVS can be applied in the characterization of solid solutions.[94, 95] For example, the powder product of cortisone and cortisol (cortisone is obtained from cortisol by oxidation of the hydroxyl group at the 11-beta position) obtained through spray-drying is shown to be a solid solution using SSNMR.[96]

1.5.4 advantages to the use of solid solutions

The biggest advantage of solid solutions is their potential to offer multi-component crystals in a tunable ratio, which is invaluable especially in drug-drug combination. The stoichiometric ratio of cocrystals is generally fixed as 1:1, 1:2, or 2:1. The dose of cocrystal formers may therefore not be in agreement with its recommended therapeutic dose for specific indications. Solid solutions, however, offer an elegant

way to solve this. For example, two antiretroviral drugs Lamivudine and Emtricitabine can be combined at the solid state, forming a solid solution with variable drug ratio.[97] Another potential application of solid solutions is the opportunity to fine-tune the physical properties (including thermal behavior, dissolution behavior, stability and so on) of a solid dosage. For example, in the solid solution of cortisone and cortisol, the initial dissolution rate of cortisol is twice that of pure cortisol, while the dissolution rate of cortisone is decreased.[96] Similarly, the aripiprazole and dehydro-aripiprazole solid solution demonstrated a tunable melting point from 157 °C to 127 °C.[98]

1.5.5 limitation to the use of solid solutions

Unlike salts or cocrystals, the study of solid solutions remains a less explored area. Indeed, nowadays only a very limited number of publications treat such systems, with most of the works focusing on simple and classical systems like benzoic acid/fluorobenzoic acid rather than real drug molecules.[99] Without the accumulation of more examples, raising new methodology for solid solution design is impossible. Apart from that, the characterization of solid solutions is still extremely difficult. Without single crystals, it is hard to judge whether the obtained phase is a true solid solution or a mere physical mixture.

1.6 Beyond binary systems

Traditional multi-component systems are composed of two species. Some researchers have however shown more complicated multi-component crystals like ternary cocrystals, salt cocrystals, salt solid solutions and so on.

1.6.1 ternary cocrystals

As the name suggests, ternary cocrystals contain three compounds. Although supramolecular chemistry has illustrated some well-designed examples of ternary cocrystal,[100, 101] it is still hard to get pharmaceutical ternary cocrystals because the coformer selection is largely narrowed by the GRAS list. Exploratory studies mainly focus on two similar drug molecules eg. both containing an amide group, (which is one of the most favored group in cocrystal formation) bridged by a dicarboxylic acid (Figure 1.6) Using this approach, Reginald B. H. Tan et al. found two new ternary cocrystals when isoniazid and nicotinamide are combined with succinic acid or fumaric acid.[102] Similar work is also done by Cui-Wei Yan et al., who obtained a new ternary cocrystal by combining pyrazinamide, isoniazid and fumaric acid together.[103] A recent contribution adopted this idea to ionic cocrystals, synthesizing a ternary ionic

cocrystal, successfully combining levetiracetam and nicotinamide using calcium chloride as bridging molecule.[104]

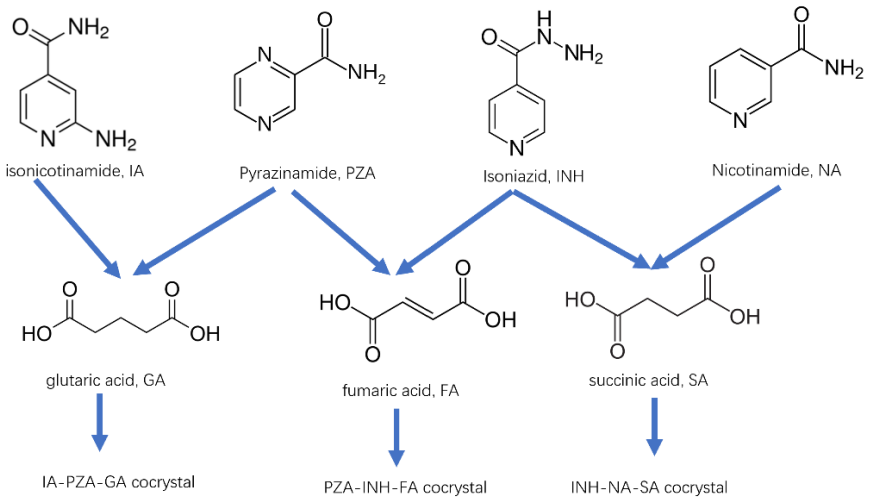

Figure 1.6 Part of the obtained ternary cocrystals up to now

1.6.2 salt cocrystals

The salt cocrystal could be regarded as a cocrystal between a salt and a coformer. For example, although cocrystalized with L-proline, the solubility of diclofenac is still lower than diclofenac sodium. To improve the solubility of diclofenac further, diclofenac sodium is cocrystallized with proline, giving a stable diclofenac sodium–proline tetrahydrate and an unstable diclofenac sodium–proline monohydrate. Their solubility and dissolution rate were superior to diclofenac sodium. [105] Similar work was presented later by Kunikazu Moribe et. al. through cocrystallization with fructose, loxoprofen sodium was found under a stable solid form under high humidity environment.[106] The salt cocrystal was also shown to exist between an organic salt and coformer. Cui-Wei Yan gave a good example, successfully combining Piperazine with ferulate through salt formation. Subsequently, the salt is cocrystallized with a second drug pyrazinamide. The solubility and dissolution analysis show that the salt cocrystal can simultaneously achieve a sustained-release effect for piperazine ferulate and superior dissolution rate for pyrazinamide.[107]

1.6.3 solid solutions of salt/cocrystals

Similar to normal solid solutions, as long as two salts or cocrystals fulfill the similarity principle, there is a high possibility to obtain a solid solution between these two compounds. Indeed, a solid solution can be obtained between the isonicotinaide-fumaric acid cocrystal and the isonicotinamide-succinic acid cocrystal, explained by their similarity.[108] Iain D. H. Oswald showed another example, using the salt 4-methylmethcathinone hydrochloride. This latter undergoes an enantiotropic phase transition upon cooling. Through formation of a solid solution with 4-methylmethcathinone hydro bromide, the polymorphic transition temperature can be altered by up to 80 °C depending on the amount of bromide.[109]

1.7 Goal of the thesis

This PhD project is performed in the group of Prof. Tom Leyssens in the Institute of Condensed Matter and Nanosciences (IMCN), UCLouvain. In this laboratory, we focused on crystal engineering of APIs, for which we not only explore the landscape of API solid forms, but also try to develop innovative methodologies for pharmaceutical crystals design. These new solid forms may present desired physical properties like improved solubility, thermal stability compared the original molecules, which is valuable in pharmaceutical industry.

In this context, we focused on exploring innovative methods for combining different molecules in one crystal through rational design rather than simple try and error. If successful, the physical properties of these newly designed multi-component crystals will be further characterized to investigatee if there are improvements or not. Moreover, we will seek opportunities to prepare them on a large scale.

Three methods are put forward for multi-components pharmaceutical crystal design, which include:

1) Ternary cocrystals: following the success examples given by previous work, the ternary cocrystal method was applied in the design of multi-component crystals. It is expected that two suitable pharmaceutical compounds will be interconnected by urea. Although new cocrystals between urea and three pharmaceutical compounds are identified and characterized, the attempt to obtain ternary cocrystals met complete failure, which will be presented in chapter 2.

2) Complexation: in this part, a new method was investigated. Through transforming acidic compounds to their salt, combination with another neutral molecule could be achieved. This method met great success. In the first part of chapter 3, we try to combine saccharine, a well-known sweetener, with a series of bitter drugs, racetams. In the second part, we focused on achieving drug combination with this method.

3) cocrystal solid solution: inflexibility in the ratio of two desired compounds is a large limitation to the application of multicomponent crystals. In chapter 4, we therefore focused on a crystal form allowing to vary the drug ratio through the formation of solid solution.

At the end of the thesis, a brief overview is given and overall conclusions are drawn leading to perspectives for future work. All the Supporting Materials related to the articles are given into the appendices at the end of this document.

References

(1) Nangia, A. K.; Desiraju, G. R. Crystal Engineering: An Outlook for the Future. *Angew Chem Int Ed Engl* **2019**, *58* (13), 4100-4107.

(2) Desiraju, G. R. Crystal engineering: from molecule to crystal. *J Am Chem Soc* **2013**, *135* (27), 9952-9967.

(3) Moulton, B.; Zaworotko, M. J. From molecules to crystal engineering: supramolecular isomerism and polymorphism in network solids. *Chem Rev* **2001**, *101* (6), 1629-1658.

(4) Bragg, S. W. H. The Structure of Organic Crystals. *Proceedings of the Physical Society of London* **1921**, *34* (1), 33-50.

(5) Lonsdale, K. The Structure of the Benzene Ring. *Nature* **1928**, *122* (3082), 810-810.

(6) Pepinsky, R. Crystal engineering-new concept in crystallography. In *Physical Review*, 1955; AMERICAN PHYSICAL SOC ONE PHYSICS ELLIPSE, COLLEGE PK, MD 20740-3844 USA: Vol. 100, pp 971-971.

(7) Little, M. A.; Cooper, A. I. The Chemistry of Porous Organic Molecular Materials. *Advanced Functional Materials* **2020**, *30* (41).

(8) Zhang, C.; Jiao, F.; Li, H. Crystal Engineering for Creating Low Sensitivity and Highly Energetic Materials. *Crystal Growth & Design* **2018**, *18* (10), 5713-5726.

(9) Laramy, C. R.; O'Brien, M. N.; Mirkin, C. A. Crystal engineering with DNA. *Nature Reviews Materials* **2019**, *4* (3), 201-224.

(10) Mattei, A.; Li, T. *Pharmaceutical crystals: science and engineering*; John Wiley & Sons, 2018.

(11) Wouters, J.; Quéré, L. *Pharmaceutical salts and co-crystals*; Royal Society of Chemistry, 2011.

(12) Byrn, S. R.; Zografi, G.; Chen, X. S. *Solid-state properties of pharmaceutical materials*; John Wiley & Sons, 2017.

(13) Berry, D. J.; Steed, J. W. Pharmaceutical cocrystals, salts and multicomponent systems; intermolecular interactions and property based design. *Adv Drug Deliv Rev* **2017**, *117*, 3-24.

(14) Aitipamula, S.; Banerjee, R.; Bansal, A. K.; Biradha, K.; Cheney, M. L.; Choudhury, A. R.; Desiraju, G. R.; Dikundwar, A. G.; Dubey, R.; Duggirala, N.; et al. Polymorphs, Salts, and Cocrystals: What's in a Name? *Crystal Growth & Design* **2012**, *12* (5), 2147-2152.

(15) Bond, A. D. What is a co-crystal? *CrystEngComm* **2007**, *9* (9).

(16) Karagianni, A.; Malamatari, M.; Kachrimanis, K. Pharmaceutical Cocrystals: New Solid Phase Modification Approaches for the Formulation of APIs. *Pharmaceutics* **2018**, *10* (1).

(17) Gupta, D.; Bhatia, D.; Dave, V.; Sutariya, V.; Varghese Gupta, S. Salts of Therapeutic Agents: Chemical, Physicochemical, and Biological Considerations. *Molecules* **2018**, *23* (7).

(18) Serajuddin, A. T. Salt formation to improve drug solubility. *Adv Drug Deliv Rev* **2007**, *59* (7), 603-616.

(19) Hossain Mithu, M. S.; Economidou, S.; Trivedi, V.; Bhatt, S.; Douroumis, D. Advanced Methodologies for Pharmaceutical Salt Synthesis. *Crystal Growth & Design* **2021**, *21* (2), 1358-1374.

(20) Wiedmann, T. S.; Naqwi, A. Pharmaceutical salts: Theory, use in solid dosage forms and in situ preparation in an aerosol. *Asian Journal of Pharmaceutical Sciences* **2016**, *11* (6), 722-734.

(21) Tan, D.; Loots, L.; Friscic, T. Towards medicinal mechanochemistry: evolution of milling from pharmaceutical solid form screening to the synthesis of active pharmaceutical ingredients (APIs). *Chem Commun (Camb)* **2016**, *52* (50), 7760-7781.

(22) Zhou, W.-X.; Zhao, H.-W.; Chen, H.-H.; Zhang, Z.-Y.; Chen, D.-Y. Characterization of drug–drug salt forms of metformin and aspirin with improved physicochemical properties. *CrystEngComm* **2019**, *21* (25), 3770-3773.

(23) Cruz-Cabeza, A. J. Acid–base crystalline complexes and the pKa rule. *CrystEngComm* **2012**, *14* (20).

(24) Trask, A. V.; Haynes, D. A.; Motherwell, W. D.; Jones, W. Screening for crystalline salts via mechanochemistry. *Chem Commun (Camb)* **2006**, (1), 51-53.

(25) Galcera, J.; Friščić, T.; Hejczyk, K. E.; Fábián, L.; Clarke, S. M.; Day, G. M.; Molins, E.; Jones, W. Isostructural organic binary-host frameworks with tuneable and diversely decorated inclusion cavities. *CrystEngComm* **2012**, *14* (23).

(26) Cerreia Vioglio, P.; Chierotti, M. R.; Gobetto, R. Pharmaceutical aspects of salt and cocrystal forms of APIs and characterization challenges. *Adv Drug Deliv Rev* **2017**, *117*, 86-110.

(27) Harris, R. K. NMR crystallography: the use of chemical shifts. *Solid State Sciences* **2004**, *6* (10), 1025-1037.

(28) Xu, Y.; Southern, S. A.; Szell, P. M. J.; Bryce, D. L. The role of solid-state nuclear magnetic resonance in crystal engineering. *CrystEngComm* **2016**, *18* (28), 5236-5252.

(29) Braga, D.; Chelazzi, L.; Grepioni, F.; Dichiarante, E.; Chierotti, M. R.; Gobetto, R. Molecular Salts of Anesthetic Lidocaine with Dicarboxylic Acids: Solid-State Properties and a Combined Structural and Spectroscopic Study. *Crystal Growth & Design* **2013**, *13* (6), 2564-2572.

(30) Peng, B.; Zhang, Z.; Wang, J. R.; Li, M.; Zhang, Q.; Mei, X. Confocal Raman micro-spectral evidence and physicochemical evaluation of triamterene salts. *Analyst* **2019**, *144* (2), 530-535.

(31) Bastin, R. J.; Bowker, M. J.; Slater, B. J. Salt Selection and Optimisation Procedures for Pharmaceutical New Chemical Entities. *Organic Process Research & Development* **2000**, *4* (5), 427-435.

(32) Saal, C. SOLUBILITY: Pharmaceutical Salts Optimization of Solubility or Even More? *American Pharmaceutical Review* **2010**, *13* (2), 18.

(33) Thackaberry, E. A. Non-clinical toxicological considerations for pharmaceutical salt selection. *Expert Opin Drug Metab Toxicol* **2012**, *8* (11), 1419-1433.

(34) Bharate, S. S. Modulation of biopharmaceutical properties of drugs using sulfonate counterions: A critical analysis of FDA-approved pharmaceutical salts. *Journal of Drug Delivery Science and Technology* **2021**, *66*.

(35) Thakuria, R.; Sarma, B. Drug‐Drug and Drug‐Nutraceutical Cocrystal/Salt as Alternative Medicine for Combination Therapy: A Crystal Engineering Approach. *Crystals* **2018**, *8* (2).

(36) Liu, S.; Wang, C.; Chen, H.; Sun, C. C. Sweet Sulfamethazine Acesulfamate Crystals with Improved Compaction Property. *Crystal Growth & Design* **2021**, *21* (2), 1077-1085.

(37) Kong, M.; Fu, X.; Li, J.; Li, J.; Chen, M.; Deng, Z.; Zhang, H. Sweet pharmaceutical salts of stanozolol with enhanced solubility and physical stability. *CrystEngComm* **2016**, *18* (45), 8739-8746.

(38) Martins, F. T.; Paparidis, N.; Doriguetto, A. C.; Ellena, J. Crystal Engineering of an Anti-HIV Drug Based on the Recognition of Assembling Molecular Frameworks. *Crystal Growth & Design* **2009**, *9* (12), 5283-5292.

(39) Li, A.-Y.; Xu, L.-L.; Chen, J.-M.; Lu, T.-B. Solubility and Dissolution Rate Enhancement of Triamterene by a Cocrystallization Method. *Crystal Growth & Design* **2015**, *15* (8), 3785-3791.

(40) Banerjee, R.; Bhatt, P. M.; Ravindra, N. V.; Desiraju, G. R. Saccharin Salts of Active Pharmaceutical Ingredients, Their Crystal Structures, and Increased Water Solubilities. *Crystal Growth & Design* **2005**, *5* (6), 2299-2309.

(41) Vakil, V.; Trappe, W. Drug Combinations: Mathematical Modeling and Networking Methods. *Pharmaceutics* **2019**, *11* (5).

(42) Wan, X.; Ma, P.; Zhang, X. A promising choice in hypertension treatment: Fixed-dose combinations. *Asian Journal of Pharmaceutical Sciences* **2014**, *9* (1), 1-7.

(43) Frantz, S. The trouble with making combination drugs. *Nat Rev Drug Discov* **2006**, *5* (11), 881-882.

(44) Putra, O. D.; Furuishi, T.; Yonemochi, E.; Terada, K.; Uekusa, H. Drug–Drug Multicomponent Crystals as an Effective Technique to Overcome Weaknesses in Parent Drugs. *Crystal Growth & Design* **2016**, *16* (7), 3577-3581.

(45) Zhu, Q.; Wang, J.; Bian, X.; Zhang, L.; Wei, P.; Xu, Y. Novel Synthesis of Antiobesity Drug Lorcaserin Hydrochloride. *Organic Process Research & Development* **2015**, *19* (9), 1263-1267.

(46) Liu, L.-W.; Wang, F.-Y.; Tian, F.; Peng, L.; Wang, L.-X. An Improved and Enantioselective Preparation of the Telaprevir Bicyclic [3.3.0] Proline Intermediate and Reuse of Unwanted Enantiomer. *Organic Process Research & Development* **2016**, *20* (2), 320-324.

(47) Siedlecka, R. Recent developments in optical resolution. *Tetrahedron* **2013**, *69* (31), 6331-6363.

(48) Bharate, S. S. Recent developments in pharmaceutical salts: FDA approvals from 2015 to 2019. *Drug Discov Today* **2021**, *26* (2), 384-398.

(49) Bogardus, J. B.; Blackwood, R. K., Jr. Solubility of doxycycline in aqueous solution. *J Pharm Sci* **1979**, *68* (2), 188-194.

(50) Kavanagh, O. N.; Croker, D. M.; Walker, G. M.; Zaworotko, M. J. Pharmaceutical cocrystals: from serendipity to design to application. *Drug Discov Today* **2019**, *24* (3), 796-804.

(51) Duggirala, N. K.; Perry, M. L.; Almarsson, O.; Zaworotko, M. J. Pharmaceutical cocrystals: along the path to improved medicines. *Chem Commun (Camb)* **2016**, *52* (4), 640-655.

(52) Braga, D.; Grepioni, F.; Shemchuk, O. Organic–inorganic ionic co-crystals: a new class of multipurpose compounds. *CrystEngComm* **2018**, *20* (16), 2212-2220.

(53) Etter, M. C. Hydrogen bonds as design elements in organic chemistry. *The Journal of Physical Chemistry* **2002**, *95* (12), 4601-4610.

(54) Etter, M. C. Encoding and decoding hydrogen-bond patterns of organic compounds. *Accounts of Chemical Research* **2002**, *23* (4), 120-126.

(55) Donohue, J. The Hydrogen Bond in Organic Crystals. *The Journal of Physical Chemistry* **2002**, *56* (4), 502-510.

(56) Leng, F.; Shemchuk, O.; Robeyns, K.; Leyssens, T. Complexation: An Interesting Pathway for Combining Two APIs at the Solid State. *Pharmaceutics* **2022**, *14* (9).

(57) Desiraju, G. R. A bond by any other name. *Angew Chem Int Ed Engl* **2011**, *50* (1), 52-59.

(58) Kumar Bandaru, R.; Rout, S. R.; Kenguva, G.; Gorain, B.; Alhakamy, N. A.; Kesharwani, P.; Dandela, R. Recent Advances in Pharmaceutical Cocrystals: From Bench to Market. *Front Pharmacol* **2021**, *12*, 780582.

(59) Stevens, J. S.; Newton, L. K.; Jaye, C.; Muryn, C. A.; Fischer, D. A.; Schroeder, S. L. M. Proton Transfer, Hydrogen Bonding, and Disorder: Nitrogen Near-Edge X-ray Absorption Fine Structure and X-ray Photoelectron Spectroscopy of Bipyridine–Acid Salts and Co-crystals. *Crystal Growth & Design* **2015**, *15* (4), 1776-1783.

(60) Childs, S. L.; Kandi, P.; Lingireddy, S. R. Formulation of a danazol cocrystal with controlled supersaturation plays an essential role in improving bioavailability. *Mol Pharm* **2013**, *10* (8), 3112-3127.

(61) Karimi-Jafari, M.; Padrela, L.; Walker, G. M.; Croker, D. M. Creating Cocrystals: A Review of Pharmaceutical Cocrystal Preparation Routes and Applications. *Crystal Growth & Design* **2018**, *18* (10), 6370-6387.

(62) Trask, A. V.; Motherwell, W. D. S.; Jones, W. Pharmaceutical Cocrystallization: Engineering a Remedy for Caffeine Hydration. *Crystal Growth & Design* **2005**, *5* (3), 1013-1021.

(63) Karki, S.; FrisÌŒcÌŒicÌ• , T.; FÃ¡biÃ¡n, L. s.; Laity, P. R.; Day, G. M.; Jones, W. Improving Mechanical Properties of Crystalline Solids by Cocrystal Formation: New Compressible Forms of Paracetamol. *Advanced Materials* **2009**, *21* (38â€“39), 3905-3909.

(64) Sun, C. C.; Hou, H. Improving Mechanical Properties of Caffeine and Methyl Gallate Crystals by Cocrystallization. *Crystal Growth & Design* **2008**, *8* (5), 1575-1579.

(65) Takata, N.; Takano, R.; Uekusa, H.; Hayashi, Y.; Terada, K. A Spironolactone−Saccharin 1:1 Cocrystal Hemihydrate. *Crystal Growth & Design* **2010**, *10* (5), 2116-2122.

(66) Hickey, M. B.; Peterson, M. L.; Scoppettuolo, L. A.; Morrisette, S. L.; Vetter, A.; Guzman, H.; Remenar, J. F.; Zhang, Z.; Tawa, M. D.; Haley, S.; et al. Performance comparison of a co-crystal of carbamazepine with marketed product. *Eur J Pharm Biopharm* **2007**, *67* (1), 112-119.

(67) Chadha, R.; Saini, A.; Jain, D. S.; Venugopalan, P. Preparation and Solid-State Characterization of Three Novel Multicomponent Solid Forms of Oxcarbazepine: Improvement in Solubility through Saccharin Cocrystal. *Crystal Growth & Design* **2012**, *12* (8), 4211-4224.

(68) Thipparaboina, R.; Kumar, D.; Chavan, R. B.; Shastri, N. R. Multidrug co-crystals: towards the development of effective therapeutic hybrids. *Drug Discov Today* **2016**, *21* (3), 481-490.

(69) Wang, X.; Du, S.; Zhang, R.; Jia, X.; Yang, T.; Zhang, X. Drug-Drug Cocrystals: Opportunities and Challenges. *Asian Journal of Pharmaceutical Sciences* **2020**.

(70) Cheney, M. L.; Weyna, D. R.; Shan, N.; Hanna, M.; Wojtas, L.; Zaworotko, M. J. Coformer selection in pharmaceutical cocrystal development: a case study of a meloxicam aspirin cocrystal that exhibits enhanced solubility and pharmacokinetics. *J Pharm Sci* **2011**, *100* (6), 2172-2181.

(71) Braga, D.; Grepioni, F.; Maini, L.; Capucci, D.; Nanna, S.; Wouters, J.; Aerts, L.; Quere, L. Combining piracetam and lithium salts: ionic co-crystals and co-drugs? *Chem Commun (Camb)* **2012**, *48* (66), 8219-8221.

(72) Sanphui, P.; Goud, N. R.; Khandavilli, U. B. R.; Nangia, A. Fast Dissolving Curcumin Cocrystals. *Crystal Growth & Design* **2011**, *11* (9), 4135-4145.

(73) Videla, S.; Lahjou, M.; Vaque, A.; Sust, M.; Encabo, M.; Soler, L.; Sans, A.; Sicard, E.; Gascon, N.; Encina, G.; et al. Single-dose pharmacokinetics of co-crystal of tramadol-celecoxib: Results of a four-way randomized open-label phase I clinical trial in healthy subjects. *Br J Clin Pharmacol* **2017**, *83* (12), 2718-2728.

(74) Hsi, K. H.-Y.; Chadwick, K.; Fried, A.; Kenny, M.; Myerson, A. S. Separation of impurities from solution by selective co-crystal formation. *CrystEngComm* **2012**, *14* (7), 2386-2388.

(75) Zhou, F.; Shemchuk, O.; Charpentier, M. D.; Matheys, C.; Collard, L.; Ter Horst, J. H.; Leyssens, T. Simultaneous Chiral Resolution of Two Racemic Compounds by Preferential Cocrystallization*. *Angew Chem Int Ed Engl* **2021**, *60* (37), 20264-20268.

(76) Leng, F.; Robeyns, K.; Leyssens, T. Urea as a Cocrystal Former-Study of 3 Urea Based Pharmaceutical Cocrystals. *Pharmaceutics* **2021**, *13* (5).

(77) Buol, X.; Robeyns, K.; Caro Garrido, C.; Tumanov, N.; Collard, L.; Wouters, J.; Leyssens, T. Improving Nefiracetam Dissolution and Solubility Behavior Using a Cocrystallization Approach. *Pharmaceutics* **2020**, *12* (7).

(78) Jagia, M.; Daptardar, R.; Patel, K.; Bansal, A. K.; Patel, S. Role of Structure, Microenvironmental pH, and Speciation To Understand the Formation and Properties of Febuxostat Eutectics. *Mol Pharm* **2019**, *16* (11), 4610-4620.

(79) Wong, S. N.; Chen, Y. C. S.; Xuan, B.; Sun, C. C.; Chow, S. F. Cocrystal engineering of pharmaceutical solids: therapeutic potential and challenges. *CrystEngComm* **2021**.

(80) Van Klooster, H. S. Bakhuis Roozeboom and the phase rule. *Journal of Chemical Education* **1954**, *31* (11).

(81) Batten, S. R.; Champness, N. R.; Chen, X.-M.; Garcia-Martinez, J.; Kitagawa, S.; Öhrström, L.; O'Keeffe, M.; Paik Suh, M.; Reedijk, J. Terminology of metal–organic frameworks and coordination polymers

(IUPAC Recommendations 2013). *Pure and Applied Chemistry* **2013**, *85* (8), 1715-1724.

(82) Lusi, M. A rough guide to molecular solid solutions: design, synthesis and characterization of mixed crystals. *CrystEngComm* **2018**, *20* (44), 7042-7052.

(83) Lusi, M. Engineering Crystal Properties through Solid Solutions. *Crystal Growth & Design* **2018**, *18* (6), 3704-3712.

(84) Lestari, M.; Lusi, M. A mixed molecular salt of lithium and sodium breaks the Hume-Rothery rules for solid solutions. *Chem Commun (Camb)* **2019**, *55* (16), 2297-2300.

(85) Schur, E.; Nauha, E.; Lusi, M.; Bernstein, J. Kitaigorodsky revisited: polymorphism and mixed crystals of acridine/phenazine. *Chemistry* **2015**, *21* (4), 1735-1742.

(86) Scott, D. A.; Schwab, R. The Structure of Metals and Alloys. In *Metallography in Archaeology and Art*, Springer International Publishing, 2019; pp 69-132.

(87) Cruz-Cabeza, A. J.; Lestari, M.; Lusi, M. Cocrystals Help Break the "Rules" of Isostructurality: Solid Solutions and Polymorphism in the Malic/Tartaric Acid System. *Crystal Growth & Design* **2017**, *18* (2), 855-863.

(88) Sada, K.; Inoue, K.; Tanaka, T.; Epergyes, A.; Tanaka, A.; Tohnai, N.; Matsumoto, A.; Miyata, M. Multicomponent organic alloys based on organic layered crystals. *Angew Chem Int Ed Engl* **2005**, *44* (43), 7059-7062.

(89) Braun, D. E.; Griesser, U. J. Prediction and experimental validation of solid solutions and isopolymorphs of cytosine/5-flucytosine. *CrystEngComm* **2017**, *19* (26), 3566-3572.

(90) Belitzky, A.; Weissbuch, I.; Posner-Diskin, Y.; Lahav, M.; Lubomirsky, I. Design of Pyroelectric Mixed Crystals Having a Varying Degree of Polarity: The l-Asparagine·H2O/l-Aspartic Acid System. *Crystal Growth & Design* **2015**, *15* (5), 2445-2451.

(91) Schultz, P.; Keller, E. Strong positive and negative deviations from Vegard's rule: X-ray powder investigations of the three quasi-binary phase systems BiSX(1 - x)Y(x) (X, Y = Cl, Br, I). *Acta Crystallogr B Struct Sci Cryst Eng Mater* **2014**, *70* (Pt 2), 372-378.

(92) Shemchuk, O.; Braga, D.; Grepioni, F. Alloying barbituric and thiobarbituric acids: from solid solutions to a highly stable keto co-crystal form. *Chem Commun (Camb)* **2016**, *52* (79), 11815-11818.

(93) Le Bail, A. Whole powder pattern decomposition methods and applications: A retrospection. *Powder Diffraction* **2012**, *20* (4), 316-326.

(94) Braun, D. E.; Kahlenberg, V.; Griesser, U. J. Experimental and Computational Hydrate Screening: Cytosine, 5-Flucytosine and Their Solid Solution. *Cryst Growth Des* **2017**, *17* (8), 4347-4364.

(95) Pina, M. F.; Pinto, J. F.; Sousa, J. J.; Fabian, L.; Zhao, M.; Craig, D. Q. Identification and characterization of stoichiometric and nonstoichiometric hydrate forms of paroxetine HCl: reversible changes in crystal dimensions as a function of water absorption. *Mol Pharm* **2012**, *9* (12), 3515-3525.

(96) Verma, V.; Bordignon, S.; Chierotti, M. R.; Lestari, M.; Lyons, K.; Padrela, L.; Ryan, K. M.; Lusi, M. Cortisone and cortisol break hydrogen-bonding rules to make a drug-prodrug solid solution. *IUCrJ* **2020**, *7* (Pt 6), 1124-1130.

(97) Fonseca, J. d. C.; Tenorio Clavijo, J. C.; Alvarez, N.; Ellena, J.; Ayala, A. P. Novel Solid Solution of the Antiretroviral Drugs Lamivudine and Emtricitabine. *Crystal Growth & Design* **2018**, *18* (6), 3441-3448.

(98) Trotta, J. T.; Zeidan, T. A.; Tilak, P. A.; Foxman, B. M.; Almarsson, Ö.; Oliveira, M. A.; Chiarella, R. A.; Hickey, M. B.; Remenar, J. F. Aripiprazole and Dehydro-Aripiprazole Solid Solutions: Crystalline Combinations of Drug and Active Metabolite in Tailored Compositions. *Crystal Growth & Design* **2020**, *20* (6), 3944-3956.

(99) Seera, R.; Cherukuvada, S.; Guru Row, T. N. Evolution of Cocrystals from Solid Solutions in Benzoic Acid–Mono/poly-fluorobenzoic Acid Combinations. *Crystal Growth & Design* **2021**, *21* (8), 4607-4618.

(100) Adsmond, D. A.; Sinha, A. S.; Khandavilli, U. B. R.; Maguire, A. R.; Lawrence, S. E. Design and Synthesis of Ternary Cocrystals Using Carboxyphenols and Two Complementary Acceptor Compounds. *Crystal Growth & Design* **2015**, *16* (1), 59-69.

(101) Allu, S.; Bolla, G.; Tothadi, S.; Nangia, A. Supramolecular Synthons in Bumetanide Cocrystals and Ternary Products. *Crystal Growth & Design* **2017**, *17* (8), 4225-4236.

(102) Aitipamula, S.; Wong, A. B. H.; Chow, P. S.; Tan, R. B. H. Novel solid forms of the anti-tuberculosis drug, Isoniazid: ternary and polymorphic cocrystals. *CrystEngComm* **2013**, *15* (29).

(103) Liu, F.; Song, Y.; Liu, Y.-N.; Li, Y.-T.; Wu, Z.-Y.; Yan, C.-W. Drug-Bridge-Drug Ternary Cocrystallization Strategy for Antituberculosis Drugs Combination. *Crystal Growth & Design* **2018**, *18* (3), 1283-1286.

(104) Song, L.; Robeyns, K.; Tumanov, N.; Wouters, J.; Leyssens, T. Combining API in a dual-drug ternary cocrystal approach. *Chem Commun (Camb)* **2020**.

(105) Nugrahani, I.; Kumalasari, R. A.; Auli, W. N.; Horikawa, A.; Uekusa, H. Salt Cocrystal of Diclofenac Sodium-L-Proline: Structural, Pseudopolymorphism, and Pharmaceutics Performance Study. *Pharmaceutics* **2020**, *12* (7).

(106) Fujito, T.; Oshima, T.; Higashi, K.; Ueda, K.; Ito, M.; Masu, H.; Noguchi, S.; Moribe, K. Salt Cocrystallization of Loxoprofen Sodium with Sugar: Reduction of the Propensity for Hydrate Formation by Forming a Continuous One-Dimensional Chain Structure of Sodium and Sugar. *Crystal Growth & Design* **2021**.

(107) Yu, X.-Z.; Wang, L.-Y.; Liu, F.; Li, Y.-T.; Wu, Z.-Y.; Yan, C.-W. Sustained-Release Dual-Drug Ternary Salt Cocrystal of Piperazine Ferulate with Pyrazinamide: Synthesis, Structure, and Hirshfeld Surface Analysis. *Crystal Growth & Design* **2020**, *20* (3), 2064-2073.

(108) Oliveira, M. A.; Peterson, M. L.; Klein, D. Continuously Substituted Solid Solutions of Organic Co-Crystals. *Crystal Growth & Design* **2008**, *8* (12), 4487-4493.

(109) Delori, A.; Maclure, P.; Bhardwaj, R. M.; Johnston, A.; Florence, A. J.; Sutcliffe, O. B.; Oswald, I. D. H. Drug solid solutions – a method for tuning phase transformations. *CrystEngComm* **2014**, *16* (26), 5827-5831.

Chapter 2

2.Urea Cocrystals: A Failed Attempt

This chapter is based on the article published by Leng F, Robeyns K, Leyssens T. *Pharmaceutics*, **2021**, 13(5): 671.

As mentioned in part 1.7, our initial idea was to use urea as a sort of coupling agent between two organic compounds. Focusing on two different API that both cocrystallize with urea, we hoped to use urea as a bridge to couple both API together in a ternary cocrystal. These attempts however failed, likely due to the lack of similarity between cocrystal structures. This approach can therefore be considered a 'failed attempt'. However, as we did get a multitude of novel solid forms including the GRAS compound urea, we valorized this work through a publication focusing on urea.

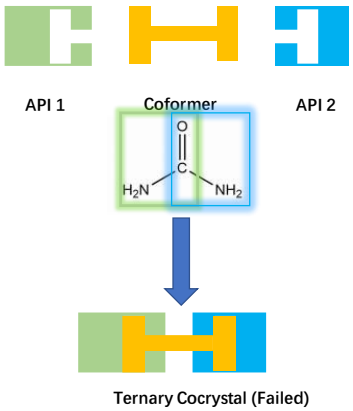

Conceptualization, T.L. and K.R.; methodology, T.L.; software, K.R.; validation, T.L., K.R. and F.L.; formal analysis, F.L.; investigation, F.L.; data curation, F.L.; writing—original draft preparation, F.L.; writing—review and editing, T.L. and K.R.; supervision, T.L. and K.R.; project administration, T.L.; funding acquisition, T.L. All authors have read and agreed to the published version of the manuscript.

2.1 Abstract

Cocrystallization is commonly used for its ability to improve the physical properties of APIs, such as solubility, bioavailability, compressibility, etc. The pharmaceutical industry is particularly interested in those cocrystals comprising a GRAS former in

connection with the target API. In this work, we focus on the potential of urea as a cocrystal former, identifying three novel pharmaceutical cocrystal systems with catechin, 3-hydroxyl-2-naphthoic and ellagic acid. Interestingly, the stability of catechin under high humidity or high temperature environment is improved upon cocrystallization with urea. Moreover, the solubility of ellagic acid is improved about 17 times. This work displays the latent possibility of urea in improving the physical property of drug molecules using a cocrystallization approach.

2.2 Introduction

Cocrystals have drawn increasing attention in recent years due to their ability to improve physical properties of APIs without changing the chemical structure of the original drug[1-4]. Although still in debate, a well-accepted definition describes cocrystals as "solids that are crystalline single-phase materials composed of two or more different molecules and/or ionic compounds generally in a stoichiometric ratio which are neither solvates nor simple salts"[5]. More specifically, pharmaceutical cocrystals combine a drug compound and a pharmaceutically acceptable coformer. There have been several pharmaceutical cocrystals marketed up to date, with an even more important number undergoing clinical trials.[6]

Indexed as a GRAS compound, urea is an excellent choice of coformer from the pharmaceutical (safe) and economic (inexpensive) point of view. Until now, 5 urea polymorphs have been reported,[7] it is worth noting that the structure of polymorph I possesses an unusual channel.[8] High water solubility coformers in general increase the solubility of the API when the cocrystal is formed [2, 9, 10]. Urea cocrystals are therefore expected to strongly impact the API solubility. Urea furthermore has functional groups frequently encountered in cocrystal hydrogen bonding patterns, and therefore forms an ideal candidate for co-crystal screening [11, 12]. Various contributions already show the potential of urea for the improvement of physical properties compared to the original API [13-16]. Urea co-crystals raised the solubility of agomelatine 2.2 times[17]. Urea also improved the intrinsic dissolution rate of bumetanide[13], febuxostat[15] and niclosamide[16] in a variety of solvents.

We here present, three novel urea comprising pharmaceutical cocrystals with catechin, 3-hydroxyl-2-naphthoic acid and ellagic acid, all of which show interesting bioactivity. Specifically, ellagic acid is widely used in food and pharmaceutical industry owing to its antioxidant and anti-inflammatory effect [18, 19]. The anti-diabetic effect of 3-hydroxyl-2-naphthoic acid has also been proved by previous reports [20]. Catechin is a flavanol which has been effectiveness as an antioxidant, and for improvement of the

immune system response [21-24]. In this work we show how cocrystallization with urea, leads to a 17-fold solubility increase of ellagic acid, as well as an improvement of the physical stability of catechin. This work therefore further underlines the potential of urea for the improvement of physical properties of API through cocrystallization.

2.3 Materials and methods

Materials. Catechin (98%) and 3-hydroxyl-2-naphthoic acid (98%) were bought from sigma-Aldrich, St. Louis, MO, USA. Ellagic acid (97%) was bought from Alfa Aesar, Haverhill, MA, USA. Urea was bought from Merck. Catechin hydrate is obtained by slurring catechin in water for 2 days, apart from that, all reagents were used as received.

Cocrystal screen. In a typical cocrystal screening experiment, 0.25 mmol urea and an equimolar amount of API are placed in an Eppendorf adding one stainless steel ball. After that, grinding was performed using a RETSCH Mixer Mill MM 400 with a beating frequency of 30 Hz for 90 min. Subsequently, the PXRD of the ground material is compared to that of the parent compounds. Upon apparition of novel peaks, grinding is performed under various ratios as well. When neat grinding did not lead to a full transformation, LAG was performed in parallel, adding 20 μL of solvent to the initial mixture of urea and target compound prior to grinding (solvents include methanol, ethanol, water, acetonitrile and isopropanol).

Mechanical synthesis of cocrystals. The UE can be obtained by LAG of 30 mg urea and 75 mg ellagic acid (2:1 molar ratio) using 20 μL of water or isopropanol. The UH as well as UC can be obtained by dry grinding in a 1:1 molar ratio

Single crystal growth. Methanol is added in a drop-wise manner to a vial containing 25 mg of catechin and 24 mg urea (1:5 molar ratio) until full dissolution is achieved. After that, the solution is left to evaporate. After one week, UC crystals are obtained of sufficient quality for SCXRD. In a similar approach, single crystals of UH are obtained by evaporating an undersaturated methanol solution of urea and 3-hydroxyl-2-naphthoic acid (in a 1:3 molar ratio).

PXRD and VT-PXRD. Powder X-ray diffraction of all samples are conducted on a Siemens D5000 diffractometer equipped with a Cu X-ray source operating at 40 kV and 40 mA (λ = 1.5418 Å) from 2 to 50 degree at the rate of 0.6 degree per minute. VT-PXRD of catechin hydrate is collected on a PANalytical X'Pert PRO automated diffractometer from 3 to 40 degree, equipped with an X'Celerator detector and an Anton Paar TTK 450 system for measurements at controlled temperature. Data were

collected in open air in Bragg-Brentano geometry, using Cu-Kα radiation without a monochromator.

Structure Determination. Single crystal diffraction data for UC and UH were collected on a MAR345 image plate detector using Mo Kα radiation (λ = 0.71073 Å), generated by a Rigaku Ultra X18S rotating anode (Xenocs fox3d mirrors). For UC the crystal was flash frozen at 150 K in a N_2 flow prior to data collection. Data integration and reduction was performed by CrystAlisPro and the implemented absorption correction was applied. Structure solution was performed by the dual-space algorithm in SHELXT [25] and the structure was further refined against F^2 using SHELXL2014/7. All non-hydrogen atoms were refined anisotropically and hydrogen atoms were placed at calculated positions with temperature factors set at 1.2Ueq of the parent atoms (1.5Ueq for methyl and OH hydrogens). For UE the structure was solved from powder diffraction measured on a STOE STADI P diffractometer using monochromated CuKα1 radiation in transmission mode (with the sample placed between zero scattering foils). Unit cell determination was performed by DICVOL and the structure was solved by DASH [26], the structure was subsequently optimized by Rietveld refinement in Fullprof [27].

TGA. Typically, the TGA analyses of all samples are performed from 30 to 450 °C using a heating rate of 5 °C/min with a continuous nitrogen flow of 50 mL/min, on a Mettler Toledo TGA/SDTA851e.

DSC. DSC measurements are performed on a TA DSC2500. Deposited in an aluminum Tzero pans with punctured hermetic lid, samples were heated from 20 °C up to 240 °C using a heating rate of 2 °C/min under a 50 mL/min continuous nitrogen flow.

Congruence experiments. Stoichiometric amounts of urea and API were added to 1 mL of solvent until dissolution no longer occurred and a suspension was obtained. After that, ground traces of cocrystal material were added to the suspension as seed material. After 3 days of slurrying at room temperature, the suspension was filtered and the solid analyzed by PXRD.

Solubility measurement. The solubility measurement is conducted in ethanol at room temperature. An excess amount of solid is added to 2 mL of ethanol and the suspension is left to slurry for 2 days reaching saturation. After that, the suspension is filtered, and the filtrate weighed and left for evaporation. Weighing the recovered solids, allows determining the amount of solvent as well as solid present in the filtrate, and hence the solubility.

2.4 Results and discussion

2.4.1Cocrystal screening

As our main goal was to show the potential of urea as a pharmaceutical cocrystal former, a screen involving 62 APIs was performed (Table A.1). Seven positive hits were identified in agreement with literature reported success rates of about 10% (Figure 2.1) [28]. From this data, APIs containing a phenol group have a higher likelihood of forming a cocrystal with urea. Four cocrystals were already reported in literature (Figures A.1–A.4) (theophylline, nicotinamide, salicylic acid, and hydroquinone) [29-31]. We report here three new cocrystal systems with catechin, ellagic acid, and 3-hdyroxyl-2-naphthoic acid, which are discussed in detail.

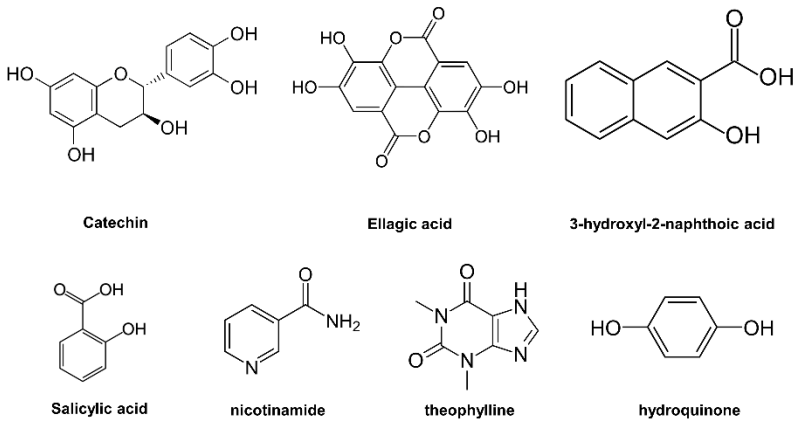

Figure 2.1. Chemical structure of the active pharmaceutical ingredients used in our screen which form cocrystals with urea.

2.4.2 UC

Urea and catechin cocrystallize in the monoclinic $P2_1$ space group (Table 2.1). The unit cell contains two urea and two catechin molecules. As a hydrogen bond acceptor, the oxygen atom of each urea molecule is connected to a N–H group of a second urea molecule and to a phenolic hydroxyl of catechin. Furthermore, all hydroxyl groups are engaged in hydrogen bonds with hydroxyl groups of neighboring catechin molecules (Figure 2.2).

Table 2.1. crystallographic data for the UC and UH cocrystals.

Compound	UC Cocrystal	UH Cocrystal	UE Cocrystal*
Formula	$C_{16}H_{18}N_2O_7$	$C_{12}H_{12}N_2O_4$	$C_{16}H_{14}N_4O_{10}$
$D_{calc.}$**/ g cm^{-3}**	1.544	1.398	1.048
m**/mm^{-1}**	0.123	0.107	0.148
Formula Weight	350.32	248.24	422.31
Colour	brown	colourless	light yellow
Shape	needle	rod	powder
Size/mm^3	0.35 × 0.02 × 0.02	0.30 × 0.10 × 0.05	
T**/K**	150(2)	293(2)	293
Crystal System	monoclinic	monoclinic	Triclinic
Space Group	$P2_1$	$C2/c$	P-1
a**/Å**	10.7771(12)	24.353(2)	11.6585(8)
b**/Å**	5.0024(5)	5.0996(4)	6.8608(2)
c**/Å**	14.960(3)	20.7056(19)	6.1960(3)
α**/°**	90	90	72.901(3)
β**/°**	110.849(17)	113.490(11)	114.356(3)
γ**/°**	90	90	115.482(2)
V/Å^3	753.68(19)	2358.3(4)	403.36(4)
Z	2	8	1
Z'	1	1	0.5
Wavelength/Å	0.71073	0.71073	1.54056
Radiation type	MoK_α	MoK_α	$CuK_{\alpha 1}$
Measured Refl's.	3867	8859	-
Indep't Refl's	2127	2341	557
Refl's I ≥ 2 s(I)	1217	1938	-
R_{int}	0.1191	0.0365	-
GooF	1.026	1.063	-
wR_2 **(all data)**	0.1510	0.1192	-
wR_2	0.1240	0.1125	-
R_1 **(all data)**	0.1472	0.0511	-
R_1	0.0775	0.0421	5.0768

* UE cocrystal was solved from PXRD

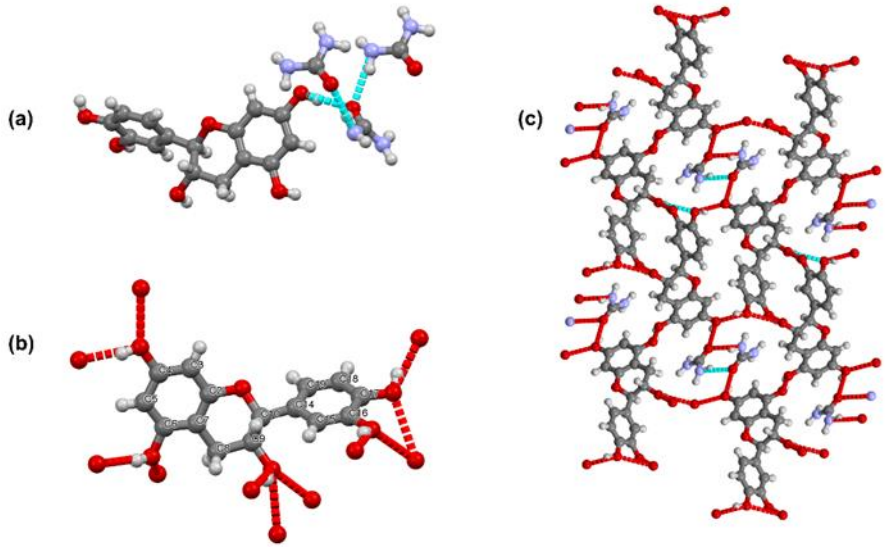

Figure 2.2. (a) Hydrogen bonding around a urea molecule in the UC cocrystal. (b) Hydrogen bonding around a catechin molecule in the cocrystal. (c) View along the a axis.

Figure 2.3 shows a PXRD overlay of the ground and starting materials (catechin is not displayed because the used catechin was amorphous), as well as the pattern simulated from the single crystal structure. As shown in this figure, the ground material matches the one from single crystal analysis, corresponding to the 1:1 cocrystal.

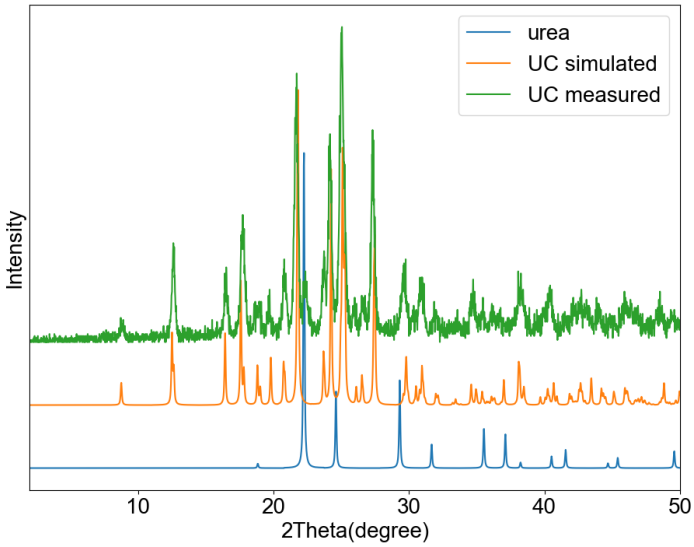

Figure 2.3. PXRD profiles of UC obtained by grinding (green), the simulated pattern of the UC cocrystal (orange), and urea (blue).

Urea shows a single melting point with onset at 134 °C immediately followed by a degradation as illustrated by the TGA analysis, similar to previous report[32]. The UC cocrystal shows a melting temperature of 176 °C with a corresponding heat of fusion of 162.78 J/g (Figure 2.4), which is followed by a degradation endotherm. Comparing the UC and the amorphous catechin material in terms of humidity stability, one notices the UC cocrystal to remain stable at 75% RH at 25 °C for a period of two weeks (Figure A.5), whilst storing the amorphous material, leads to crystalline catechin hydrate under these conditions. Catechin hydrate in turn starts losing water at temperatures above 50 °C (Figure A.6), transforming into the amorphous phase upon dehydration (Figure A.7). Cocrystallization with urea, therefore, leads to a solid form of catechin which is much less moisture or thermo-sensitive.

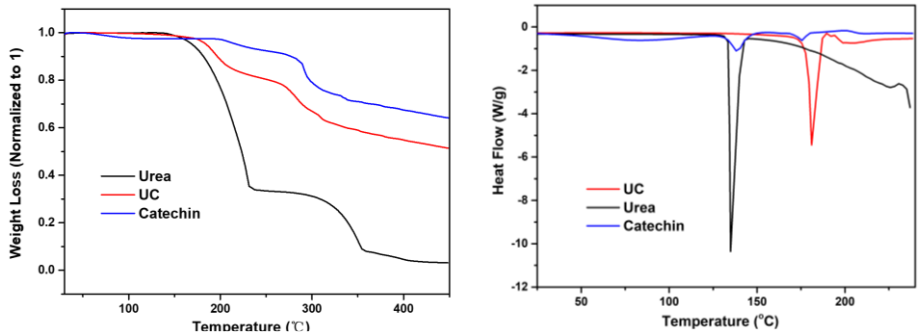

(a) (b)

Figure 2.4. (a) TGA curves of urea, catechin and UC. (b) DSC curves of urea, catechin and UC.

2.3.3 UH

Urea and 3-hydroxyl-2-naphthoic acid crystallize in the monoclinic C2/c space group in a 1:1 ratio. The carboxylic acid of 3-hydroxyl-2naphthoic acid, is connected to the amide group of urea through an amide-acid hetero-synthon. The phenyl hydroxyl forms an intramolecular hydrogen bond, as well as an intermolecular hydrogen bond with urea (Figure 2.5). Other hydrogen bonding patterns involve different urea molecules and are of the C = O–H–N type (Figure 2.5).

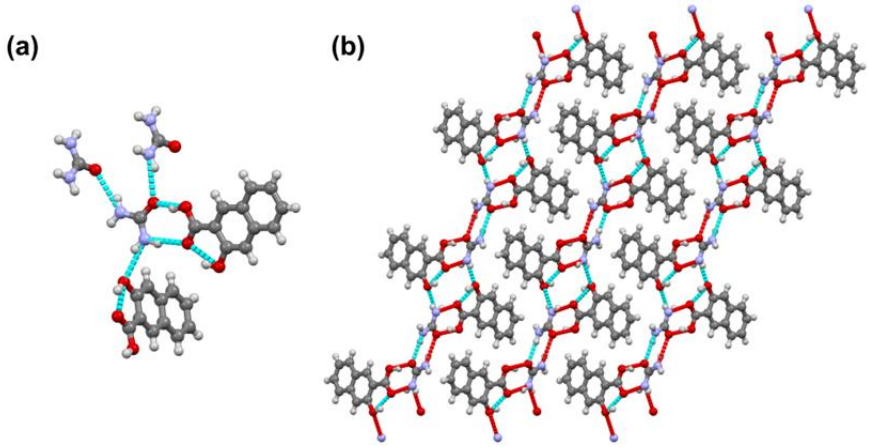

(a) (b)

Figure 2.5. (a) Hydrogen bonds in UH. (b) View of crystal structure of UH along the b axis.

Figure 2.6 shows a PXRD overlay of the ground and starting materials, as well as the simulated pattern from the single crystal data. As shown in this figure, the ground material matches the single crystal phase, corresponding to a 1:1 cocrystal.

Further, 3-hydroxyl-2-naphthoic acid shows a single melting point with onset at 218 °C and an associated 173.3 J/g heat of fusion. The cocrystal in turn shows a single melting temperature at 155 °C with a heat of fusion 156.78 J/g followed by immediate degradation. As common for cocrystals, this melting point lies between that of both parent compounds. TGA confirms degradation upon melting for all phases (Figure 2.7).

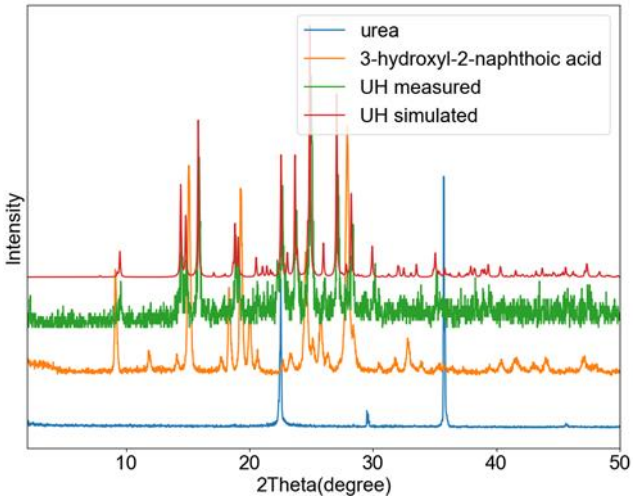

Figure 2.6. PXRD profiles of urea (blue), UH co-crystal obtained by grinding (green), the simulated UH pattern (red) and the experimental 3-hydroxyl-2-naphthoic acid pattern (orange).

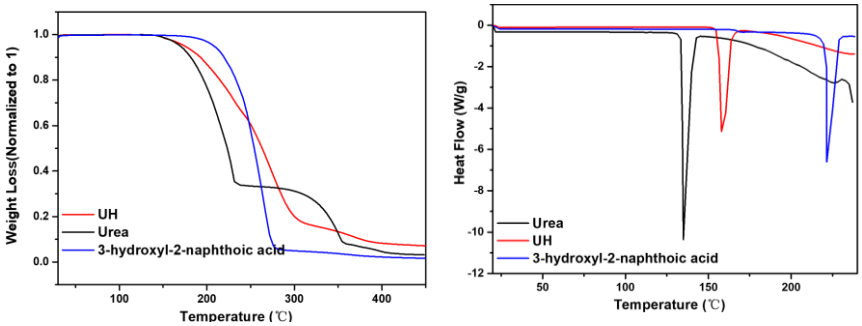

Figure 2.7. (a) TGA curves of urea, catechin and UC. (b) DSC curves of urea, catechin and UC.

2.3.4 UE

The UE cocrystal can be obtained by LAG of two equivalents of urea and one equivalent of ellagic acid using water (Figure 2.8). Grinding a 1:1 ratio, leads to cocrystal material with excess amount of ellagic acid. As attempts at growing a single crystal failed, the structure was resolved from the powder pattern. Urea and ellagic acid cocrystallize in the P-1 space group, with two urea and one ellagic acid molecule in the unit cell (Table 2.1). Ellagic acid is found on a crystallographic inversion center. For ellagic acid, the oxygen atoms in the ester group of ellagic acid serve as hydrogen bond acceptor, connecting to amide groups from urea molecules. On the other hand, the phenolic hydroxyl groups in ellagic acid serve as hydrogen bond donor to the carbonyl oxygen of a urea molecule (Figure 2.9).

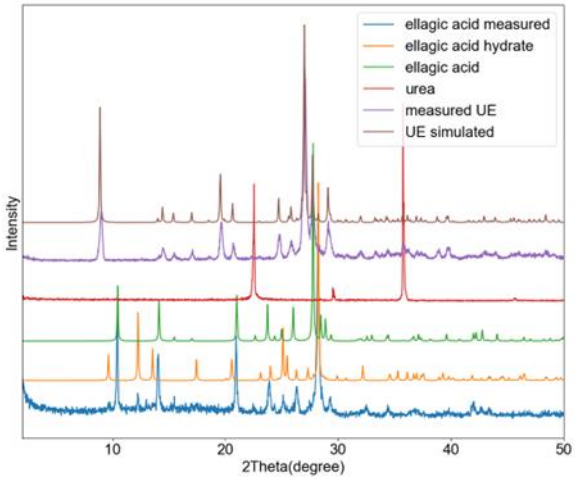

Figure 2.8. PXRD profiles of ellagic acid (blue), simulated ellagic acid hydrate(orange), simulated ellagic acid (green), urea (red), UE co-crystal obtained by grinding (purple), the simulated UH pattern (brown).

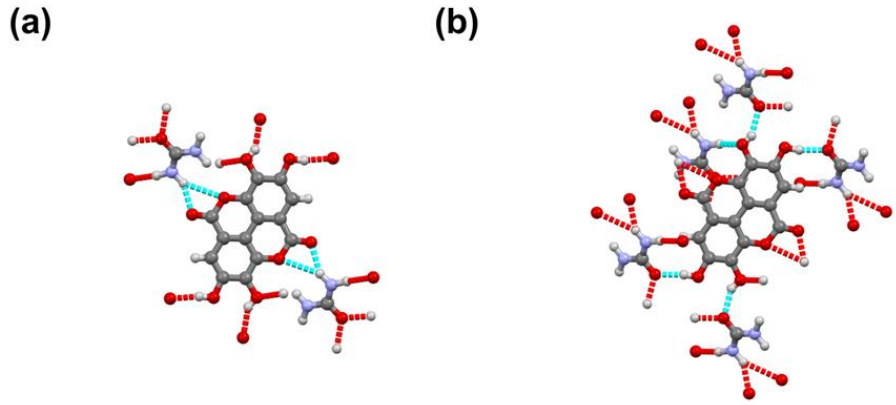

Figure 2.9. (a) Hydrogen bonds in UE between urea amide group and ellagic acid carbonyl group. (b) Hydrogen bonds formed by the phenol group in UE.

Thermal analysis of ellagic acid showed our initial powder to contain a mixture of the hydrate and anhydrate phase as shown in Figure 2.9. TGA of ellagic acid shows a mass loss of 2.5% at 103 °C, suggesting a quarter of ellagic acid used here is under the dihydrate form. DSC confirms this water loss. Ellagic acid has a reported melting temperature of 350 °C[33]. The cocrystal shows a single endotherm peak at 222 °C, corresponding to the melting point of the cocrystal. TGA shows melting to be followed by immediate degradation (Figure 2.10).

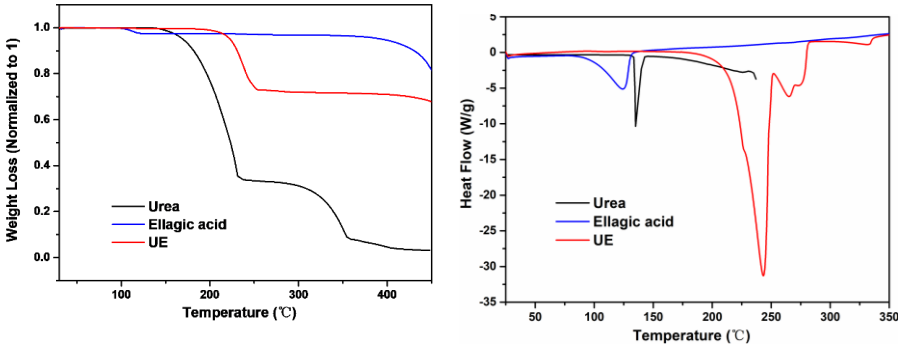

(**a**) (**b**)

Figure 2.10. (a) TGA curves of urea, ellagic acid and UE. (b) DSC curves of urea, ellagic acid and UE.

Solution Behavior

The solution behavior of the novel phases was evaluated in various solvents. Initially, the cocrystals were suspended in a solvent to evaluate their congruency. Congruency implies that stoichiometric amounts of the cocrystal components lead to the cocrystal as the only stable phase in suspension, while non-congruency means that one of the parent compounds crystallizes out (or a mixture of cocrystal and a parent compound). UH behaves congruently in ethanol, acetonitrile, and isopropanol, whereas it is not congruent in water or methanol (Figure A.8), with 3-hydroxyl-2-naphthoic acid crystallizing out. UE behaves congruently in methanol, ethanol, acetonitrile, and iso-propanol. In water, ellagic acid hydrate is obtained (Figure A.9). UC crystalizes congruently in all organic solvents used here and incongruently in water, with catechin hydrate crystallizing out (Figure 2.11). In mixed water/methanol solvents, UC behaves congruently for solvent mixtures of 1:9 to 4:6 water/methanol ratios (Figure A.10). When the water/methanol ratio varies from 5:5 to 6:4, a recently identified catechin methanol solvate-hydrate crystallizes out (catechin: water: methanol 2:2:1) (Figure A.11) [34]. With an even higher water/methanol ratio, a PXRD profile different from any known form is obtained (Figures A.12 and A.13). Drying this phase under ambient conditions yields catechin hydrate, suggesting another solvate of catechin was likely obtained. Slurrying catechin on its own in water/methanol ratios from 7:3 to 9:1, only gives the catechin hydrate, which means urea likely plays a role in the stabilization of the yet unknown catechin solvate (Figure A.14).

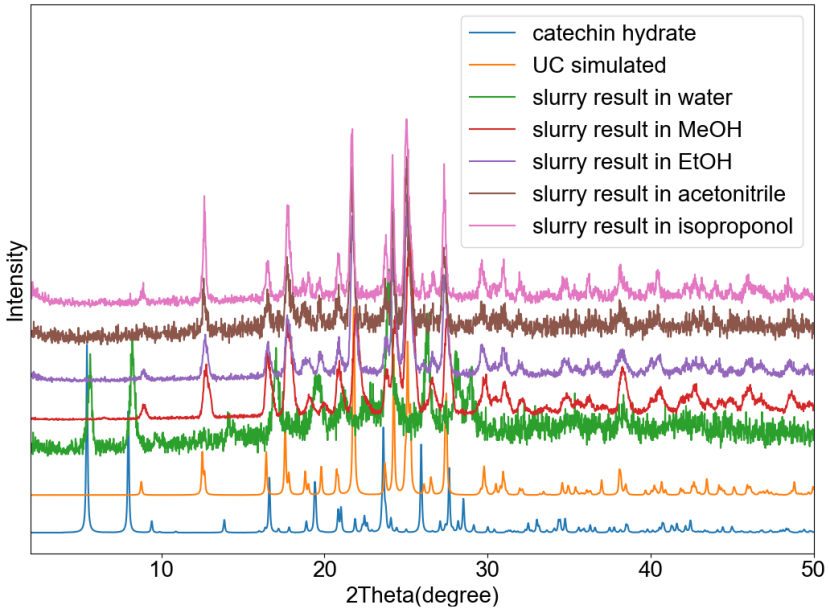

(a)

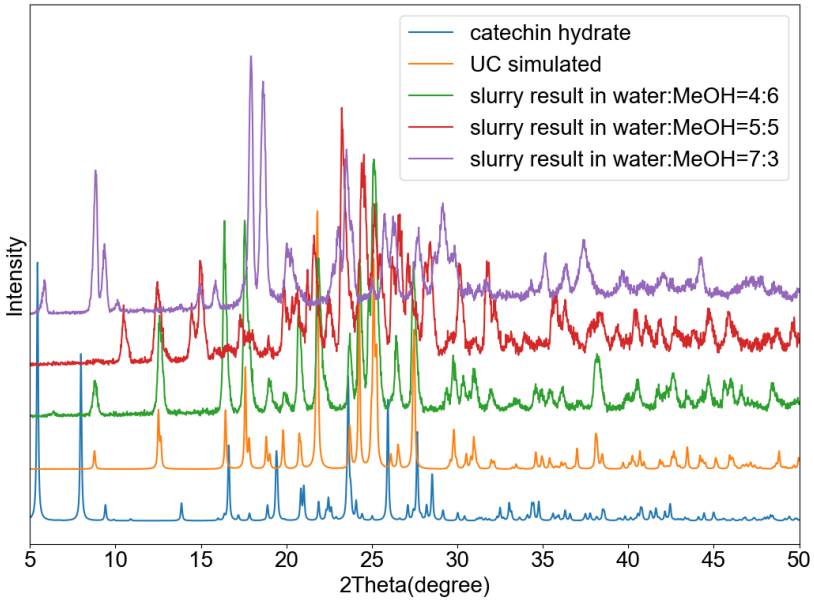

(b)

Figure 2.11. (a) PXRD profiles of congruence experiments results of UC in different solvents. (b) Various products obtained using different methanol/water ratio when suspending stoichiometric ratio of urea and catechin.

As all three new cocrystals behave congruently in ethanol, solubility measurements were conducted in this solvent. For UC and UH cocrystal, a solubility of 0.595 mol/L and 0.439 mol/L is obtained, which is lower than that of the parent compound (0.736 mol/L and 0.599 mol/L respectively). For ellagic acid, the behavior is inverted, with the solubility being raised from 0.52 mmol/L to 9.04 mmol/L, showing the potential of cocrystallization to strongly impact the solubility behavior of poorly soluble drugs. Solubility of a cocrystal depends on the free energy of the novel cocrystal as well as the solution free energy of dissolved compounds and their solution interaction. Predicting this solubility merely on the structure is not feasible. The increase in solubility for ellagic acid is not surprising as the solubility of ellagic acid is extremely low. Very likely a variation of free energy of the solid structure as well as a positive interaction between both components in solution needs to be taken into account.

2.4 Conclusion

In this work, three novel cocrystals involving urea were identified, targeting catechin, ellagic acid, and 3-hydroxyl-2-naphthoic acid. Urea is a GRAS compound that is a promising coformer with a potential strong impact on the solubility of the target compound, as shown here for a 18-fold solubility increase for ellagic acid. Furthermore, we showed how the stability of the target compounds can be impacted and improved upon by cocrystallization with urea.

References

(1) Sun, C. C. Cocrystallization for successful drug delivery. *Expert Opin Drug Deliv* **2013**, *10* (2), 201-213.

(2) Kuminek, G.; Cao, F.; Bahia de Oliveira da Rocha, A.; Goncalves Cardoso, S.; Rodriguez-Hornedo, N. Cocrystals to facilitate delivery of poorly soluble compounds beyond-rule-of-5. *Adv Drug Deliv Rev* **2016**, *101*, 143-166.

(3) Bolla, G.; Nangia, A. Pharmaceutical cocrystals: walking the talk. *Chem Commun (Camb)* **2016**, *52* (54), 8342-8360.

(4) Karimi-Jafari, M.; Padrela, L.; Walker, G. M.; Croker, D. M. Creating Cocrystals: A Review of Pharmaceutical Cocrystal Preparation Routes and Applications. *Crystal Growth & Design* **2018**, *18* (10), 6370-6387.

(5) Aitipamula, S.; Banerjee, R.; Bansal, A. K.; Biradha, K.; Cheney, M. L.; Choudhury, A. R.; Desiraju, G. R.; Dikundwar, A. G.; Dubey, R.; Duggirala, N.; et al. Polymorphs, Salts, and Cocrystals: What's in a Name? *Crystal Growth & Design* **2012**, *12* (5), 2147-2152.

(6) Kavanagh, O. N.; Croker, D. M.; Walker, G. M.; Zaworotko, M. J. Pharmaceutical cocrystals: from serendipity to design to application. *Drug Discov Today* **2019**, *24* (3), 796-804.

(7) Piaggi, P. M.; Parrinello, M. Predicting polymorphism in molecular crystals using orientational entropy. *Proc Natl Acad Sci U S A* **2018**, *115* (41), 10251-10256.

(8) Safari, F.; Tkacz, M.; Katrusiak, A. High-Pressure Sorption of Hydrogen in Urea. *J Phys Chem C Nanomater Interfaces* **2021**, *125* (14), 7756-7762.

(9) Good, D. J.; Rodríguez-Hornedo, N. Solubility Advantage of Pharmaceutical Cocrystals. *Crystal Growth & Design* **2009**, *9* (5), 2252-2264.

(10) Machado, T. C.; Kuminek, G.; Cardoso, S. G.; Rodriguez-Hornedo, N. The role of pH and dose/solubility ratio on cocrystal dissolution, drug supersaturation and precipitation. *Eur J Pharm Sci* **2020**, *152*, 105422.

(11) Desiraju, G. R. Supramolecular Synthons in Crystal Engineering—A New Organic Synthesis. *Angewandte Chemie International Edition in English* **1995**, *34* (21), 2311-2327.

(12) Gunawardana, C. A.; Aakeroy, C. B. Co-crystal synthesis: fact, fancy, and great expectations. *Chem Commun (Camb)* **2018**, *54* (100), 14047-14060.

(13) Allu, S.; Bolla, G.; Tothadi, S.; Nangia, A. K. Novel Pharmaceutical Cocrystals and Salts of Bumetanide. *Crystal Growth & Design* **2019**, *20* (2), 793-803.

(14) Li, Z.; Li, M.; Peng, B.; Zhu, B.; Wang, J.-r.; Mei, X. Improving Compliance and Decreasing Drug Accumulation of Diethylstilbestrol through Cocrystallization. *Crystal Growth & Design* **2019**, *19* (3), 1942-1953.

(15) Maddileti, D.; Jayabun, S. K.; Nangia, A. Soluble Cocrystals of the Xanthine Oxidase Inhibitor Febuxostat. *Crystal Growth & Design* **2013**, *13* (7), 3188-3196.

(16) Sanphui, P.; Kumar, S. S.; Nangia, A. Pharmaceutical Cocrystals of Niclosamide. *Crystal Growth & Design* **2012**, *12* (9), 4588-4599.

(17) Yan, Y.; Chen, J.-M.; Geng, N.; Lu, T.-B. Improving the Solubility of Agomelatine via Cocrystals. *Crystal Growth & Design* **2012**, *12* (5), 2226-2233.

(18) Ceci, C.; Graziani, G.; Faraoni, I.; Cacciotti, I. Strategies to improve ellagic acid bioavailability: from natural or semisynthetic derivatives to nanotechnological approaches based on innovative carriers. *Nanotechnology* **2020**, *31* (38), 382001.

(19) Priyadarsini, K. I.; Khopde, S. M.; Kumar, S. S.; Mohan, H. Free radical studies of ellagic acid, a natural phenolic antioxidant. *J Agric Food Chem* **2002**, *50* (7), 2200-2206.

(20) Park, S. M.; Choi, J.; Nam, T. G.; Ku, J. M.; Jeong, K. Anti-diabetic effect of 3-hydroxy-2-naphthoic acid, an endoplasmic reticulum stress-reducing chemical chaperone. *Eur J Pharmacol* **2016**, *779*, 157-167.

(21) Chen, Z.; Zhu, Q. Y.; Tsang, D.; Huang, Y. Degradation of green tea catechins in tea drinks. *J Agric Food Chem* **2001**, *49* (1), 477-482.

(22) de Araujo, F. F.; de Paulo Farias, D.; Neri-Numa, I. A.; Pastore, G. M. Polyphenols and their applications: An approach in food chemistry and innovation potential. *Food Chem* **2021**, *338*, 127535.

(23) Li, N.; Taylor, L. S.; Ferruzzi, M. G.; Mauer, L. J. Kinetic study of catechin stability: effects of pH, concentration, and temperature. *J Agric Food Chem* **2012**, *60* (51), 12531-12539.

(24) Labbé, D.; Têtu, B.; Trudel, D.; Bazinet, L. Catechin stability of EGC- and EGCG-enriched tea drinks produced by a two-step extraction procedure. *Food Chemistry* **2008**, *111* (1), 139-143.

(25) Sheldrick, G. M. Crystal structure refinement with SHELXL. *Acta Crystallogr C Struct Chem* **2015**, *71* (Pt 1), 3-8.

(26) Boultif, A.; Louër, D. Powder pattern indexing with the dichotomy method. *Journal of Applied Crystallography* **2004**, *37* (5), 724-731.

(27) Rodríguez-Carvajal, J. Recent advances in magnetic structure determination by neutron powder diffraction. *Physica B: Condensed Matter* **1993**, *192* (1-2), 55-69.

(28) Buol, X.; Robeyns, K.; Caro Garrido, C.; Tumanov, N.; Collard, L.; Wouters, J.; Leyssens, T. Improving Nefiracetam Dissolution and Solubility Behavior Using a Cocrystallization Approach. *Pharmaceutics* **2020**, *12* (7).

(29) Mahmoud, M. M.; Wallwork, S. C. The crystal structure of the 1:1 complex between quinol and urea. *Acta Crystallographica Section B Structural Crystallography and Crystal Chemistry* **1975**, *31* (2), 338-342.

(30) Wiedenfeld, H.; Knoch, F. Zur Kristallstruktur des Theophyllin-Harnstoff-Komplexes. *Archiv der Pharmazie* **1986**, *319* (7), 654-659.

(31) Preut, H.; Haupt, H. J. Packing analyses on organometallic compounds. *Acta Crystallographica Section A Foundations of Crystallography* **1981**, *37* (a1), C93-C93.

(32) Mazzei, L.; Broll, V.; Casali, L.; Silva, M.; Braga, D.; Grepioni, F.; Baltrusaitis, J.; Ciurli, S. Multifunctional Urea Cocrystal with Combined Ureolysis and Nitrification Inhibiting Capabilities for Enhanced Nitrogen Management. *ACS Sustainable Chemistry & Engineering* **2019**, *7* (15), 13369-13378.

(33) Sepúlveda, L.; Ascacio, A.; Rodríguez-Herrera, R.; Aguilera-Carbó, A.; Aguilar, C. N. Ellagic acid: Biological properties and biotechnological development for production processes. *African Journal of Biotechnology* **2011**, *10* (22), 4518-4523.

(34) Dudek, M. K.; Paluch, P.; Śniechowska, J.; Nartowski, K. P.; Day, G. M.; Potrzebowski, M. J. Crystal structure determination of an elusive methanol solvate – hydrate of catechin using crystal structure prediction and NMR crystallography. *CrystEngComm* **2020**, *22* (30), 4969-4981.

Chapter 3

3 Designing crystals through complexation

This chapter is based on two articles:

(1) **Leng F**, Robeyns K, Leyssens T, et al. Combining Racetams with a Sweetener through Complexation[J]. *Crystal Growth & Design*, **2022**, 22(5): 3016-3023.

(2) **Leng F**, Shemchuk O, Robeyns K, et al. Complexation: An Interesting Pathway for Combining Two APIs at the Solid State[J]. *Pharmaceutics*, **2022**, 14(9): 1960.

The failure of our ternary cocrystal strategy forced us to seek a new methodology for molecular combination. We proposed another methodology, complexation, which met great success in both taste masking and drug combination. In the first part of this chapter, we were able to couple a series of racetam drugs to the sweetener by transforming saccharin to its zinc salt. Similarly, in the second part of this chapter, a series of carboxylic acid containing drugs were also transformed to their zinc salt form and further combined with a series of pyridine containing drugs in high success rate.

3.1 Combining racetams with a sweetener through complexation

3.1.1 Abstract:

Combining APIs with sweeteners through crystal engineering is an attractive way to mask the bitter taste of drugs. However, traditional methods like salt or cocrystal formation still suffer some major limitations. Herein, racetams, a series of normally bitter drugs, cannot be combined with the popular sweetener saccharin through either salt or cocrystal formation. We here, however, show how these compounds can be combined, when zinc saccharinate is used rather than saccharin. The obtained complexes can either be identified starting from a binary target API/Zn saccharinate or a ternary API/ZnO/saccharin combination. This work opens novel pathways to couple two compounds of interest through a crystal engineering approach.

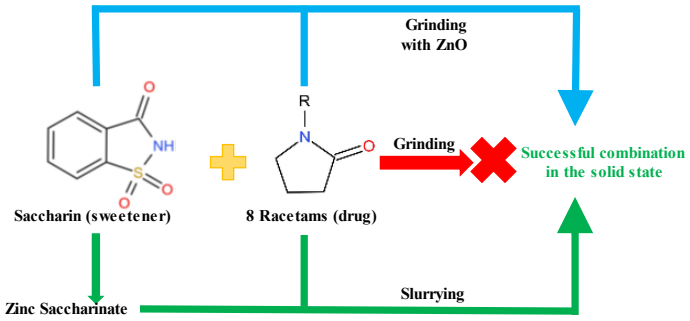

Conceptualization, F.L. and T.L.; methodology, F.L. and T.L.; software, F.L. and K.R.; validation, T.L., K.R. and F.L.; formal analysis, F.L.; investigation, F.L.; data curation, F.L.; writing—original draft preparation, F.L.; writing—review and editing, T.L. and K.R.; supervision, T.L. and K.R.; project administration, T.L.; funding acquisition, T.L.

3.1.2 Introduction

Racetams are a series of APIs that impact the central nervous system.[1-4] Their unpleasant taste still forms a hurdle in the development of their oral dosage form.[5, 6] For example, Levetiracetam, marketed as Keppra®, is used for the treatment of epilepsy.[7] Its intensively bitter taste usually leads to poor patient compliance, especially with children.[8, 9] Similarly, Piracetam which has been marketed and used for the treatment of memory and balance problems, [10] met the refusal of patients in clinical trials because of its bitter taste.[6]

Combining suitable sweeteners with racetams through crystal engineering is an attractive way to overcome such problems as they mask the bad taste of drug molecules but do not change their original chemical structure.[11-14] For drugs containing basic groups like quinine, venlafaxine, haloperidol, stanozolol, lamivudine, triamterene or mirtazapine, the acidic sweetener saccharin can easily be combined in the same solid form through the formation of salts.[15-19] For unionizable drugs, previous works have proven the possibility of combining sweeteners through cocrystallization.[20, 21] For example, oxcarbazepine, spironolactone and carbamazepine were cocrystallized with saccharin, a sweetener widely used in the pharmaceutical and food industry[22, 23] with obtained solids showing improved solubility.[24-26] Albeit elegant, cocrystallization suffers from a low success rate in identifying suitable coformers.[27-29]

In this study, we introduce an innovative approach showing how saccharin can be successfully combined at the solid state with unionizable drug compounds for which no molecular cocrystals between drug and saccharin exist. Inspired by ionic cocrystallization,[30] we show how zinc saccharinate can be successfully combined with 6 racetams (Figure 3.1.1), which do not form a molecular cocrystal with saccharin. We, furthermore, highlight an efficient three-component grinding strategy to the identification of these complexes, which often show increased thermal stability with respect to the parent drug compound. The approach used in this work, not only shows a novel way to combine sweeteners with drugs, but also opens a new perspective on how two target compounds can be combined at the solid state.

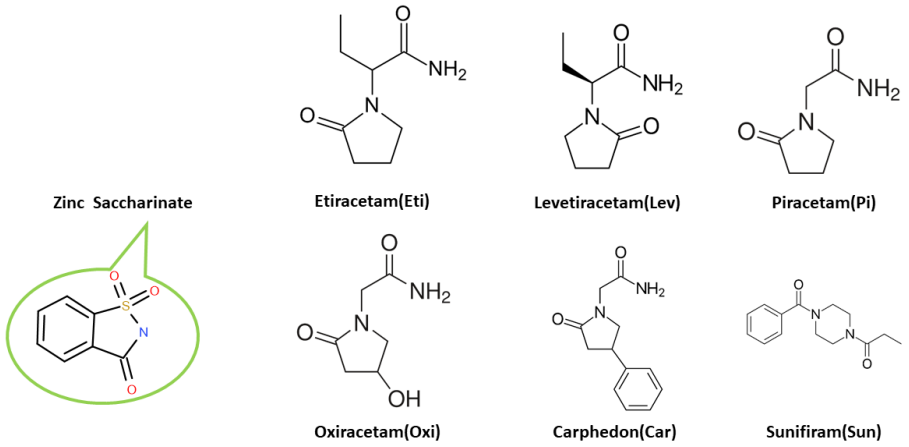

Figure 3.1.1 Zinc saccharinate and racetams used.

3.1.3 Experimental section

Materials. Racetams, including levetiracetam; piracetam; oxiracetam; sunifiram and carphedon, were bought from Xiamen Top Health Biochem Tech. Co., Ltd. Etiracetam is the racemate of levetiracetam, obtained from this latter following a literature based procedure.[31] Saccharin was purchased from Alfa Aesar. Zinc acetate was bought from Carlroth. Zinc oxide was bought from Merck. All the solvents and reagents were used as received without further treatment.

Preparation of zinc saccharinate hexahydrate [$ZnSac_2(H_2O)_4$]·$2H_2O$. [$ZnSac_2(H_2O)_4$]·$2H_2O$ (zinc saccharinate hereafter, Figure B.1) was obtained by slurrying saccharin and zinc acetate in a 2:1 ratio in water at room temperature for 2 days. After that, the suspension was filtered, the filtered cake collected and dried under ambient conditions.

Three-component grinding for screening. Generally, 0.5 mmol saccharin, 0.25 mmol ZnO, 0.25 mmol racetam, and 2-3 stainless metal balls (Ø 3 mm) were added to a plastic Eppendorf tube. After adding 40 µL of solvent (methanol, ethanol, isopropanol, acetonitrile, or water), the samples were ground in a RETSCH Mixer Mill MM 400 with a beating frequency of 30Hz for 90 minutes. The PXRD profiles of the resulting powders were compared to the parent compounds as well as the different zinc saccharinate solvates.

Two-component grinding for screening. For levetiracetam, two component grinding is performed starting directly from zinc saccharinate. 0.1 mmol of zinc

saccharinate, 0.1mmol of levetiracetam and 3 stainless-steel balls were added to an plastic Eppendorf tube. After adding 20 μL of solvent (methanol, ethanol, isopropanol, acetonitrile, or water), samples were ground using a RETSCH Mixer Mill MM 400 with a beating frequency of 30Hz for 90 minutes. The PXRD profiles were compared to those of the parent compounds as well as all zinc saccharinate solvates (Table B.1).

Single crystal growth.

$ZnSac_2Lev$, $ZnSac_2Eti_2$, $[ZnSac_2Pi]•CH_3CN$, $[ZnSac_2Oxi]•CH_3CN$, $[ZnSac_2Sun]•CH_3CN$ were obtained following a similar procedure: to 0.1 mmol of zinc saccharinate and the corresponding racetams, 1 mL of acetonitrile was added and the solution was heated to 80 °C. Afterwards, seeds of the respective complexes obtained from grinding were added to the solution, the glass vial was sealed and left to cool down slowly overnight.

$[ZnSac_2(H_2O)_2]•Car•EtOH•H_2O$ and $Zn_3Sac_6Pi_2(H_2O)_4$ were obtained following procedure 2.4.1, apart from using a water-ethanol mixture (0.05:0.95 in volume) instead of acetonitrile.

$[ZnSac_2Lev(H_2O)]•EtOH$. To a physical mixture of 0.1 mmol zinc saccharinate and 0.4 mmol levetiracetam, ethanol was added dropwise until all solid dissolved. Single crystals of $[ZnSac_2Lev(H_2O)]•EtOH$ were obtained after leaving the solution to partially evaporate after one day.

$[ZnSac_2Lev(H_2O)]•CH_3CN$. 0.1 mmol of zinc saccharinate was dissolved in 1 mL of acetonitrile by heating. The obtained solution was mixed with an equimolar quantity of levetiracetam dissolved in 1 mL of acetonitrile at RT. The solution was kept at 9 °C and single crystals suitable for structure determination were collected after 24 hours.

$ZnSac_2Car$. 0.1 mmol of zinc saccharinate and 0.1 mmol of carphedon were stirred in 2 mL of ethanol for 2 hours. Afterwards, the solution was heated to 85 °C. At this temperature, ethanol was added dropwise until all solids dissolved. Seeds, obtained from grinding experiments, were added to the solution. The glass vial was sealed and left to cool down slowly overnight, after which single crystals were harvested.

PXRD and VT-PXRD. Powder X-ray diffraction of all samples were conducted on a Siemens D5000 diffractometer equipped with a Cu X-ray source operating at 40 kV and 40 mA (λ = 1.5418 Å) at a scanning range of 2θ values from 5° to 50° at a scan rate of 0.6° min^{-1}. VT-PXRD profiles were collected on a PANalytical X'Pert PRO automated diffractometer at a scanning range of 2θ values from 3° to 40°, equipped

with an X'Celerator detector and an Anton Paar TTK 450 system for measurements at controlled temperature. Data were collected in the open air in Bragg-Brentano geometry, using Cu-Kα radiation without a monochromator.

SCXRD. Data were collected on a MAR345 image plate detector using Mo Kα radiation (λ = 0.71073 Å), generated by an Incoatec IμS microfocus source. Data integration and reduction was performed by CrystAlis^{PRO} and the implemented absorption correction was applied. Structure solution was performed by the dual-space algorithm in SHELXT and the structure was further refined against F^2 using SHELXL.[32] All non-hydrogen atoms were refined anisotropically and hydrogen atoms were placed at calculated positions with temperature factors set at 1.2Ueq of the parent atoms (1.5Ueq for methyl and OH hydrogens).

TGA. TGA analyses of all samples were performed from 30 °C to 500°C using a heating rate of 10°C/min with a continuous nitrogen flow of 50 mL/min, on a Mettler Toledo TGA/SDTA851e.

DSC. DSC measurements were performed on a TA DSC2500. Deposited in aluminum Tzero pans with punctured lid, samples were heated from 20 °C up to 350 °C using a heating rate of 10 °C/min under a 50 mL/min continuous nitrogen flow.

3.1.4 Results and discussion

The unexplored potential of using complexation to bind a drug and a sweetener.

Due to the lack of ionizable groups in all investigated racetams (Figure 3.1.1), combining them with saccharin through salt formation is not possible. On top, all attempts to directly cocrystallize saccharin with these racetams were unsuccessful. This failure in cocrystallization can be explained by the fact that the intermolecular interactions in the expected cocrystals are of the same type as those in the starting compounds (hydrogen bonding, *π-π* interactions, …) but overall less favorable for the potential cocrystal compared to the starting compounds. Aiming for a stronger stabilization of the resulting crystalline solid, we focused on inducing stronger interactions. Recently, ionic cocrystals have emerged showing stronger interaction between the metal center and the organic compounds, resulting often in a higher success rate to cocrystal formation.[31, 33-35] Unlike molecular cocrystals, the dominating force that combines different compounds together is not hydrogen bonding or π–π stacking, but rather coordination and electrostatic interactions, which are much

stronger. [30] Considering zinc is pharmaceutically acceptable and its inorganic salt was shown to cocrystallize with different racetams,[28, 36] we took an innovative approach, converting saccharin to zinc saccharinate and using this latter to form complexes combining both saccharin as well as the target API.

Mechanochemical strategies.

Previous contributions in metallopharmaceuticals have shown the effectiveness of mechanochemistry in finding metal complexes.[37, 38] In our case, saccharin shows a pKa of 1.6 and easily deprotonates.[27] The most obvious method here would be to convert saccharin to the zinc saccharinate salt. This salt can then be ground with the API, to screen for complex formation (two-component grinding). Although successful, the supplementary synthetic step of synthesizing the zinc saccharinate salt makes this procedure lengthily and time-consuming. However, as LAG has already proven capable of promoting the reaction between metal oxides and organic acids in a one-step synthesis of multiple ligand complexes,[39-41] a similar approach proofed successful here. The combination of saccharin, zinc oxide and API in a single-step grinding approach yielded the desired complexes (three-component grinding).

To evaluate the usefulness of both grinding approach, a series of two- and three-component grinding experiments were performed for the mechanochemical coupling of levetiracetam, zinc, and saccharin. This highlighted the importance of the solvent used during the grinding experiments. In all cases, neat grinding failed to yield the desired complexes: the mixture of starting materials was observed for both two- and three-component grinding experiments even after 90 minutes of milling. A similar observation was made by Chow. et al. working on magnesium oxide (Figure B.2-B.3).[41]

LAG using water also did not lead to successful transformation for the two- as well as the three-component grinding experiments. In both cases, a mixture of the zinc saccharinate hexahydrate and levetiracetam was obtained (Figure B.4). This can be explained as the stability of zinc saccharinate hexahydrate is directly related to the water activity (eq. 1). whereas high water activity led to the formation of levetiracetam physically mixed with the zinc saccharinate hexahydrate. Water assisted LAG can be assimilated to high water activity under which the equilibrium is completely shifted to the hexahydrate phase.

$$[ZnSac_2(H_2O)_4]\bullet 2H_2O_{solid} + Lev_{solid} \rightleftharpoons ZnSac_2Lev_{solid} + 6\ H_2O_{liquid} \quad \text{(eq. 1)}$$

LAG using organic solvents (Figure B.5), leads to a reduced overall water activity, pulling the reaction towards the formation of the various desired complex. As the use of two equivalents of saccharin and one equivalent of ZnO during the three-component grinding only introduces one equivalent of water,(the only water introduced in the reaction is the byproduct of two saccharin and one zinc oxide) versus the 6 equivalents introduced when performing the two-component grinding using zinc saccharinate hexahydrate, the transformation is more advanced, as shown by the weaker peaks from zinc saccharinate residue in the three-components grinding experiments compared to two-components grinding experiments.(Figure B.6-B.8). Furthermore, to our surprise, different patterns appeared when using methanol, ethanol and acetonitrile, which were shown to correspond to unsolvated form $ZnSac_2Lev$ and the solvated form of the complex containing one molecule of water, and one molecule of solvent ($ZnSac_2Lev(H_2O)$•EtOH and $ZnSac_2Lev(H_2O)$•CH_3CN respectively) (Table B.2, Figure B.9-B.11). This result shows the importance of the solvent used during LAG, and highlights the crucial role of the water activity when hydrates are involved in the transformation process.

Based on the results above the three-component LAG using organic solvents was opted as the principal approach for the coupling of the other racetams to saccharin.

Saccharinate-Zn-racetam complexes

The coupling of zinc saccharinate and racetams at the solid state, was successfully achieved for six racetams studied here, through three-components grinding. This is in strong contrast to the direct coupling attempts between saccharin and racetams, which all failed (B.6-B.8, B.12-B.19).

To gain structural insight, into how racetams couple to zinc saccharinate a series of single crystals were grown. Interestingly, all crystals were easily crystalized from solution without experiencing annoying oil product formation. Considering most racetams share common structural motifs one could reasonably expect some likeness in the crystal structures of the obtained complexes. In most complexes, zinc shows a tetrahedral coordination involving the nitrogen atoms of two saccharinate anions and two oxygen atoms of respectively a pyrrolidone and amide group of two different racetam molecules (Figure 2). As for each racetam molecule the pyrrolidone and amide group link to two different zinc atoms, an infinite 1D chain structure or 0D complex is formed. This coordination mode is observed in $ZnSac_2Lev$, $ZnSac_2Car$, [$ZnSac_2Pi$]•CH_3CN, [$ZnSac_2Oxi$]•CH_3CN, and [$ZnSac_2Sun$]•CH_3CN complexes. $ZnSac_2Lev$ is shown here while the other complexes shown in the supporting

information (Figure 3.1.2, Figure 3.1.3a, B.20-B.24, Tables B.2-B.4).

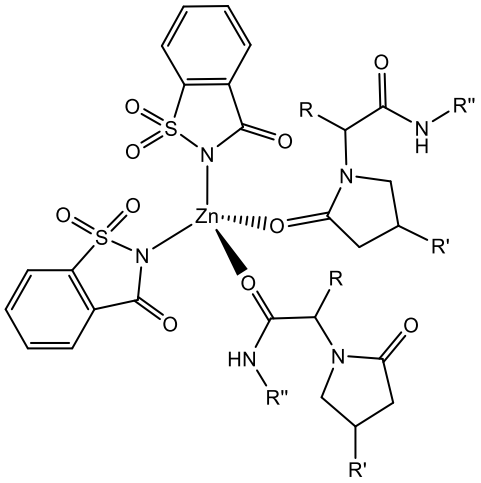

Figure 3.1.2. The most common coordination environment around Zn^{2+} in the obtained complexes.

$ZnSac_2Lev$, $ZnSac_2Eti_2$, **[**$ZnSac_2Lev(H_2O)$]•EtOH, [$ZnSac_2Lev(H_2O)$]•CH_3CN, $Zn_3Sac_6Pi_2(H_2O)_4$ and [$ZnSac_2$ $(H_2O)_2$]•Car•EtOH•H_2O show different coordination mode around the zinc cation, which is why these structures are discussed in more detail , keeping in mind the tetrahedral coordination mentioned above is most frequent.

Upon attempting to obtain single crystals of the complexes, four new solvates of zinc saccharinate were discovered and structurally characterized: [$Zn(Sac)_2(MeOH)_2$], [$Zn(Sac)_2(EtOH)_2$] [$Zn(Sac)_2$(Isopropanol)(H_2O)], [$ZnSac_2(CH_3CN)(H_2O)$] (Table S1).

Complexation with levetiracetam

Three different solid forms involving complexation of zinc saccharinate with levetiracetam were identified in this work. $ZnSac_2Lev$, **[**$ZnSac_2Lev(H_2O)$]•EtOH and [$ZnSac_2Lev(H_2O)$]•CH_3CN (Figure B.5-B.8) were accessed mechanochemically, and single crystals of these phases were identified.

$ZnSac_2Lev$. $ZnSac_2Lev$ adopts a tetrahedral coordination leading to the 1D coordination mode mentioned above, in which every two adjacent zinc atoms are bridged by one levetiracetam molecule (Figure 3.1.3). $ZnSac_2Lev$ can be obtained through three-component LAG using methanol or isopropanol or by slurrying zinc saccharinate and levetiracetam in isopropanol in 1:1.2 ratio (Figure B.9, and B.25).

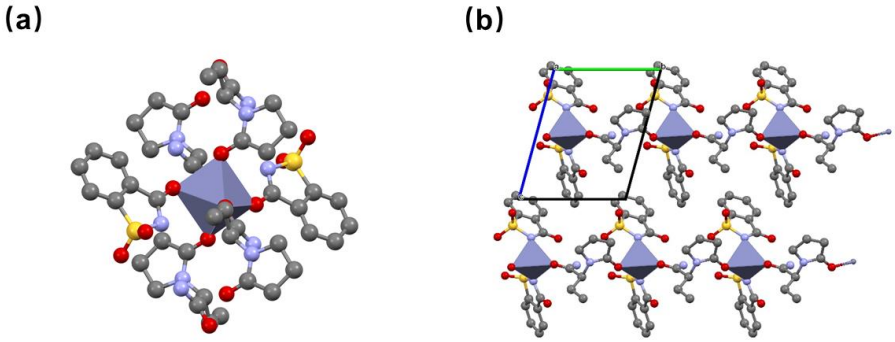

Figure 3.1.3. (a) The coordination environment of Zn^{2+} in $ZnSac_2Lev$. (b) Crystal packing of $ZnSac_2Lev$, view along crystallographic *a*-axis. Hydrogen atoms are omitted for clarity.

In addition, $ZnSac_2Lev$ shows considerable thermal stability compared to levetiracetam (levetiracetam shows a melting point of 116 °C). In its TGA curve, the rapid mass decline starts from 220 °C, corresponding to the single endothermic peak at 243 °C in the DSC thermogram, demonstrating the melting and further decomposition of the complex (Figure 3.1.4).

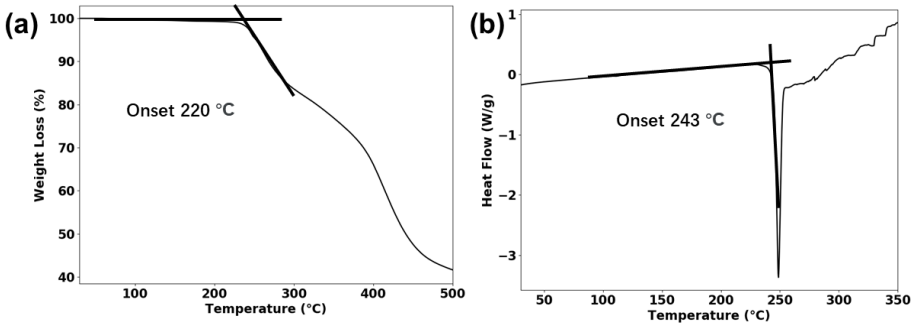

Figure 3.1.4. (a) TGA curve of $ZnSac_2Lev$. (b) DSC curve of $ZnSac_2Lev$.

$[ZnSac_2Lev(H_2O)]\bullet CH_3CN$ and **$[ZnSac_2Lev(H_2O)]\bullet EtOH$.** Both solvated complexes share a similar coordination sphere around the zinc cation (Figure 3.1.5a). Once again, zinc accepts a tetrahedral coordination formed by two nitrogen atoms from saccharinate and two oxygen atoms. However, while in $ZnSac_2Lev$ both oxygens of levetiracetam are involved in the complexation to Zn^{2+}, resulting in the infinite 1D chain formation, in the solvated complexes only the oxygen of pyrrolidone is bound

to the cation, resulting in 0D complexes. In both solvates a water molecule coordinates to the cation instead of the oxygen of the amide group. This latter interacts with adjacent molecules via $OH_{water}\cdots O_{amide}$ and $NH_{amide}\cdots O_{SO}$ hydrogen bonds (Figure 3.1.5b, Figure B.24). Thus, $[ZnSac_2Lev(H_2O)]\bullet CH_3CN$ and $[ZnSac_2Lev(H_2O)]\bullet$EtOH can be considered as acetonitrile and ethanol solvates of $ZnSac_2Lev(H_2O)$ respectively (Figure 3.1.5, Figure B.24). Both complexes can be obtained in bulk using three-component acetonitrile or ethanol LAG or alternatively slurrying a stoichiometric ratio of zinc saccharinate and levetiracetam in acetonitrile or ethanol (Figure B.10, B.11, B.26, B.27).

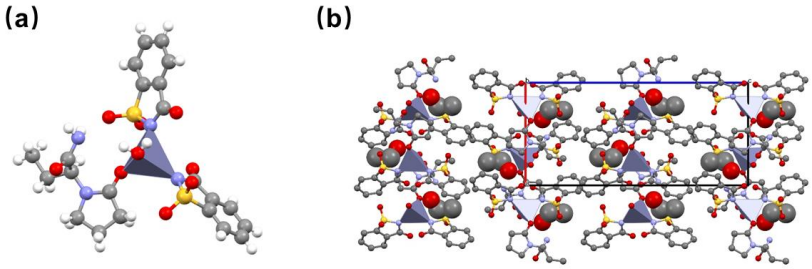

Figure 3.1.5. (a) The coordination environment of zinc in $[ZnSac_2Lev(H_2O)]\bullet$EtOH. (b) Crystal packing of $[ZnSac_2Lev(H_2O)]\bullet$EtOH view along crystallographic *a*-axis. Hydrogen atoms are omitted for clarity.

Thermal analysis of $[ZnSac_2Lev(H_2O)]\bullet CH_3CN$ shows an 8% weight loss starting from 75 °C which can be attributed to the loss of acetonitrile and water (theoretical weight loss = 7.8%). This endothermic event is also visible in the DSC thermogram (Figure. 3.1.6). After the weight loss, a single endothermal peak is presented in 241 °C, which is almost the same with the melting point of $ZnSac_2Lev$ (243 °C). VT-PXRD shows the solvent loss to lead to the unsolvated $ZnSac_2Lev$ complex (Figure B.28) $[ZnSac_2Lev(H_2O)]\bullet$EtOH shows similar thermal behavior The 8.44% weight loss start from about 69 °C, which is corresponding to the first endothermal peak on its DSC curve start from about 65 °C. Similarly, after the loss of solvent, $[ZnSac_2Lev(H_2O)]\bullet$EtOH is transformed to $ZnSac_2Lev$ and further melt at about 236 °C, similar to the measured melting point of $ZnSac_2Lev$ (243 °C).(Figures B.29-B.31)

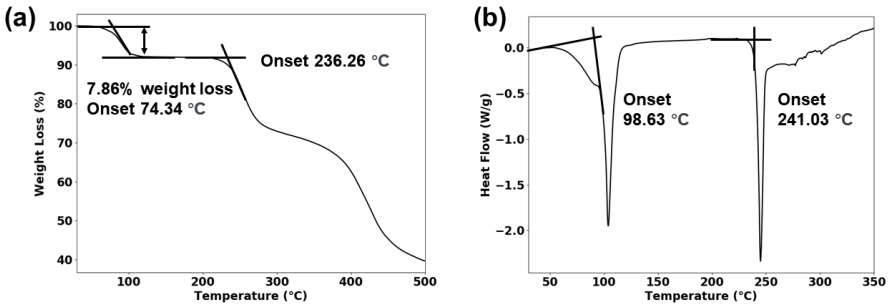

Figure 3.1.6. (a) TGA curve of $[ZnSac_2Lev(H_2O)]•CH_3CN$. (b) TGA curve of $[ZnSac_2Lev(H_2O)]•CH_3CN$.

Complexation with etiracetam.

Complexation of levetiracetam's racemic counterpart, etiracetam did not show any solvate formation, resulting in the formation of $ZnSac_2Eti_2$ which crystalizes in a $P2_1/c$ space group. Unlike the majority of complexes obtained, an octahedral coordination is observed around the zinc cation. $ZnSac_2Eti_2$ can furthermore be regarded as a 1D coordination polymer with etiracetam molecules bridging two zinc cations (Figure 3.1.7). Two etiracetam molecules coordinating to two adjacent cations act as a bridge through their pyrrolidone and amide groups. The octahedral coordination is fulfilled by two saccharinate anions through the carbonyl oxygen instead of the nitrogen atoms unlike all other complexes obtained. This is a rare occurrence for this type of coordination involving saccharinate, as a CSD search confirms that nitrogen coordination is more likely.[42-44]

The simulated PXRD pattern overlaps with that of the ground material (Figure. B.32), showing the same phase was obtained. In addition, the synthesis of Sac_2ZnEti_2 was upscaled to several grams by slurrying stoichiometric amounts of zinc saccharinate and etiracetam in ethanol or isopropanol. (Figure B.33)

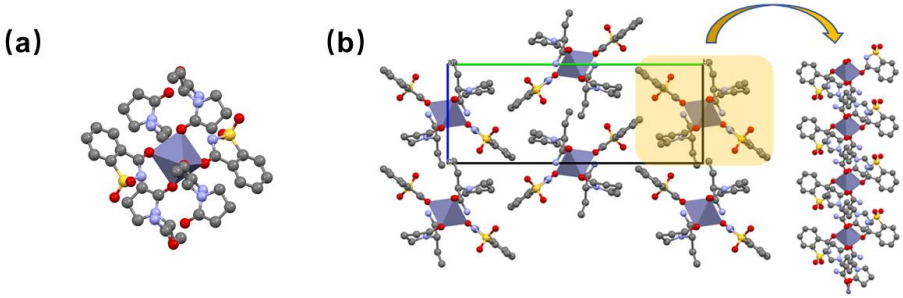

Figure 3.1.7. $ZnSac_2Eti_2$. (a) The coordination environment of zinc; (b) crystal packing, view along crystallographic *a*-axis and the one-dimensional chain. Hydrogen atoms are omitted for clarity.

Thermal analysis (DSC and TGA) of $ZnSac_2Eti_2$ shows a single melting endotherm at 189 °C followed by immediate degradation (Figure 3.1.8). The introduction of zinc saccharinate, thermally stabilizes etiracetam at the solid state by about 70°C (etiracetam shows a melting point of 119 °C).[45] Merely cocrystallizing etiracetam with $ZnCl_2$ shows almost no increase of etiracetam's melting point (around 118°C), highlighting the importance of saccharinate in this stabilization.[36]

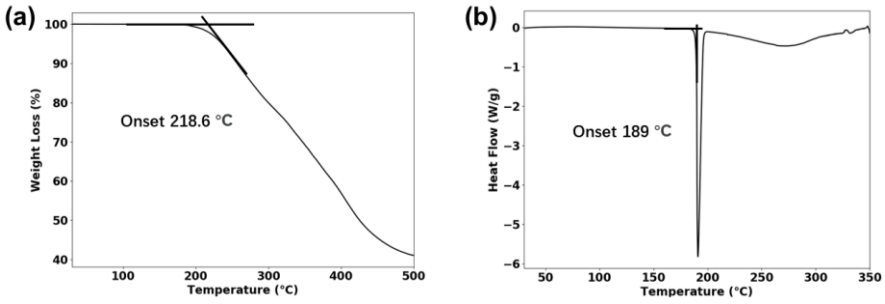

Figure 3.1.8. (a) TGA curve of $ZnSac_2Eti_2$ (b) DSC curve of $ZnSac_2Eti_2$

Complexation with piracetam

Complexation of piracetam with zinc saccharinate always resulted in the formation the hydrated $Zn_3Sac_6Pi_2(H_2O)_4$ complex regardless of the synthetic method (LAG or slurrying in ethanol, acetonitrile or isopropanol (Figures B.34-B.35).

The structure of $Zn_3Sac_6Pi_2(H_2O)_4$ differs significantly from the other complexes (Figure 3.1.9). Firstly, the stoichiometric ratio of zinc saccharinate to piracetam is different, showing a 3:2 instead of the most common 1:1 ratio. Secondly, this complex is characterized by both tetrahedral as well as octahedral coordination around the zinc cation. Two zinc cations have a tetrahedral coordination formed by three nitrogen atoms of saccharinate and an oxygen from a piracetam amide group. The pyrrolidone oxygens of piracetam, in turn, are coordinated to the octahedrally coordinated zinc cation which is situated in between the above mentioned tetrahedra. The octahedral coordination is completed by 4 water molecules. This combination of tetra- and octahedrally coordinated zinc leads to $Zn_3Sac_6Pi_2(H_2O)_4$ monomer. These monomers

interact with each other via hydrogen bonds between the water molecules and amide group of piracetam and oxygen atoms of saccharinate (Figure. 3.1.9a).

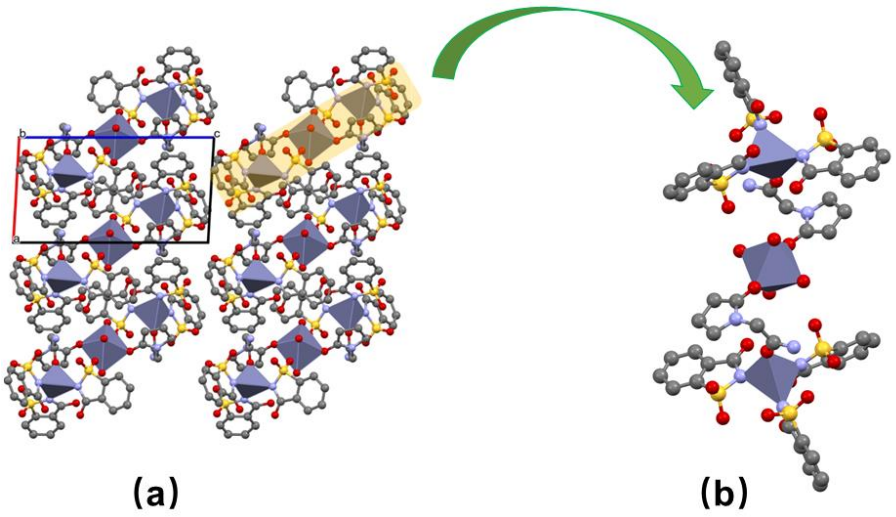

Figure 3.1.9. (a) Crystal packing of $Zn_3Sac_6Pi_2(H_2O)_4$, view down crystallographic *b*-axis. The yellowish rectangle represents one $Zn_3Sac_6Pi_2(H_2O)_4$ monomer (b).The structure of $Zn_3Sac_6Pi_2(H_2O)_4$ monomer.

Complexation with carphedon

The complexation of zinc saccharinate with carphedon revealed a unique molecular cocrystal $[ZnSac_2(H_2O)_2]$•Car•EtOH•H_2O, which can be obtained by slurrying or LAG methods using ethanol as a solvent (Figure B.36, B.37). $[ZnSac_2(H_2O)_2]$•Car•EtOH•H_2O is the only complex, in which the racetam compound is not coordinated to the zinc cation. The tetrahedral coordination of Zn^{2+} is formed by two saccharinate and two water molecules (Figure 3.1.10a), with carphedon interacting with the $[ZnSac_2(H_2O)_2]$ motif through hydrogen bonding (Figure 3.1.10b). $[ZnSac_2\ (H_2O)_2]$•Car•EtOH•H_2O can therefore be described as a solvated cocrystal between $[ZnSac_2(H_2O)_2]$ and carphedon.

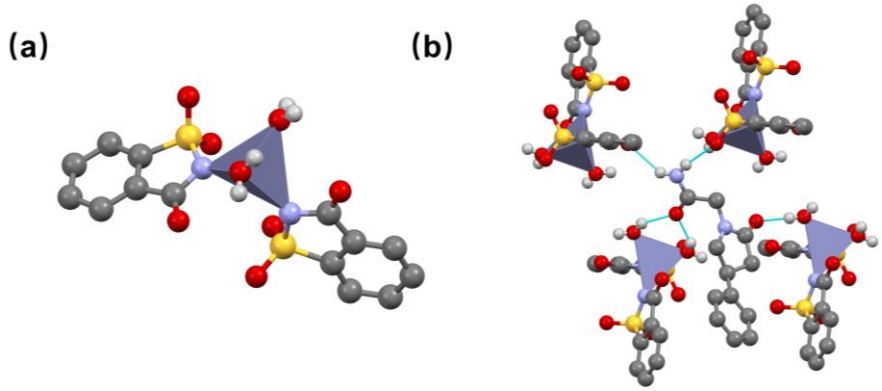

Figure 3.1.10. (a) The coordination environment of Zn^{2+}; (b) Hydrogen bonding interaction between carphedon and $[ZnSac_2(H_2O)_2]$. H_{CH} were omitted for the sake of clarity.

3.1.5 Conclusion

This paper introduces a novel methodology to couple a sweetener to a drug compound, as demonstrated for the racetam family. Whereas salt or cocrystal formation between the sweetener saccharin and racetams is not feasible, they can however be coupled together at the solid state, complexing the racetam compound with zinc saccharinate. We successfully applied this methodology to 6 different racetams, leading to 10 solid forms structurally identified in this paper. Interestingly, various structural features occur for these complexes with tetrahedral as well as octahedral coordination modes around the zinc cation, for which well-chosen examples of the various cases presented here. Furthermore, the solid-state landscape can be expanded through the existence of various solvates of the obtained complexes, involving water as well as organic solvents. This shows the complexity surrounding these complexes rendering the prediction of their structural assembly non-trivial. Albeit the large variety in structural features, all complexes remain stable under ambient conditions and can easily be obtained through mechanochemical or solution-based methodologies, all showing increased thermal stability.

This methodology can easily be transposed to other systems for which cocrystallization between the target compound and the coformer (a sweetener in our case) cannot be achieved, once more expanding the solid-state landscape of target compounds.

3.2. Complexation: An Interesting Pathway for Combining Two APIs at the Solid State

3.2.1 Abstract:

Combining different drugs into a single crystal form is one of the current challenges in crystal engineering, with the number of reported multi-drug solid forms remaining limited. This paper builds upon an efficient approach to combining Active Pharmaceutical Ingredients (APIs) containing carboxylic groups in their structure with APIs containing pyridine moieties. By transforming the former into their zinc salts, they can be successfully combined with the pyridine-containing APIs. This work highlights the successfulness of this approach, as well as the improvement in the physical properties of the obtained solid forms.

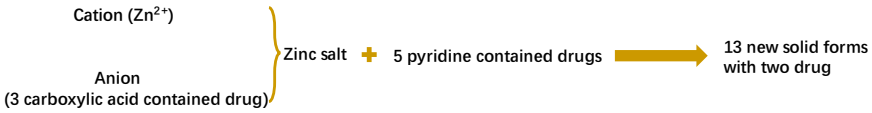

	aspirin	ibuprofen	4-aminobenzoic acid
methylnicotate	New form		New form
nicotinamide		New form	New form
isonicotinamide	New form	New form	New form
isoniazid		New form	New form
Amifampridine	New form	new form	New form

Conceptualization, T.L. and F.L. methodology, F.L.; software, K.R.; validation, O.S. and T.L.; formal analysis, F.L.; investigation, F.L.; resources, T.L.; data curation, O.S.; writing—original draft preparation, F.L.; writing—review and editing, O.S.; visualization, T.L.; supervision, O.S.; project administration, T.L.; funding acquisition, T.L. and K.R. All authors have read and agreed to the published version of the manuscript.

3.2.2 Introduction

The last few decades have witnessed a rapid increase in life expectancy around the world. This is, however, accompanied by an increased number of cases of age-associated chronic and complex diseases such as diabetes, cancer, and cardiovascular disorders[46, 47]. Multi-drug combinations have demonstrated superiority compared to traditional mono-therapy approaches for the treatment of such diseases[48-51]. Administrating several drugs in parallel will decrease the patient's compliance, especially for elderly people. Formulating different drugs into one solid dosage form, which is also called FDC, seems to be an easy and straightforward choice to solve this problem. Unfortunately, in some cases, the difference in physicochemical properties of the combined APIs does not allow one-dose compatibility.[51, 52]

Combining different drugs in a single solid form could potentially offer a solution to this problem, allowing the overcoming of potential issues observed with fixed-dose combinations, and at the same time, allowing for improving physicochemical properties and even bioactivity [11, 53-55]. To this end, cocrystallization and salt formation are two main approaches in the attempt to combine different drugs into one crystal structure [55]. To date, dozens of drug–drug cocrystals have been reported [49, 51, 53]; some of them (e.g., meloxicam-aspirin, piracetam–lithium chloride, and curcumin–pyrogallol) exhibit superior solubility profiles compared to the parent compounds [56-58]. The cocrystal between monosodium sacubitril and disodium valsartan, which has been marketed by Novartis under the name Entresto for the treatment of chronic heart failure, shows improved bioavailability compared to valsartan [59]. Recently, Hidehiro Uekusa et al. reported[60] a salt–salt antidiabetic drug combination, coupling gliclazide and metformin. This form not only showed improved solubility and dissolution rate characteristics with respect to gliclazide but also solved the hygroscopicity of metformin.[60]

The goal of this contribution is to explore a recent design strategy, based on complexation, to combine two APIs into the same solid form. This approach is based on the potential of coupling a second neutral API to a pharmaceutical metal-based salt of the first API, hereby achieving multi-component drug–drug systems. As model systems, we focused on the zinc salts of the CADs, ibuprofen, aspirin, and 4-aminobenzoic acid, which we aimed to couple with five PDs, nicotinamide, isonicotinamide, isoniazid, amifampridine, and methyl nicotinate, as the nitrogen is expected to easily couple with the metal center. We indeed showed that this

approach is highly successful as, in almost all cases, a successful drug–drug solid form was obtained. In addition, zinc ibuprofenate complexes showed improved physicochemical properties compared to the parent compounds.

3.2.3 Experimental Section

Materials

ASP, IBU, NC, INC, INZ, and MN were bought from Acros (Geel, Belgium). AMI was acquired from Sigma-Aldrich (St. Louis, MO, USA), PABA from Alfa Aesar (Haverhill, MA, USA), and zinc oxide from Merck (Kenilworth, NJ, USA). All the solvents and reagents were used as received without further treatment.

Preparation of Zinc Ibuprofenate ($Zn(IBU)_2 \cdot 2H_2O$), $Zn(PABA)_2$ and Zinc Aspirinate ($Zn(ASP)_2$)

Zinc aspirinate and zinc ibuprofenate were prepared following previously reported experimental procedures[61, 62]. $Zn(PABA)_2$ was prepared by suspending 4-aminobenzoic acid and zinc acetate in a 2:1 ratio in acetonitrile for 2 days at room temperature. Afterward, the suspension was filtered, and the filtered cake was left to dry under ambient conditions.

Mechanochemical Synthesis of Drug-Drug Complexes

First, 0.25 mmol of zinc oxide, 0.5 mmol of CAD, and 0.25 mmol of PD (Table 3.2.1) were added to an Eppendorf tube together with 40 μL of water and 2–3 stainless-steel balls. The mixtures were left to grind at 30 Hz for 90 min using a vibrating mill. Grinding experiments were also performed using double the amount of PD (0.5 mmol) to verify the existence of stoichiometrically diverse complexes. The resulting PXRD patterns were compared to the parent compounds as well as to the grinding results of the binary combination of CAD and zinc oxide to exclude false positives due to the potential formation of the physical mixture between a CAD-Zn salt and neutral PD.

Table 3.2.1. Complexation screening results. Green stands for the successful mechanochemical combination; grey means an oil-like product was obtained. SC means the combination was confirmed by structural analysis of a single crystal (SC).

	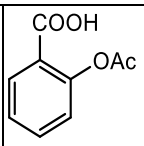 **Aspirin (ASP)**	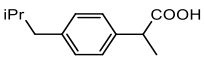 **Ibuprofen (IBU)**	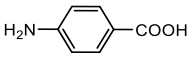 **4-aminobenzoic acid (PABA)**
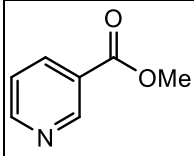 **Methylnicotinate (MN)**	SC		SC
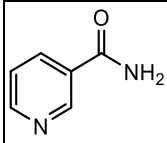 **Nicotinamide (NC)**		SC	SC
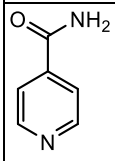 **Isonicotinamide (INC)**	SC	SC	SC
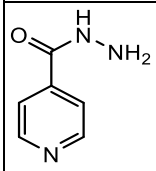 **Isoniazid (INZ)**		SC	SC [1]
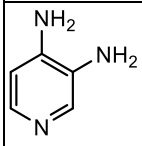 **Amifampridine (AMI)**		SC	SC

[1] The complex was obtained in the form of methanolate solvate.

Single Crystal and Bulk Material Preparation

Table 3.2.2. Overview of the single crystal and Bulk Material preparation for the reported compounds.

Material	Single Crystal Growth	Bulk Preparation
$Zn(IBU)_2(NC)$	Zinc acetate, Ibu, NC dissolved by methanol in 1:2:1 ratio, then evaporation	Slurrying $Zn(IBU)_2$ and NC in 1:1 ratio with ethyl acetate as solvent
$Zn(PABA)_2(INC)_2 \cdot 0.5H_2O$	Zinc acetate, PABA, INC dissolved by methanol in 1:2:2 ratio, then evaporation	
$Zn(PABA)(Ac)(MN)_2 \cdot H_2O$	Zinc acetate, PABA, MN dissolved by methanol in 1:1:2 ratio, then evaporation	
$Zn(PABA)_2(NC)_2$	Zinc acetate, PABA, NC dissolved by methanol in 1:2:2 ratio, then evaporation	
$Zn(PABA)_2(INZ) \cdot CH_3OH$	Zinc acetate, PABA, INZ dissolved by methanol in 1:2:1 ratio, then evaporation	
$Zn(IBU)_2(INC)$	$Zn(IBU)_2$, INC dissolved by methanol in 1:1 ratio, then evaporation	Slurrying $Zn(IBU)_2$ and INC in 1:1 ratio with methanol as solvent
$Zn(ASP)_2(MN)_2$	$Zn(ASP)_2$, MN dissolved by methanol in 1:2 ratio, then evaporation	

Material	Single Crystal Growth	Bulk Preparation
$Zn(ASP)_2(INC)$	$Zn(ASP)_2$, INC dissolve by methanol in 1:1 ratio, then evaporation	
$Zn(PABA)_2(MN)_2 \cdot H_2O$	$Zn(PABA)_2$, MN dissolve by methanol in 1:2 ratio, then evaporation	
$Zn(IBU)_2(AMI)$	$Zn(IBU)_2$, AMI dissolved by methanol in 1:4 ratio, then evaporation and cool in fridge	Slurrying $Zn(IBU)_2$ and AMI in 1:1 ratio with isopropanol as solvent
$Zn(IBU)_2(INC)_2(H_2O)_2$	$Zn(IBU)_2$, INC dissolved by methanol/H_2O mixed solvent (7:3) in 1:2 ratio, then evaporation	Slurrying $Zn(IBU)_2$ and INC in 1:2 ratio with water as solvent
$Zn(IBU)_2(INZ)$	$Zn(IBU)_2$, INZ dissolved by methanol/H_2O mixed solvent (7:3) in 1:1, then evaporation	Slurrying $Zn(IBU)_2$ and INZ in 1:1 ratio with water as solvent
$Zn(PABA)_2(AMI)_2$	stoichiometric quantities of Zinc acetate, Ibu, NC dissolve in methanol than evaporation	

Powder X-ray Diffraction (PXRD) and Variable-Temperature X-ray Powder Diffraction (VT-PXRD)

Powder X-ray diffraction was conducted on a Siemens D5000 diffractometer (Munich, Germany) equipped with a Cu X-ray source operating at 40 kV and 40 mA ($\lambda = 1.5418$

Å) from 4 to 50 degrees at the rate of 0.6 degrees per minute. VT-PXRD profiles were collected on a PANalytical X'Pert PRO automated diffractometer (Malvern Panalytical, Malvern, UK) at a scanning range of 2θ values from 3° to 40°, equipped with an X'Celerator detector and an Anton Paar TTK 450 system (Rigaku, Tokyo, Japan) for measurements at a controlled temperature. Data were collected in the open air in Bragg–Brentano geometry, using Cu–Kα radiation without a monochromator.

SCXRD

Data were collected on a MAR345 image plate detector (marXperts, Norderstedt, Germany) using Mo Kα radiation (λ = 0.71073 Å), generated by an Incoatec IμS microfocus source (Geesthacht, Germany). Data integration and reduction were performed by CrysAlisPRO (Rigaku), and the implemented absorption correction was applied. The structure solution was performed by the dual-space algorithm in SHELXT, and the structure was further refined against F^2 using SHELXL2014/7 [32]. All non-hydrogen atoms were refined anisotropically, and hydrogen atoms were placed at calculated positions with temperature factors set at 1.2 Ueq of the parent atoms (1.5 Ueq for methyl and OH hydrogens).

TGA

TGA analyses of all samples were performed from 30 °C to 500 °C using a heating rate of 10 °C/min with a continuous nitrogen flow of 50 mL/min, on a Mettler Toledo TGA/SDTA851e (Columbus, OH, USA).

DSC

DSC measurements were performed on a TA DSC2500. Samples in aluminum Tzero pans with a punctured lid were heated from 20 °C up to 350 °C using a heating rate of 10 °C/min under a 50 mL/min continuous nitrogen flow.

Solubility Measurement

Solubilities were determined for Ibuprofen, $Zn(IBU)_2(H_2O)_2$, $Zn(IBU)_2(INC)_2(H_2O)_2$, and $Zn(IBU)_2(INZ)$ at room temperature. To do so, an excess amount of compound was suspended in water at room temperature for two days. The suspension was filtered, and the mass of the clear saturated solution was determined. After evaporation of the solvent, the remaining solid was weighed once again, allowing us to determine the solubility. The original residue was verified by PXRD to confirm no solid transition occurred.

3.2.4 Results and discussion

Coupling API through Complexation

Converting acidic drugs into the corresponding metal salts is a widely used approach to improve their solubility and thermal stability [63-65]. Low-valent metals such as sodium, potassium, calcium, magnesium, or zinc are the most popular cations used in salt formation as they are pharmaceutically acceptable. The use of these metals often leads to 1:1 or 2:1 organic anion-metal cation complexes [66, 67]. These cations, however, often favor high coordination numbers (4, 6, or even higher), with full coordination only achievable using perfectly chelated multidentate API. When such full coordination cannot be achieved by the API, water molecules can fulfil this role, explaining the frequent occurrence of ion-coordinated hydrates among such pharmaceutical salts [68, 69]. Interestingly, one is not limited to the use of water, as any neutral organic compound linking to a metal cation could be used to fulfil this purpose. This opens an interesting strategy to design multi-component drug solid forms, as an API can be used as such a second component. We decided to test this strategy on the Zn salts of ibuprofen, aspirin, and 4-aminobenzoic acid. Among all pharmaceutically accepted metals, zinc possesses the most records in the CCDC database. This suggests zinc could be a good potential coordination center for a multi-component complexation. In addition, several contributions have demonstrated that converting acidic drugs such as ibuprofen or aspirin into their zinc salts led to improved bioactivity [61, 70]. Zinc is furthermore characterized by low toxicity, with symptoms such as nausea, vomiting, and fatigue only occurring with extremely high zinc intake, making it an ideal metal for pharmaceutical purposes [71].

The first step in achieving multi-component systems implies identifying suitable APIs to couple to these salts. Synthon analysis has been shown to be an efficient approach in the context of cocrystal design. Selecting a suitable coformer based on frequently occurring and reproducible patterns of intermolecular interactions often leads to high success rates in cocrystal screening [72-74]. A similar strategy can be applied here as metal ions often show favored coordination modes [75, 76]. Going through the CCDC, mixed-ligand zinc complexes are often encountered when one compound contains a carboxylic acid, while the other contains a pyridine function [77, 78]. We, therefore, selected a series of five different pyridine-based drugs (nicotinamide, isonicotinamide,

isoniazid, amifampridine, and methyl nicotinate) to test the coupling strategy suggested here.

Following our recent success working on saccharinate-Zn-racetam complexes [79], we used a three-component grinding approach to identify potential drug–drug complexes. In this approach, ZnO, the carboxylic acid drug, and the pyridine-containing drug are ground together, leading to a multi-component complex. Table 3.2.1 shows that out of the 15 potential combinations tried here, 11 show a different PXRD profile compared to the parent compounds upon grinding (Table 3.2.1, Figures B.22-B.32). To confirm these hits were not due to the mere formation of different polymorphs or that the complexes contained only a single drug component, single crystals of the multi-component complexes were grown. This was successfully achieved for 10 of the complexes. $Zn(ASP)_2$-AMI is also expected to be a drug–drug metal complex, but up to now, we have not yet been able to grow single crystals suitable for structural analysis. The four remaining combinations, namely ($Zn(IBU)_2$-MN, $Zn(ASP)_2$-NC, $Zn(ASP)_2$-INZ, and $Zn(PABA)_2$-INZ), were not successful in a mechanochemical approach, with an oil-like substance occurring upon grinding. This can be due to a low melting eutectic or a highly hygroscopic product. These combinations, however, can still be achievable if the right conditions are applied (e.g., crystals of complex $Zn(PABA)_2$-INZ in the form of methanolate solvate were obtained from solution crystallization). Interestingly, although PABA is a zwitterion, it can be converted to a salt, therefore the successful combination can still be expected.

It should be mentioned that, in most cases, successful cocrystal formation also occurs (see appendices) between the organic compounds (without the need for the zinc cation). However, as the acids are under ionized form in the complexes, large changes in properties such as solubility can be expected compared to a mere binary cocrystal. Furthermore, complexes form for those cases where the binary combination is unsuccessful.

Structural and Thermal Characterization of Drug-Drug Complexes

Analysis of the 11 crystal structures allows us to regroup them into three different categories according to the observed coordination mode. All three coordination modes (Figure 3.2.1) are typically observed for Zn complexes. $Zn(PABA)_2(INC)_2{\cdot}0.5H_2O$, $Zn(PABA)_2(NC)_2$, $Zn(PABA)_2(AMI)_2$, $Zn(IBU)_2(INZ)$, $Zn(IBU)_2(INC)_2$, $Zn(PABA)_2(INZ){\cdot}CH_3OH$, and Zn

$(ASP)_2(INC)$) show a tetrahedral coordination mode. $Zn(ASP)_2(MN)$, $Zn(PABA)(Ac)(MN)\cdot H_2O$, $Zn(IBU)_2(AMI)$, and $Zn(IBU)_2(NC)$ show a pyramidal paddle-wheel coordination around the zinc cation. Finally, a hexa-coordinated octahedron mode is observed for the $Zn(IBU)_2(INC)_2(H_2O)_2$ and $Zn(PABA)_2(MN)_2\cdot H_2O$ complexes. $Zn(IBU)_2$-PDs will be described in more detail below as their examples cover each coordination mode. Furthermore, ibuprofen has low thermal stability (79.04 °C m.p.) and low solubility[80], so we investigated the potential of these complexes to improve drug properties. A mere transformation of ibuprofen into its zinc salt does not solve the issue of low thermal stability as it crystallizes as a dihydrate, which becomes amorphous upon dehydration at essentially the same temperature as the melting point of ibuprofen (Figure C.13).

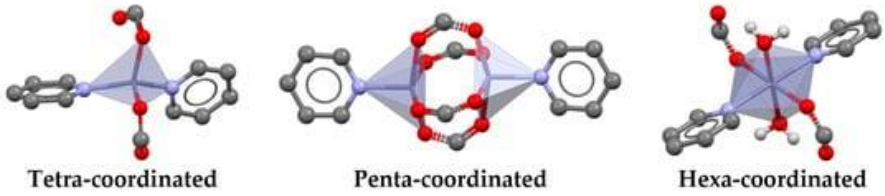

Figure 3.2.1.Three favored coordination modes of zinc complexes involving pyridine and carboxylate ligands, as identified in the CSD.

Tetra-Coordinated $Zn(IBU)_2(INC)_2$ and Hexa-Coordinated $Zn(IBU)_2(INC)_2(H_2O)_2$

The tetrahedral coordination mode is the most frequently observed in our results. $Zn(IBU)_2(INC)_2$ shows a central zinc cation tetrahedrally coordinated by two oxygens from two ibuprofen carboxylate groups and two pyridine nitrogen atoms from two isonicotinamide molecules giving an overall $Zn(IBU)_2(INC)_2$ monomer (Figure 3.2.2a). Furthermore, the 3D network shows one-dimensional chains formed through $NH_{amide}\cdots O_{carboxylate}$ hydrogen bonding between adjacent monomers (Figure 3.2).

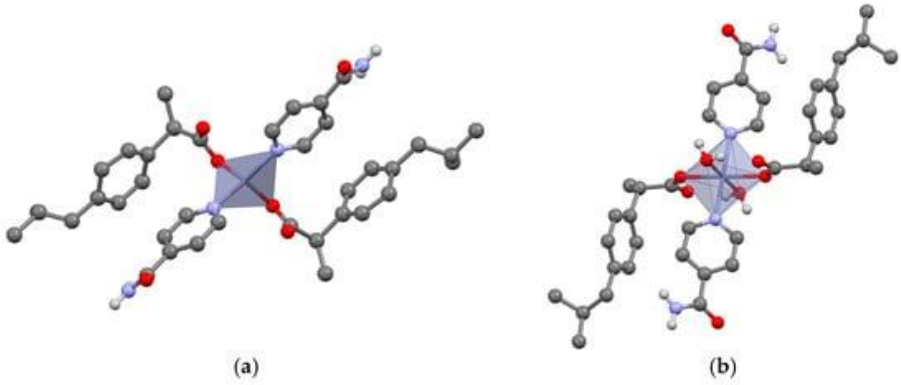

Figure 3.2.2. Monomers in $Zn(IBU)_2(INC)_2$ (a) and $Zn(IBU)_2(INC)_2(H_2O)_2$ (b); H_{CH} omitted for clarity.

Interestingly, looking for a single crystal, a hydrated complex $Zn(IBU)_2(INC)_2(H_2O)_2$ was encountered. It shows a hexacoordinated octahedral coordination mode in which the zinc cation is coordinated by two oxygens from water molecules, two oxygens from ibuprofenate moieties, and two pyridine nitrogens from isonicotinamide (Figure 3.2.2b). Unlike for $Zn(IBU)_2(INC)_2$, the neighboring monomers interact via a two-dimensional hydrogen bonding network, which is built by $NH_{amide}\cdots O_{carboxylate}$ and $OH_{water}\cdots O_{carboxylate}$ interactions (Figure C.3). This observation also shows that water molecules have the potential to complete the coordination mode around the central cation and that hydrated phases can also be encountered for drug–drug complexes.

Thermal analysis of $Zn(IBU)_2(INC)_2$ shows a single melting event at 176 °C (Figure 3.2.3a). It highlights the remarkable thermal stability of $Zn(IBU)_2(INC)_2$ (isonicotinamide melts at 120 °C [80]). Furthermore, this melting point is also substantially higher than that of Ibuprofen (79.04 °C [79]) and the 1:1 ibuprofen-isonicotinamide cocrystal (119 °C [81]).

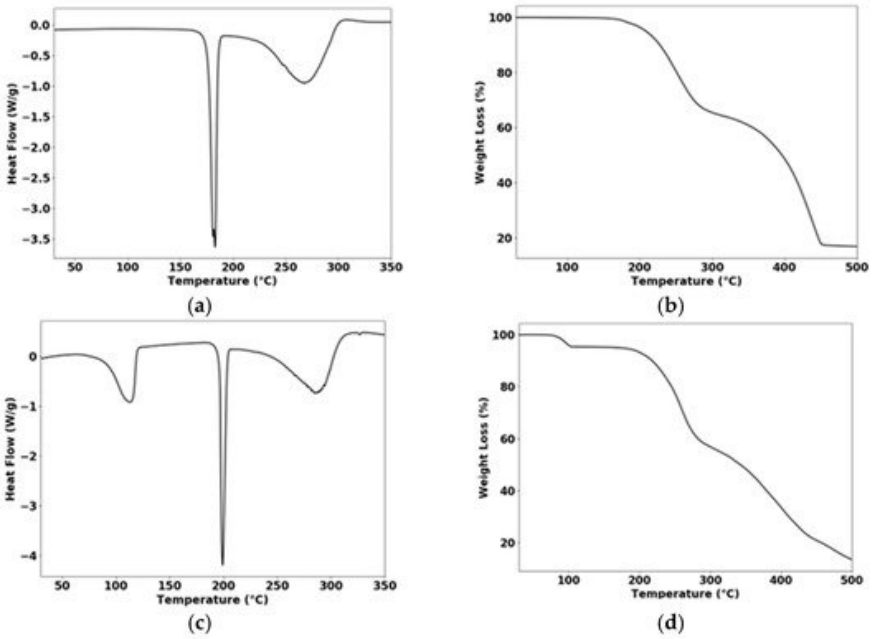

Figure 3.2.3. TGA and DSC thermograms of $Zn(IBU)_2(INC)_2$ (a,b) and of $Zn(IBU)_2(INC)_2(H_2O)_2$ (c,d).

The thermal behavior of the hydrated complex—$Zn(IBU)_2(INC)_2(H_2O)_2$—shows a 4.75% weight loss at approximately 100 °C corresponding to the loss of two coordinated water molecules (Figure 3.2.3d). This water loss leads to the $Zn(IBU)_2(INC)_2$ phase with a melting point of 196 °C (Figure 3.2.3c), which is 20 °C above the temperature reported above. VT-PXRD confirms that upon dehydration, the hydrated complex transforms into a different polymorph of the $Zn(IBU)_2(INC)_2$ complex (Figure C.33). If drug–drug complexes are considered for the formulation, it is recommended to always investigate polymorphism and hydrate formation.

Penta-Coordinated $Zn(IBU)_2$(AMI) and $Zn(IBU)_2$(NC)

Both complexes have similar crystal packings. Only the crystal structure of $Zn(IBU)_2$(AMI) will be discussed here. $Zn(IBU)_2$(AMI) is characterized by a penta-coordinated mode (Figure 3.2.4). One monomeric unit shows two zinc cations surrounded by four bridging carboxylates from four ibuprofen molecules. The pyridine nitrogen atoms from amifampridine coordinate to both zinc cations along the Zn-Zn axis. Monomers form a one-dimensional chain

through hydrogen bonds between the amide groups and the carboxylates (Figure C.4) in a similar manner to the tetra-coordinated $Zn(IBU)_2(INC)_2$ complex. The overall 3D structure should be seen as the packing result of these one-dimensional chains.

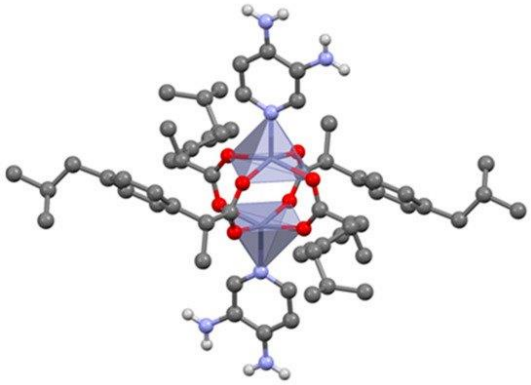

Figure 3.2.4. Monomer in $Zn(IBU)_2(AMI)$, H_{CH} omitted for clarity.

Interestingly, mechanochemical screening revealed the existence of a stoichiometrically diverse complex $Zn(IBU)_2(AMI)_2$. Both $Zn(IBU)_2(AMI)$ and $Zn(IBU)_2(AMI)_2$ complexes can be obtained from solution, slurrying $Zn(IBU)_2$ and AMI in isopropanol under different ratios (see experimental part). As for other drug–drug systems (cocrystals or salts), drug–drug complexes also show the potential for stoichiometrical diversity, besides polymorphism and hydrate formation, once more highlighting the importance of a full solid-state screening when considering these forms for formulation.

Thermal analysis shows single endothermal melting peaks at 137 °C and 157 °C for $Zn(IBU)_2(AMI)$ and $Zn(IBU)_2(AMI)_2$, respectively (see Figure C.14b,d). The thermal stability of the solid form complexes $Zn(IBU)_2(AMI)$ and $Zn(IBU)_2(AMI)_2$ is between those of the parent compounds (the melting point of amifampridine is 218 °C).

The crystal structure of $Zn(IBU)_2(NC)$ was recently reported by Moura et al. focusing on bioactivity improvement using this complex [82]. The investigation of thermal stability reveals a temperature comparable to that of nicotinamide (128–129 °C) (Figure C.15b). Furthermore, $Zn(IBU)_2(NC)$ shows higher thermal stability compared to the ibuprofen-nicotinamide cocrystal, which shows a melting temperature of 96 °C [80, 83].

Tetra-Coordinated $Zn(IBU)_2(INZ)$

$Zn(IBU)_2(INZ)$ is an example of an alternative crystal packing. As in the majority of the complexes described in this work, zinc is coordinated to two oxygen atoms from ibuprofenate and to one pyridine-type nitrogen. Contrary to the other complexes, its coordination not only involves pyridine nitrogens. Specifically, coordination also occurs with a hydrazide group (Figure 3.2.5a). As coordinating nitrogen atoms of an isoniazid molecule link to different zinc cations, these molecules act as bridging ligands leading to one-dimensional chains (Figure 3.2.5b). An identical coordination mode is observed in the $Zn(PABA)_2(INZ)\cdot CH_3OH$ complex (see Figure C.8).

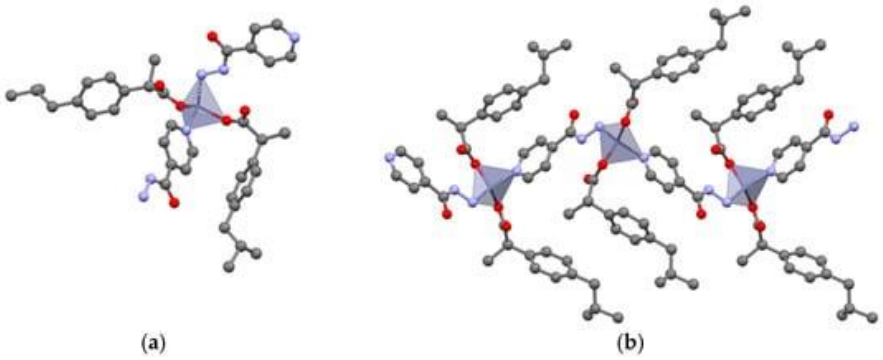

Figure 3.2.5. $Zn(IBU)_2(INZ)$: Tetra-coordinated zinc cation (a); one-dimensional chain (b). Hydrogen atoms omitted for clarity.

A single melting peak is observed at 212 °C (Figure C.16b) highlighting, once again, the improvement in thermal stability compared to both isoniazid (melting at 172 °C [84]) and zinc ibuprofenate.

Solubility Improvement

The water solubility of salts, cocrystals, or multi-component complexes is only directly comparable to the parent compound if the system behaves congruently. $Zn(IBU)_2(INC)_2(H_2O)_2$and $Zn(IBU)_2(INZ)$ were shown to be congruent in water, and their solubilities were determined gravimetrically. For easy comparison, the solubility is represented in mmol of ibuprofen per liter. Compared to ibuprofen, $Zn(IBU)_2(INC)_2(H_2O)_2$ and $Zn(IBU)_2(INZ)$ show a 17- and 9-fold increase in solubility, respectively, at room temperature. These complexes, however, do show lower solubility compared to the zinc ibuprofenate dihydrate (5.36 mmol/L) (Figure 3.2.6).

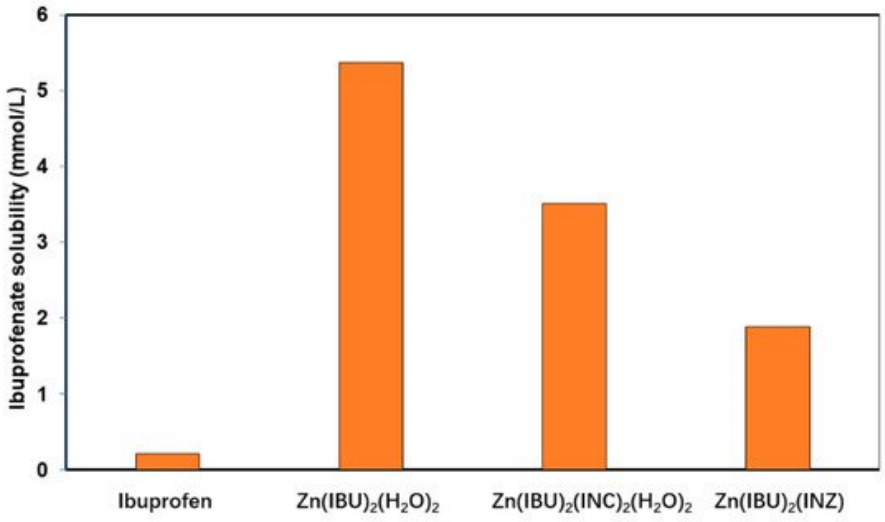

Figure 3.2.6. Solubility of ibuprofen, $Zn(IBU)_2(H_2O)_2$, $Zn(IBU)_2(INC)_2(H_2O)_2$, and $Zn(IBU)_2(INZ)$ calculated based on the amount of ibuprofenate.

This lower solubility compared to the parent salt is not a general rule, as reported complexes between L-proline and diclofenac sodium show improved solubility compared to anhydrous diclofenac sodium. Too few examples currently exist in the literature to draw conclusions on the general behavior of the solubility of the complexes vs. the solubility of parent salts [85].

Interestingly, a strong reduction in solubility is observed for isonicotinamide and isoniazid showing a respective solubility of 1.56 mol/L and 1.02 mol/L, showing a strong impact even for the non-ionized compound involved in the complex.

3.2.5 Conclusion

We explored a recent strategy for dual-drug solid forms, using complexation to achieve our goal. We showed how zinc salts of APIs containing a carboxylic group can be complexed with drug compounds that contain a pyridine moiety. A straightforward three-component mechanochemical screen using the carboxylic acid API, ZnO, and the pyridine-containing API led to the identification of dual-drug solid forms for almost all combinations. Tetra-, Penta-, and Hexa-coordination were encountered around the zinc cation in agreement with literature-based structures. As for any solid-state form, the dual-

drug complexes studied in this work also show solvatism and polymorphism, as well as stoichiometric diversity.

References

(1) Spignoli, G.; Pepeu, G. Interactions between oxiracetam, aniracetam and scopolamine on behavior and brain acetylcholine. *Pharmacology Biochemistry and Behavior* **1987**, *27* (3), 491-495.

(2) Ghelardini, C.; Galeotti, N.; Gualtieri, F.; Romanelli, M. N.; Bucherelli, C.; Baldi, E.; Bartolini, A. DM235 (sunifiram): a novel nootropic with potential as a cognitive enhancer. *Naunyn Schmiedebergs Arch Pharmacol* **2002**, *365* (6), 419-426.

(3) Löscher, W.; Richter, A. Piracetam and levetiracetam, two pyrrolidone derivatives, exert antidystonic activity in a hamster model of paroxysmal dystonia. *European Journal of Pharmacology* **2000**, *391* (3), 251-254.

(4) Malykh, A. G.; Sadaie, M. R. Piracetam and piracetam-like drugs: from basic science to novel clinical applications to CNS disorders. *Drugs* **2010**, *70* (3), 287-312.

(5) Kavanagh, O. N.; Wang, C.; Walker, G. M.; Sun, C. C. Modulation of the powder properties of lamotrigine by crystal forms. *Int J Pharm* **2021**, *595*, 120274.

(6) Pranzatelli, M. R.; Tate, E. D.; Galvan, I.; Wheeler, A. Controlled pilot study of piracetam for pediatric opsoclonus-myoclonus. *Clin Neuropharmacol* **2001**, *24* (6), 352-357.

(7) Hovinga, C. A. Levetiracetam: a novel antiepileptic drug. *Pharmacotherapy* **2001**, *21* (11), 1375-1388.

(8) Sivaneswari, S.; Karthikeyan, E.; Veena, D.; Chandana, P.; Sai Sumana, P.; Subhashree, P.; Ramya, L.; Rajalakshmi, R.; Ashok, K. C. Physiochemical characterization of taste masking levetiracetam ion exchange resinates in the solid state and formulation of stable liquid suspension for pediatric use. *Beni-Suef University Journal of Basic and Applied Sciences* **2016**, *5* (2), 126-133.

(9) Crepeau, A. Z.; Treiman, D. M. Levetiracetam: a comprehensive review. *Expert Review of Neurotherapeutics* **2014**, *10* (2), 159-171.

(10) Winblad, B. Piracetam: a review of pharmacological properties and clinical uses. *CNS Drug Rev* **2005**, *11* (2), 169-182.

(11) Karimi-Jafari, M.; Padrela, L.; Walker, G. M.; Croker, D. M. Creating Cocrystals: A Review of Pharmaceutical Cocrystal Preparation Routes and Applications. *Crystal Growth & Design* **2018**, *18* (10), 6370-6387.

(12) Sun, C. C. Cocrystallization for successful drug delivery. *Expert Opin Drug Deliv* **2013**, *10* (2), 201-213.

(13) Bhatt, P. M.; Ravindra, N. V.; Banerjee, R.; Desiraju, G. R. Saccharin as a salt former. Enhanced solubilities of saccharinates of active pharmaceutical ingredients. *Chem Commun (Camb)* **2005**, (8), 1073-1075.

(14) Blagden, N.; de Matas, M.; Gavan, P. T.; York, P. Crystal engineering of active pharmaceutical ingredients to improve solubility and dissolution rates. *Adv Drug Deliv Rev* **2007**, *59* (7), 617-630.

(15) Liu, S.; Wang, C.; Chen, H.; Sun, C. C. Sweet Sulfamethazine Acesulfamate Crystals with Improved Compaction Property. *Crystal Growth & Design* **2021**, *21* (2), 1077-1085.

(16) Kong, M.; Fu, X.; Li, J.; Li, J.; Chen, M.; Deng, Z.; Zhang, H. Sweet pharmaceutical salts of stanozolol with enhanced solubility and physical stability. *CrystEngComm* **2016**, *18* (45), 8739-8746.

(17) Banerjee, R.; Bhatt, P. M.; Ravindra, N. V.; Desiraju, G. R. Saccharin Salts of Active Pharmaceutical Ingredients, Their Crystal Structures, and Increased Water Solubilities. *Crystal Growth & Design* **2005**, *5* (6), 2299-2309.

(18) Martins, F. T.; Paparidis, N.; Doriguetto, A. C.; Ellena, J. Crystal Engineering of an Anti-HIV Drug Based on the Recognition of Assembling Molecular Frameworks. *Crystal Growth & Design* **2009**, *9* (12), 5283-5292.

(19) Li, A.-Y.; Xu, L.-L.; Chen, J.-M.; Lu, T.-B. Solubility and Dissolution Rate Enhancement of Triamterene by a Cocrystallization Method. *Crystal Growth & Design* **2015**, *15* (8), 3785-3791.

(20) Basavoju, S.; Bostrom, D.; Velaga, S. P. Indomethacin-saccharin cocrystal: design, synthesis and preliminary pharmaceutical characterization. *Pharm Res* **2008**, *25* (3), 530-541.

(21) Hou, X.; Feng, Y.; Zhang, P.; Wei, H.; Dang, L. Selective Crystal Growth of Theophylline-Saccharin Cocrystal on Self-Assembled Monolayer from Incongruent System. *Crystal Growth & Design* **2015**, *15* (10), 4918-4924.

(22) Zhao, X.; Li, Q.; Wang, C.; Hu, S.; He, X.; Sun, C. C. Simultaneous taste-masking and oral bioavailability enhancement of Ligustrazine by forming sweet salts. *Int J Pharm* **2020**, *577*, 119089.

(23) Chattopadhyay, S.; Raychaudhuri, U.; Chakraborty, R. Artificial sweeteners - a review. *J Food Sci Technol* **2014**, *51* (4), 611-621.

(24) Takata, N.; Takano, R.; Uekusa, H.; Hayashi, Y.; Terada, K. A Spironolactone−Saccharin 1:1 Cocrystal Hemihydrate. *Crystal Growth & Design* **2010**, *10* (5), 2116-2122.

(25) Hickey, M. B.; Peterson, M. L.; Scoppettuolo, L. A.; Morrisette, S. L.; Vetter, A.; Guzman, H.; Remenar, J. F.; Zhang, Z.; Tawa, M. D.; Haley, S.; et al. Performance comparison of a co-crystal of carbamazepine with marketed product. *Eur J Pharm Biopharm* **2007**, *67* (1), 112-119.

(26) Chadha, R.; Saini, A.; Jain, D. S.; Venugopalan, P. Preparation and Solid-State Characterization of Three Novel Multicomponent Solid Forms of Oxcarbazepine: Improvement in Solubility through Saccharin Cocrystal. *Crystal Growth & Design* **2012**, *12* (8), 4211-4224.

(27) Wang, C.; Perumalla, S. R.; Sun, C. C. Anion Exchange Reaction for Preparing Acesulfame Solid Forms. *Crystal Growth & Design* **2018**, *18* (8), 4215-4219.

(28) Buol, X.; Robeyns, K.; Caro Garrido, C.; Tumanov, N.; Collard, L.; Wouters, J.; Leyssens, T. Improving Nefiracetam Dissolution and Solubility Behavior Using a Cocrystallization Approach. *Pharmaceutics* **2020**, *12* (7).

(29) Leng, F.; Robeyns, K.; Leyssens, T. Urea as a Cocrystal Former-Study of 3 Urea Based Pharmaceutical Cocrystals. *Pharmaceutics* **2021**, *13* (5).

(30) Braga, D.; Grepioni, F.; Shemchuk, O. Organic–inorganic ionic co-crystals: a new class of multipurpose compounds. *CrystEngComm* **2018**, *20* (16), 2212-2220.

(31) Song, L.; Shemchuk, O.; Robeyns, K.; Braga, D.; Grepioni, F.; Leyssens, T. Ionic Cocrystals of Etiracetam and Levetiracetam: The Importance of Chirality for Ionic Cocrystals. *Crystal Growth & Design* **2019**, *19* (4), 2446-2454.

(32) Sheldrick, G. M. Crystal structure refinement with SHELXL. *Acta Crystallogr C Struct Chem* **2015**, *71* (Pt 1), 3-8.

(33) Shemchuk, O.; Spoletti, E.; Braga, D.; Grepioni, F. Solvent Effect on the Preparation of Ionic Cocrystals of dl-Amino Acids with Lithium Chloride: Conglomerate versus Racemate Formation. *Crystal Growth & Design* **2021**, *21* (6), 3438-3448.

(34) Shemchuk, O.; Grepioni, F.; Braga, D. Co-crystallization of racemic amino acids with ZnCl2: an investigation of chiral selectivity upon coordination to the metal centre. *CrystEngComm* **2020**, *22* (34), 5613-5619.

(35) Braga, D.; Degli Esposti, L.; Rubini, K.; Shemchuk, O.; Grepioni, F. Ionic Cocrystals of Racemic and Enantiopure Histidine: An Intriguing Case of Homochiral Preference. *Crystal Growth & Design* **2016**, *16* (12), 7263-7270.

(36) Shemchuk, O.; Song, L.; Robeyns, K.; Braga, D.; Grepioni, F.; Leyssens, T. Solid-state chiral resolution mediated by stoichiometry: crystallizing etiracetam with ZnCl2. *Chem Commun (Camb)* **2018**, *54* (77), 10890-10892.

(37) Bravo, C.; Galego, F.; André, V. Hydrogen bonding networks of nalidixic acid–copper(ii) complexes. *CrystEngComm* **2019**, *21* (47), 7199-7203.

(38) Domingos, S.; Andre, V.; Quaresma, S.; Martins, I. C.; Minas da Piedade, M. F.; Duarte, M. T. New forms of old drugs: improving without changing. *J Pharm Pharmacol* **2015**, *67* (6), 830-846.

(39) Friščić, T.; Halasz, I.; Strobridge, F. C.; Dinnebier, R. E.; Stein, R. S.; Fábián, L.; Curfs, C. A rational approach to screen for hydrated forms of the pharmaceutical

derivative magnesium naproxen using liquid-assisted grinding. *CrystEngComm* **2011**, *13* (9).

(40) Friščić, T.; Fábián, L. Mechanochemical conversion of a metal oxide into coordination polymers and porous frameworks using liquid-assisted grinding (LAG). *CrystEngComm* **2009**, *11* (5).

(41) Chow, E. H.; Strobridge, F. C.; Friscic, T. Mechanochemistry of magnesium oxide revisited: facile derivatisation of pharmaceuticals using coordination and supramolecular chemistry. *Chem Commun (Camb)* **2010**, *46* (34), 6368-6370.

(42) Yilmaz, V. T.; Topcu, Y.; Yilmaz, F.; Thoene, C. Saccharin complexes of Co(II), Ni(II), Cu(II), Zn(II), Cd(II) and Hg(II) with ethanolamine and diethanolamine: synthesis, spectroscopic and thermal characteristics. Crystal structures of [Zn(ea)2(sac)2] and [Cu2(μ-dea)2(sac)2]. *Polyhedron* **2001**, *20* (26-27), 3209-3217.

(43) Williams, P. A. M.; Ferrer, E. G.; Correa, M. J.; Baran, E. J.; Castellano, E. E.; Piro, O. E. Characterization of two new zinc(II) complexes with saccharinate and imidazole or benzimidazole as ligands. *Journal of Chemical Crystallography* **2004**, *34* (4), 285-290.

(44) Karabulut, B.; Ucar, I.; Koksal, F.; Yerli, Y. Crystal structure and EPR studies of doped Cu(2+) ion in [Zn(sac)(2)(en)(2)] single crystal. *Spectrochim Acta A Mol Biomol Spectrosc* **2010**, *75* (4), 1195-1199.

(45) Herman, C.; Vermylen, V.; Norberg, B.; Wouters, J.; Leyssens, T. The importance of screening solid-state phases of a racemic modification of a chiral drug: thermodynamic and structural characterization of solid-state phases of etiracetam. *Acta Crystallogr B Struct Sci Cryst Eng Mater* **2013**, *69* (Pt 4), 371-378.

(46) Kavanagh, O. N.; Albadarin, A. B.; Croker, D. M.; Healy, A. M.; Walker, G. M. Maximising success in multidrug formulation development: A review. *J Control Release* **2018**, *283*, 1-19.

(47) OECD. Life expectancy at birth (indicator). 2018.

(48) Vakil, V.; Trappe, W. Drug Combinations: Mathematical Modeling and Networking Methods. *Pharmaceutics* **2019**, *11* (5).

(49) Wang, X.; Du, S.; Zhang, R.; Jia, X.; Yang, T.; Zhang, X. Drug-drug cocrystals: Opportunities and challenges. *Asian J Pharm Sci* **2021**, *16* (3), 307-317.

(50) Wan, X.; Ma, P.; Zhang, X. A promising choice in hypertension treatment: Fixed-dose combinations. *Asian Journal of Pharmaceutical Sciences* **2014**, *9* (1), 1-7.

(51) Thipparaboina, R.; Kumar, D.; Chavan, R. B.; Shastri, N. R. Multidrug co-crystals: towards the development of effective therapeutic hybrids. *Drug Discov Today* **2016**, *21* (3), 481-490.

(52) Frantz, S. The trouble with making combination drugs. *Nat Rev Drug Discov* **2006**, *5* (11), 881-882.

(53) Bolla, G.; Nangia, A. Pharmaceutical cocrystals: walking the talk. *Chem Commun (Camb)* **2016**, *52* (54), 8342-8360.

(54) Wong, S. N.; Chen, Y. C. S.; Xuan, B.; Sun, C. C.; Chow, S. F. Cocrystal engineering of pharmaceutical solids: therapeutic potential and challenges. *CrystEngComm* **2021**, *23* (40), 7005-7038.

(55) Thakuria, R.; Sarma, B. Drug‐Drug and Drug‐Nutraceutical Cocrystal/Salt as Alternative Medicine for Combination Therapy: A Crystal Engineering Approach. *Crystals* **2018**, *8* (2).

(56) Cheney, M. L.; Weyna, D. R.; Shan, N.; Hanna, M.; Wojtas, L.; Zaworotko, M. J. Coformer selection in pharmaceutical cocrystal development: a case study of a meloxicam aspirin cocrystal that exhibits enhanced solubility and pharmacokinetics. *J Pharm Sci* **2011**, *100* (6), 2172-2181.

(57) Braga, D.; Grepioni, F.; Maini, L.; Capucci, D.; Nanna, S.; Wouters, J.; Aerts, L.; Quere, L. Combining piracetam and lithium salts: ionic co-crystals and co-drugs? *Chem Commun (Camb)* **2012**, *48* (66), 8219-8221.

(58) Sanphui, P.; Goud, N. R.; Khandavilli, U. B. R.; Nangia, A. Fast Dissolving Curcumin Cocrystals. *Crystal Growth & Design* **2011**, *11* (9), 4135-4145.

(59) Videla, S.; Lahjou, M.; Vaque, A.; Sust, M.; Encabo, M.; Soler, L.; Sans, A.; Sicard, E.; Gascon, N.; Encina, G.; et al. Single-dose pharmacokinetics of co-crystal of tramadol-celecoxib: Results of a four-way randomized open-label phase I clinical trial in healthy subjects. *Br J Clin Pharmacol* **2017**, *83* (12), 2718-2728.

(60) Putra, O. D.; Furuishi, T.; Yonemochi, E.; Terada, K.; Uekusa, H. Drug–Drug Multicomponent Crystals as an Effective Technique to Overcome Weaknesses in Parent Drugs. *Crystal Growth & Design* **2016**, *16* (7), 3577-3581.

(61) Lemoine, P.; Viossat, B.; Dung, N. H.; Tomas, A.; Morgant, G.; Greenaway, F. T.; Sorenson, J. R. Synthesis, crystal structures, and anti-convulsant activities of ternary [Zn(II)(3,5-diisopropylsalicylate)(2)], [Zn(II)(salicylate)(2)] and [Zn(II)(aspirinate)(2)] complexes. *J Inorg Biochem* **2004**, *98* (11), 1734-1749.

(62) Abu Ali, H.; Omar, S. N.; Darawsheh, M. D.; Fares, H. Synthesis, characterization and antimicrobial activity of zinc(II) ibuprofen complexes with nitrogen-based ligands. *Journal of Coordination Chemistry* **2016**, *69* (6), 1110-1122.

(63) Bharate, S. S. Recent developments in pharmaceutical salts: FDA approvals from 2015 to 2019. *Drug Discov Today* **2021**, *26* (2), 384-398.

(64) Gupta, D.; Bhatia, D.; Dave, V.; Sutariya, V.; Varghese Gupta, S. Salts of Therapeutic Agents: Chemical, Physicochemical, and Biological Considerations. *Molecules* **2018**, *23* (7).

(65) Serajuddin, A. T. Salt formation to improve drug solubility. *Adv Drug Deliv Rev* **2007**, *59* (7), 603-616.

(66) Wiedmann, T. S.; Naqwi, A. Pharmaceutical salts: Theory, use in solid dosage forms and in situ preparation in an aerosol. *Asian Journal of Pharmaceutical Sciences* **2016**, *11* (6), 722-734.

(67) Korn, C.; Balbach, S. Compound selection for development - is salt formation the ultimate answer? Experiences with an extended concept of the "100mg approach". *Eur J Pharm Sci* **2014**, *57*, 257-263.

(68) Berry, D. J.; Steed, J. W. Pharmaceutical cocrystals, salts and multicomponent systems; intermolecular interactions and property based design. *Adv Drug Deliv Rev* **2017**, *117*, 3-24.

(69) Jurczak, E.; Mazurek, A. H.; Szeleszczuk, L.; Pisklak, D. M.; Zielinska-Pisklak, M. Pharmaceutical Hydrates Analysis-Overview of Methods and Recent Advances. *Pharmaceutics* **2020**, *12* (10).

(70) Jarosz, M.; Szkaradek, N.; Marona, H.; Nowak, G.; Mlyniec, K.; Librowski, T. Evaluation of anti-inflammatory and ulcerogenic potential of zinc-ibuprofen and zinc-naproxen complexes in rats. *Inflammopharmacology* **2017**, *25* (6), 653-663.

(71) Fosmire, G. J. Zinc toxicity. *Am J Clin Nutr* **1990**, *51* (2), 225-227.

(72) Saha, S.; Desiraju, G. R. Acid...Amide Supramolecular Synthon in Cocrystals: From Spectroscopic Detection to Property Engineering. *J Am Chem Soc* **2018**, *140* (20), 6361-6373.

(73) Li, D.; Kong, M.; Li, J.; Deng, Z.; Zhang, H. Amine–carboxylate supramolecular synthon in pharmaceutical cocrystals. *CrystEngComm* **2018**, *20* (35), 5112-5118.

(74) Desiraju, G. R. Supramolecular Synthons in Crystal Engineering—A New Organic Synthesis. *Angewandte Chemie International Edition in English* **1995**, *34* (21), 2311-2327.

(75) Smokrović, K.; Muratović, S.; Karadeniz, B.; Užarević, K.; Žilić, D.; Đilović, I. Synthon Robustness and Structural Modularity of Copper(II) Two-Dimensional Coordination Polymers with Isomeric Amino Acids and 4,4′-Bipyridine. *Crystal Growth & Design* **2020**, *20* (4), 2415-2423.

(76) Decurtins, S. Multifunctional Coordination Compounds: Design and Properties. *CHIMIA International Journal for Chemistry* **1998**, *52* (10), 539-546.

(77) Li, X.; Cao, R.; Sun, D.; Bi, W.; Wang, Y.; Li, X.; Hong, M. Syntheses and Characterizations of Zinc(II) Compounds Containing Three-Dimensional Interpenetrating Diamondoid Networks Constructed by Mixed Ligands. *Crystal Growth & Design* **2004**, *4* (4), 775-780.

(78) Ye, H.-T.; Ren, C.-Y.; Hou, G.-F.; Yu, Y.-H.; Xu, X.; Gao, J.-S.; Yan, P.-F.; Ng, S.-W. Syntheses, Structures, and Second-Order Nonlinear Optical Properties of Chiral Zinc(II) Coordination Polymers Based on (R)-4-(4-(1-Carboxyethoxy)phenoxy)-3-fluorobenzoic Acid and Effect of the Second Ligand with Imidazole Group. *Crystal Growth & Design* **2014**, *14* (7), 3309-3318.

(79) Leng, F.; Robeyns, K.; Leyssens, T.; Shemchuk, O. Combining Racetams with a Sweetener through Complexation. *Crystal Growth & Design* **2022**, *22* (5), 3016-3023.

(80) Yuliandra, Y.; Zaini, E.; Syofyan, S.; Pratiwi, W.; Putri, L. N.; Pratiwi, Y. S.; Arifin, H. Cocrystal of Ibuprofen(-)Nicotinamide: Solid-State Characterization and In Vivo Analgesic Activity Evaluation. *Sci Pharm* **2018**, *86* (2).

(81) Walsh, D.; Serrano, D. R.; Worku, Z. A.; Madi, A. M.; O'Connell, P.; Twamley, B.; Healy, A. M. Engineering of pharmaceutical cocrystals in an excipient matrix: Spray drying versus hot melt extrusion. *Int J Pharm* **2018**, *551* (1-2), 241-256.

(82) Dos Santos, P. R.; Pich, C. T.; Back, D.; Smiderle, F.; Dumas, F.; Moura, S. Synthesis, chemical characterization and DNA interaction study of new diclofenac and ibuprofen zinc (II)-nicotinamide ternary complexes as cyclooxygenase inhibitor prototypes. *J Inorg Biochem* **2020**, *206*, 111046.

(83) Berry, D. J.; Seaton, C. C.; Clegg, W.; Harrington, R. W.; Coles, S. J.; Horton, P. N.; Hursthouse, M. B.; Storey, R.; Jones, W.; Friščić, T.; et al. Applying Hot-Stage Microscopy to Co-Crystal Screening: A Study of Nicotinamide with Seven Active Pharmaceutical Ingredients. *Crystal Growth & Design* **2008**, *8* (5), 1697-1712.

(84) Ngilirabanga, J. B.; Aucamp, M.; Pires Rosa, P.; Samsodien, H. Mechanochemical Synthesis and Physicochemical Characterization of Isoniazid and Pyrazinamide Co-crystals With Glutaric Acid. *Front Chem* **2020**, *8*, 595908.

(85) Nugrahani, I.; Kumalasari, R. A.; Auli, W. N.; Horikawa, A.; Uekusa, H. Salt Cocrystal of Diclofenac Sodium-L-Proline: Structural, Pseudopolymorphism, and Pharmaceutics Performance Study. *Pharmaceutics* **2020**, *12* (7).

Chapter 4

4. Alloying through a cocrystal solid solution (in progress)

Until now, complexation has demonstrated great potential in the design of multi-component pharmaceutical crystals. But it still faces the problem of an inflexible compound ratio. In this chapter, a novel piracetam-oxiracetam(S)-gallic acid system was developed, in which the ratio of piracetam and oxiracetam(S) can be varied over the full range. This work is still in progress and written in article format.

4.1 Abstract:

In this work, a solid solution of two drugs both acting on the central nervous system, piracetam and S-oxiracetam, was successfully prepared by the introduction of a third component - gallic acid. These drugs cannot be formulated in a single solid form without the introduction of this additional component. To the best of our knowledge, this is the first example of a drug-drug solid solution which can be tuned freely in any ratio.

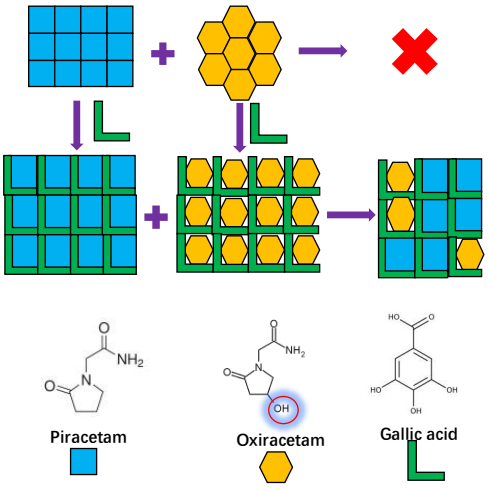

Conceptualization, T.L. and K.R.; methodology, T.L.; software, K.R.; validation, T.L., K.R. and F.L.; formal analysis, F.L.; investigation, F.L.; data curation, F.L.; writing—original draft preparation, F.L.; writing—review and editing, T.L. and K.R.; supervision, T.L. and K.R.; project administration, T.L.; funding acquisition, T.L.

4.2 Introduction

Combining multiple drugs with synergistic or complementary effect has been a widely used approach in the treatment of chronic and complex diseases like diabetes, cancer, and cardiovascular disorders.[1, 2] However, the simultaneously taking of various drugs can lead to poor patient compliance. FDC is a widely used method to combine various drugs in a single formulation.[3] However, this method cannot be applied if the various APIs have distinct physical properties, and hence interact differently with the various excipients.[4] To circumvent this issue, APIs can be combined in a single crystal form, as this not only offers a simple and elegant way to combine drugs but also endows the parent APIs with improved physical properties.[5-8] One such approach to combine multiple APIs in a single crystal form is through the formation of a salt. For instance, epalrestat and metformin were successfully incorporated in a single salt showing improved solubility (for epalrestat) and moisture stability (for metformin).[9] Alternatively, drugs can be combined in a cocrystal (e.g. the cocrystal between meloxicam and aspirin possesses improved solubility in a pH 7.4 phosphate buffer and 4-fold bioavailability[10]).

Although these crystal engineering methods have been very successful for the development of multi-drug systems, they suffer from the inflexibility to vary the API ratio.[11] Indeed, literature shows a 1:1 or 1:2 ratio for all reported drug-drug cocrystals or salts , which may not always be the ideal ratio required for clinical applications.[5] To achieve a flexible API ratio in one solid form, a different approach in crystal engineering approach can be applied based on the use of a API-API solid solutions,.[12, 13] To date, only a limited amount of API-API solid solution have been reported, namely cytosine/5-flucytosine, Aripiprazole/Dehydro-Aripiprazole, and Lamivudine/emtricitabine.[14-16] In case of the latter system, both molecules only differ by a fluoride/hydrogen atom. Even so, a complete solid solution cannot be achieved over the full range, suggesting the high requirement of structural resemblance of the two parent APIs during solid solution formation.

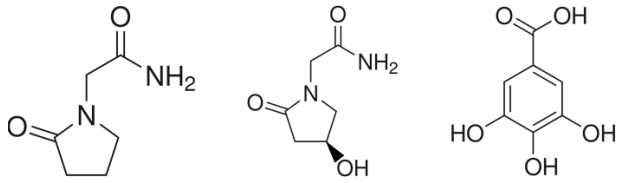

Piracetam **S-oxiracteam** **Gallic acid**

Figure 4.1. chemical structure of piracetam, S-oxiracetam and gallic acid.

Marketed in 1972, Pir (2-oxo-1-pyrrolidinyl-acetamide, Figure 4.1) has been widely used in the treatment of memory and balance problems.[17] Similarly, its analogue Oxi (4-hydroxy-2-oxo-l-pyrrolidineacetamide) has also shown its effectiveness in the treatment of cognitive impairments.[18] Recent research has shown that it is the S-enantiomer of this API (S-oxiracetam (Oxi(S)), Figure 4.1) that exhibits the desired pharmaceutical activity.[19] With similar effect on the central nerve system while different metabolic rate in the human body, it is assumed Pir and Oxi(S) may be effective at a different time after drug delivery, so as to increase the effective duration of the drug. it is Although Pir and Oxi(S) are relatively similar, differing only by the hydroxyl group, any attempt to combine them directly was found unsuccessful. We here use a crystal engineering approach, to successfully combine both APIs. To do so we engineer the structure of both parent compounds so as to come to structurally resembling solids. This can be achieved linking both parent compounds to GA. We then show how both cocrystal parents form a solid solution, leading to a system in which the Pir and Oxi(S) ratio can be freely modulated.

4.3 Materials and methods

Materials. Piracetam was bought from Xiamen Top Health Biochem Tech. Co., Ltd, S-oxiracetam from BLDpharm, GA from Sigma-Aldrich. All compounds were used as such.

Single crystal growth. Excessive amounts of Pir, Oxi(S) and GA were slurried separately in methanol overnight to obtain saturated solutions. After this, one of the various vials were combined in a volume ratio of x:1-x:1 (Pir : Oxi(S) : GA, x ranging from 0 to 1). The vials were left to evaporate slowly. Block like crystals were harvested after one to two days.

SCXRD. Data were collected on a MAR345 image plate detector using Mo Kα radiation (λ = 0.71073 Å), generated by an Incoatec IμS microfocus source. Data

integration and reduction was performed by CrysAlis^{PRO} and the implemented absorption correction was applied. Structure solution was performed by the dual-space algorithm in SHELXT and the structure was further refined against F^2 using SHELXL2014/7.[20] All non-hydrogen atoms were refined anisotropically and hydrogen atoms were placed at calculated positions with temperature factors set at 1.2Ueq of the parent atoms (1.5Ueq for methyl and OH hydrogens).

Construction of the Phase Diagram. Pir, Oxi(S) and GA were ground together in a ratio of x:1-x:1, x ranged from 0 to 1. After that, about 10 mg of the mixture was added to a 20mL vial and the solid left to slurry in 5 mL of acetonitrile for 2 hours. Subsequently, 50 μL of acetonitrile was added to the vial every 30 min until the suspension became clear. The total amount of acetonitrile is used to determine the solubility line of the phase diagram.

4.4 Results and discussion

Due to the high requirement on structure similarity in the formation of solid solutions, traditional solid solution systems are normally composed of analogues with differences in Cl/Br, Br/CH_3, H/F. The high mutual solubility in the solid state is not expected for H/OH analogues as the hydroxyl group is typically involved in hydrogen bonding networks, which usually leads to a different structure and, thus, immiscibility at the solid state.[21] Oxi(S) only has one reported polymorph, in which the hydroxyl group forms a hydrogen bond with the keto group from pyrrolidine.[22] While in Pir, due to the absence of the hydroxyl group, only the amide group is connected to the keto group from pyrrolidine of another Pir.[23] With such differences in bonding patterns, it could be expected mixing of Pir and Oxi(S) only results in the physical mixture, which is also evidenced by the experiment result.

We further considered the possibility to make Pir and Oxi(S) share identical crystal structures through crystal engineering. As salt formation is not an option for both parent compounds, we turned to cocrystal formation as engineering tool. Among all reported cocrystals, GA-Oxi(S) attracted our interest.[24] The asymmetric unit of GA-Oxi(S) is composed of two pairs of GA and Oxi(S) molecules. For every GA/OXI(S) pair, connected by a hydrogen bond between the carboxylic acid (GA) and the keto group (Oxi(S)), the benzene ring of GA and the pyrrolidine of Oxi(S) are roughly coplanar (Figure 4.2a). In plane A, the hydroxyl group of Oxi(S) is hydrogen bonded to the hydroxyl group of GA of a second pair. Expanding the structure through symmetry, one can clearly observe that four GA (almost perpendicular to plane A and B) fix two planes through hydrogen bonds (Figure 4.2b). Interestingly, although GA-

Oxi(S) and GA-Oxi(racemic) crystalize in $P2_1$ and $P2_1/c$ respectively, they still bear almost the same unit cell and hydrogen bonding network (Figure 4.2c). The most interesting thing is that all hydroxyl groups in GA-Oxi(S) join the formation of the hydrogen bonds network, while in GA-Oxi(racemic), only about 1/3 hydroxyl groups form hydrogen bond with GA, which may suggest the hydrogen bonds between hydroxyl group and GA are not necessary for the construction of the crystal packing, which means Pir could replace Oxi(S) in GA-Oxi(S).

Bearing these in mind, we started to look for the GA-Pir cocrystal, which was reported by Chick C. Wilson in 2016.[25] As expected, the lack of hydroxyl group does not influence the formation of the hydrogen bonding network. The GA-Pir cocrystal is isostructural with the GA-Oxi(S) cocrystal (Figure 4.2d) Thus, we started to explore the possibility of a GA-Pir/Oxi(S) solid solution.

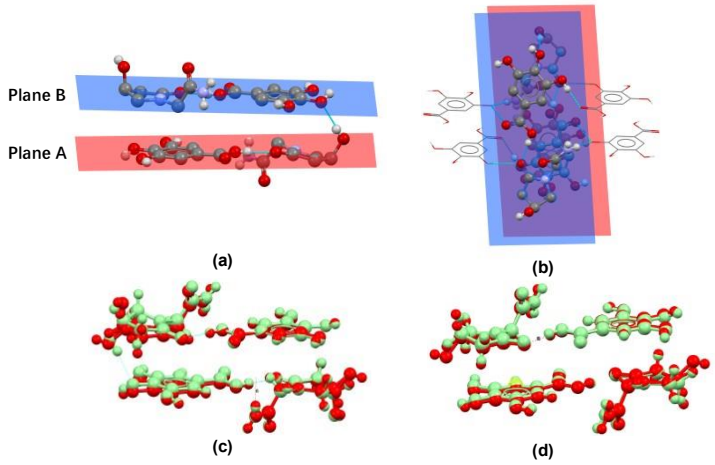

Figure 4.2. (a) the layer structure in GA-Oxi(S) (b) connecting between layers through GA. (c) structure overlay between GA-Oxi(S) and GA-Oxi(racemic) (d) structure overlay between GA-Oxi(S) and GA-Pi

As the solubility of Pir and Oxi(S) are very different in methanol, the crystals obtained from a solution of Pir and Oxi(S) always possess a much higher Pir/Oxi(S) ratio compared to the solution. To fine-tune the Pir/Oxi(S) ratio in crystals, Pir and Oxi(S) were first dissolved in methanol to obtain a saturated solution. After that, the saturated solution was mixed in a specific ratio, from which a series of GA-Pir/Oxi(S) solid solutions were successfully prepared from solution. The wide concentration range of Pir and Oxi(S) suggests GA-Pir/Oxi(S) is not a partially solid solution in which the

concentration of two starting materials could only be tuned in a limited range. Interestingly, unlike most solid solutions which obey Vegard's rule,[26] the unit cell volume of GA-Pi/Oxi(S) increases and then decreases with the increasement of Oxi(S) ratio in crystal (Figure 4.3).

Table 4.1. crystallography table of GA-Pi/Oxi(S) solid solution in different ratio

Empirical formula	$C_{26}H_{32}N_4O_{16}$ **OXI(S)**	$C_{26}H_{32}N_4O_{15.5}$ **OXI(S) / Pir**	$C_{26}H_{32}N_4O_{15.34}$ **OXI(S) / Pir**	$C_{26}H_{32}N_4O_{14.92}$ **OXI(S) / Pir**	$C_{26}H_{32}N_4O_{14.4}$ **OXI(S) / Pir**	$C_{13}H_{16}N_2O_7$ **Pir**
Space group	$P2_1$	$P2_1$	$P2_1$	$P2_1$	$P2_1$	$P2_1/c$
a/Å	12.5429(9)	12.5930 (14)	12.5773 (11)	12.5915 (11)	12.5926 (15)	12.6186(15)
b/Å	9.0041 (7)	9.0187 (10)	9.0021 (6)	8.9948 (10)	8.9679 (11)	8.9621 (11)
c/Å	12.8134(11)	12.7746(12)	12.7233(14)	12.6726(14)	12.6297(12)	12.6078(16)
α/°	90	90	90	90	90	90
β/°	103.008(8)	103.107(10)	103.234(10)	103.380(10)	103.492(11)	103.362(13)
γ/°	90	90	90	90	90	90
Volume/Å^3	1410.0 (2)	1413.0 (3)	1402.3 (2)	1396.3 (3)	1386.9 (3)	1387.2 (3)
Z	2	2	2	2	2	4
Z'	2	2	2	2	2	1
ρ_{calc}g/cm^3	1.387	1.516	1.53	1.534	1.513	1.495
μ/mm^{-1}	0.115	0.127	0.128	0.128	0.125	0.123
F(000)	589	677	677	677	663	656
2θ range /°	6.628-52.208	6.638-52.232	6.658-50.67	6.116-52.374	5.63-52.328	6.134-52.382
Refl. collected	9693	9795	8914	9636	9635	9145
R_{int}	0.0372	0.0404	0.0417	0.0701	0.0475	0.0383
Data/restr/ para	5373/1/ 425	5380/129/ 459	5041/129/ 471	5450/129/ 471	5394/116/ 471	2762/0/ 205
GooF	1.149	1.035	1.127	1.04	1.055	1.045
Final R indexes [I>=2σ (I)]	R_1=0.0423 wR_2=0.1363	R_1=0.0409 wR_2=0.1027	R_1=0.0439 wR_2=0.1275	R_1=0.0542 wR_2=0.1397	R_1=0.0502 wR_2=0.1373	R_1=0.0391 wR_2=0.0989
Final R indexes [all data]	R_1= 0.0456 wR_2=0.1397	R_1=0.0477 wR_2=0.1068	R_1=0.0517 wR_2=0.1434	R_1=0.0738 wR_2=0.1545	R_1=0.0672 wR_2=0.1509	R_1=0.049 wR_2=0.1048
Ratio of Oxi(S) in solid solution based on refinement	100%	75%	67%	46%	20%	0

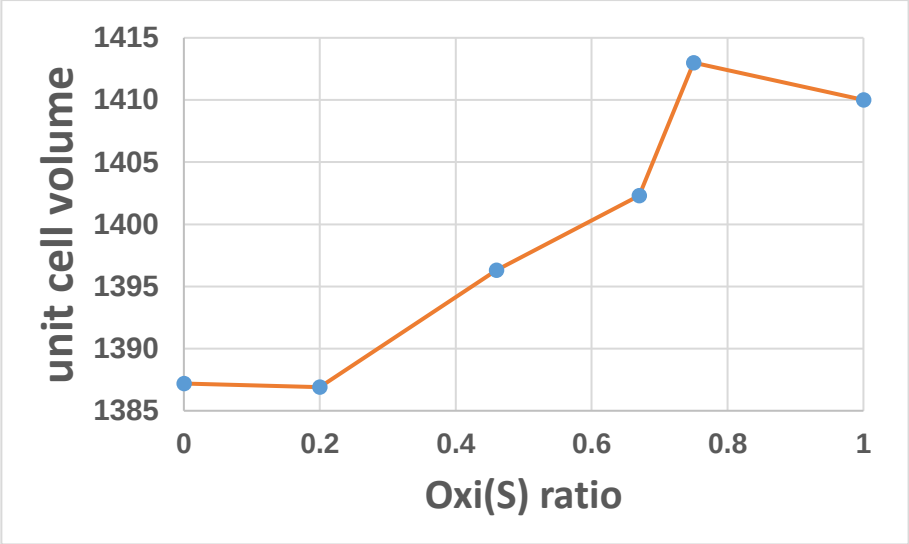

Figure 4.3 the relationship between unit cell volume and molar ratio of Oxi(S) in GA-Pi/Oxi(S).

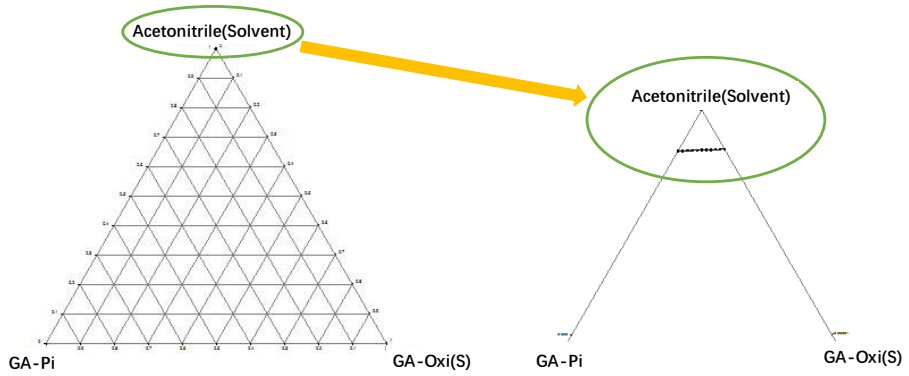

Figure 4.4. Phase diagram of GA-Pir/Oxi(S) solid solution.

A ternary phase diagram was constructed to confirm the solid solution formation. As shown on Figure 4.3, there is almost no variability in the solubility of the solid solution upon changing the Pir/Oxi(S) ratio. Such a diagram is characteristic of solid solutions. To be able to control the outcome of the crystallization experiment, appropriate tie-lines, need to be constructed. Once known, these can guide the crystallization process.

4.5 Conclusion

Through cocrystallizing with gallic acid, two immiscible drugs piracetam and S-oxiracetam were combined in one crystal form in any ratio, by formation of a cocrystal solid solution. This work offered the first drug-drug solid solution with freely tunable ratio.

References

(1) Hasselt, J. G. C. v.; Iyengar, R. Systems Pharmacology: Defining the Interactions of Drug Combinations. *Annual Review of Pharmacology and Toxicology* **2019**, *59* (1), 21-40.

(2) Vakil, V.; Trappe, W. Drug Combinations: Mathematical Modeling and Networking Methods. *Pharmaceutics* **2019**, *11* (5).

(3) Wan, X.; Ma, P.; Zhang, X. A promising choice in hypertension treatment: Fixed-dose combinations. *Asian Journal of Pharmaceutical Sciences* **2014**, *9* (1), 1-7.

(4) Frantz, S. The trouble with making combination drugs. *Nat Rev Drug Discov* **2006**, *5* (11), 881-882.

(5) Wang, X.; Du, S.; Zhang, R.; Jia, X.; Yang, T.; Zhang, X. Drug-Drug Cocrystals: Opportunities and Challenges. *Asian Journal of Pharmaceutical Sciences* **2020**.

(6) Bolla, G.; Nangia, A. Pharmaceutical cocrystals: walking the talk. *Chem Commun (Camb)* **2016**, *52* (54), 8342-8360.

(7) Thakuria, R.; Sarma, B. Drug‐Drug and Drug‐Nutraceutical Cocrystal/Salt as Alternative Medicine for Combination Therapy: A Crystal Engineering Approach. *Crystals* **2018**, *8* (2).

(8) Thipparaboina, R.; Kumar, D.; Chavan, R. B.; Shastri, N. R. Multidrug co-crystals: towards the development of effective therapeutic hybrids. *Drug Discov Today* **2016**, *21* (3), 481-490.

(9) Sun, J.; Jia, L.; Wang, M.; Liu, Y.; Li, M.; Han, D.; Gong, J. Novel Drug–Drug Multicomponent Crystals of Epalrestat–Metformin: Improved Solubility and Photostability of Epalrestat and Reduced Hygroscopicity of Metformin. *Crystal Growth & Design* **2022**, *22* (2), 1005-1016.

(10) Cheney, M. L.; Weyna, D. R.; Shan, N.; Hanna, M.; Wojtas, L.; Zaworotko, M. J. Coformer selection in pharmaceutical cocrystal development: a case study of a meloxicam aspirin cocrystal that exhibits enhanced solubility and pharmacokinetics. *J Pharm Sci* **2011**, *100* (6), 2172-2181.

(11) Wong, S. N.; Chen, Y. C. S.; Xuan, B.; Sun, C. C.; Chow, S. F. Cocrystal engineering of pharmaceutical solids: therapeutic potential and challenges. *CrystEngComm* **2021**.

(12) Lusi, M. A rough guide to molecular solid solutions: design, synthesis and characterization of mixed crystals. *CrystEngComm* **2018**, *20* (44), 7042-7052.

(13) Lusi, M. Engineering Crystal Properties through Solid Solutions. *Crystal Growth & Design* **2018**, *18* (6), 3704-3712.

(14) Braun, D. E.; Kahlenberg, V.; Griesser, U. J. Experimental and Computational Hydrate Screening: Cytosine, 5-Flucytosine and Their Solid Solution. *Cryst Growth Des* **2017**, *17* (8), 4347-4364.

(15) Trotta, J. T.; Zeidan, T. A.; Tilak, P. A.; Foxman, B. M.; Almarsson, Ö.; Oliveira, M. A.; Chiarella, R. A.; Hickey, M. B.; Remenar, J. F. Aripiprazole and Dehydro-Aripiprazole Solid Solutions: Crystalline Combinations of Drug and Active Metabolite in Tailored Compositions. *Crystal Growth & Design* **2020**, *20* (6), 3944-3956.

(16) Fonseca, J. d. C.; Tenorio Clavijo, J. C.; Alvarez, N.; Ellena, J.; Ayala, A. P. Novel Solid Solution of the Antiretroviral Drugs Lamivudine and Emtricitabine. *Crystal Growth & Design* **2018**, *18* (6), 3441-3448.

(17) Winblad, B. Piracetam: a review of pharmacological properties and clinical uses. *CNS Drug Rev* **2005**, *11* (2), 169-182.

(18) Dager, S. R.; Loebel, J. P.; Claypool, K.; Case, M.; Budech, C. B.; Dunner, D. L. Oxiracetam in the treatment of primary dementia of the Alzheimer's type: A small case series. *International Journal of Geriatric Psychiatry* **1992**, *7* (12), 905-912.

(19) Li, W.; Liu, H.; Jiang, H.; Wang, C.; Guo, Y.; Sun, Y.; Zhao, X.; Xiong, X.; Zhang, X.; Zhang, K.; et al. (S)-Oxiracetam is the Active Ingredient in Oxiracetam that Alleviates the Cognitive Impairment Induced by Chronic Cerebral Hypoperfusion in Rats. *Sci Rep* **2017**, *7* (1), 10052.

(20) Sheldrick, G. M. Crystal structure refinement with SHELXL. *Acta Crystallogr C Struct Chem* **2015**, *71* (Pt 1), 3-8.

(21) Cruz-Cabeza, A. J.; Lestari, M.; Lusi, M. Cocrystals Help Break the “Rules” of Isostructurality: Solid Solutions and Polymorphism in the Malic/Tartaric Acid System. *Crystal Growth & Design* **2017**, *18* (2), 855-863.

(22) Shemchuk, O.; Song, L.; Tumanov, N.; Wouters, J.; Braga, D.; Grepioni, F.; Leyssens, T. Chiral Resolution of RS-Oxiracetam upon Cocrystallization with Pharmaceutically Acceptable Inorganic Salts. *Crystal Growth & Design* **2020**, *20* (4), 2602-2607.

(23) Fabbiani, F. P. A.; Allan, D. R.; Parsons, S.; Pulham, C. R. An exploration of the polymorphism of piracetam using high pressure. *CrystEngComm* **2005**, *7* (29).

(24) Wang, Z.-Z.; Chen, J.-M.; Lu, T.-B. Enhancing the Hygroscopic Stability of S-Oxiracetam via Pharmaceutical Cocrystals. *Crystal Growth & Design* **2012**, *12* (9), 4562-4566.

(25) Thomas, L. H.; Wales, C.; Wilson, C. C. Selective preparation of elusive and alternative single component polymorphic solid forms through multi-component crystallisation routes. *Chem Commun (Camb)* **2016**, *52* (46), 7372-7375.

(26) Denton, A. R.; Ashcroft, N. W. Vegard's law. *Phys Rev A* **1991**, *43* (6), 3161-3164.

5. Summary, Conclusions and Perspectives

Combining desired molecules with specific APIs is an interesting approach during the design of new drug solid forms. Unfortunately, traditional design methods like binary salt or cocrystal formation, are not always feasible and suffer from low success rates. In this thesis, we explore some new crystal engineering methodologies for combining desired APIs which cannot be coupled at the solid state through the more traditional methods.

Our first approach was to explore the possibility of a ternary cocrystal using a small organic linker. Urea was selected as a bridge to connect two other APIs together. Sadly enough, this approach turned out to be unsuccessful, as no ternary cocrystal API1-urea-API2 could be identified. However, the screen between urea and a series of APIs gave three binary cocrystals including urea-catechin, urea-3-hydroxyl-2-naphthoic acid and urea-ellagic acid, which were fully characterized. Through cocrystallization with urea, the stability of catechin with respect to humidity or temperature was improved. Moreover, the solubility of ellagic acid was found 17 times higher in case of the cocrystal.

We then turned to a second strategy combining different molecules through complexation with a metal. This approach turned out to be successful (Figure 5.1a). This strategy is first tested combining a famous sweetener, saccharin, and 6 nootropic racetam drugs. Binary cocrystallization did not allow combining saccharin and racetams. However, a metal can be introduced simply converting saccharin to its salt form. Doing so, a successful combination between saccharinate salts and racetams can be obtained for all possible combinations. These solid forms are characterized by a complex solid-state landscape through the existence of various solvates of the obtained complexes, involving water as well as organic solvents. This shows the complexity surrounding these complexes, rendering the prediction of their structural assembly non-trivial. Despite the large variety in structural features, all complexes remained stable under ambient conditions and can be easily obtained through mechanochemical or solution-based methodologies, all showing increased thermal stability.

Inspired by the successes of the racetam-saccharin combination, we explored this strategy to combined two drug molecules. Going through literature, the coordination mode of zinc should favor carboxylic acid-zinc-pyridine bonding.[1, 2] Following this synthon-guided approach five different pyridine-based drugs and 3 carboxylic acid containing drugs were selected leading to successful drug-drug complex formation. Moreover, tetra-, penta-, and hexa-coordinated complexes were obtained in agreement with literature-based structures involving the zinc cation. As for any solid-state form, the dual-drug complexes studied in this work also show solvatism and polymorphism, as well as stoichiometric diversity.

Our final strategy, allowing to couple drug compounds makes use of the concept of solid solutions(Figure 5.1b). Although piracetam and S-oxiracetam share almost the same chemical structure, the introduction of the extra hydroxyl group in S-oxiracetam leads to completely different structures for these compounds. This renders a direct solid solution formation impossible. Interestingly, their cocrystal with gallic acid shows similar structures characterized by identical hydrogen bonding networks. Based on the principle of similarity, a solid solution between gallic acid-piracetam and gallic acid-oxiracetam(S) can be successfully obtained.

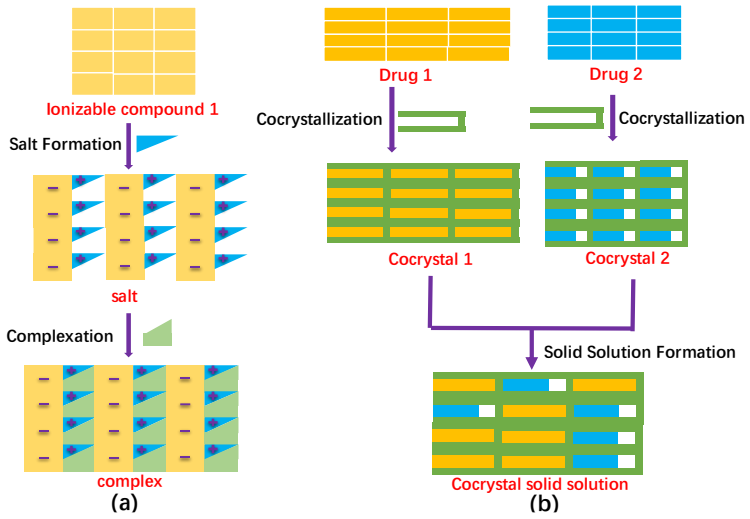

Figure 5.1. Two successful methodologies developed in this thesis for multicomponent crystal design.

In conclusion, this thesis not only presented dozens of new multi-component pharmaceutical crystals with improved physical properties but also demonstrated two innovative methodologies for designing and synthesizing multi-component crystals including complexation and cocrystal solid solution. With the guidance of structure analysis, uncombined molecules (in traditional method) could be bond in one crystal with a desired ratio. There are still plenty of unexplored areas in pharmaceutical crystal design beyond traditional pharmaceutical solid state like salt formation or cocrystallization.

From a general point of view, the strategies developed could be regarded as the combination of traditional methods: the ternary cocrystal strategy can be considered as the combination of two binary cocrystals, the complexation strategy as the combination of a salt and a neutral API and the solid solution as the solid solution between two cocrystals. From this point of view, future contributions to this work are obvious: can we use what we learned to develop more complicated systems? Some exploratory work has been done in this direction. Saccharin can be transformed to its magnesium and calcium form, and further combined with piracetam, giving two crystals having very similar structures. After that, the saccharinate-Ca/Mg-piracetam solid solution was successfully synthesized. Our exploratory experiments demonstrated saccharinate-Ca-piracetam and saccharinate-Mg-piracetam have distinct solubility as well as thermal stability. Based on our experience working with solid solutions, the melting point and solubility could be tuned freely through the modulation of the Ca/Mg ratio in this solid solution, which is meaningful in drug solid-form design.

The obvious challenge remains in the predication or design of the desired combination. For example, the success rate of cocrystallization is about 10%. Our work demonstrates a higher success rate could be achieved through complexation, but the favored coordination mode is hard to identify especially for metals like Ca/Mg/Na/K in pharmaceutical salts, whose coordination is also typically impacted by water. As for the solid solution system, our work shows molecules differing only by a hydroxyl group could form solid solutions by the assistance of third coformer. But identifying or even designing such a coformer remains problematical. Although some progress is currently being made in literature, this task remains a trial and error approach. The most important challenge or aspiration in the area of crystal engineering, remains the development of a truly predictive design strategy to multi-component crystals, in a true Lego-approach: building a multicomponent crystal purely based on molecular structure and connectivity.

(1) ZareKarizi, F.; Joharian, M.; Morsali, A. Pillar-layered MOFs: functionality, interpenetration, flexibility and applications. *Journal of Materials Chemistry A* **2018**, *6* (40), 19288-19329.

(2) Dos Santos, P. R.; Pich, C. T.; Back, D.; Smiderle, F.; Dumas, F.; Moura, S. Synthesis, chemical characterization and DNA interaction study of new diclofenac and ibuprofen zinc (II)-nicotinamide ternary complexes as cyclooxygenase inhibitor prototypes. *J Inorg Biochem* **2020**, *206*, 111046.

(1) ZareKarizi, F.; Joharian, M.; Morsali, A. Pillar-layered MOFs: functionality, interpenetration, flexibility and applications. *Journal of Materials Chemistry A* **2018**, *6* (40), 19288-19329.

(2) Dos Santos, P. R.; Pich, C. T.; Back, D.; Smiderle, F.; Dumas, F.; Moura, S. Synthesis, chemical characterization and DNA interaction study of new diclofenac and ibuprofen zinc (II)-nicotinamide ternary complexes as cyclooxygenase inhibitor prototypes. *J Inorg Biochem* **2020**, *206*, 111046.

Appendices

Appendix A

A. Supporting information for Chapter 2

Table A.1. List of APIs in cocrystal screen. Green for new cocrystals and yellow for reported cocrystals. (The CCDC numbers of UC, UH and UE are 2076912-2076914, their cif files can be obtained free of charge from The Cambridge Crystallographic Data Centre via www.ccdc.cam.ac.uk/structures. The Refcode of urea-theophylline, urea-salicylic acid, urea-nicotinamide, and urea-hydroquinone cocrystals are DUXZAX, SLCADC, ZUYLAI, QUOLUR, their cif files could also be obtained from the same webpage)

Naproxen	Ketoprofen	Ibuprofen
Aspirin	Caffeine	Phenacetine
Acetaminophen	Theophylline	Levetiracetam
Pramiracetam	Fasoracetam	Carphedon
Sunifiram	Aniracetam	Piracetam
Nefiracetam	Coluracetam	Nicotinamide
Idebenone	Fladrafinil	Oxcarbamazepine
Salicylamide	L-penicillamine	Diprophylline
Primidone	Xanthine	Sulfathiazole
Theophylline-7-acetic acid	Hydroquinone	Phloroglucinol
Isonicotinic acid	Etofylline	Dyphylline
2-Ehoxybenzamide	3-Hydroxy-2-naphthoic acid	Sulfacetamide
L-Ascorbic acid	4-Nitroaniline	Anthranilic acid
Acetanilide	Formanilide	Thiobenzamide
Nicotinic acid	3-Aminobenzamide	Praziquantel
S-methyl-L-cysteine	L-Pyroglutamic acid	Indoprofen
Lidocaine	Ellagic acid	Flurbiprofen
Quercetin	Rutin	Catechin
Epicatechin	Salicylic acid	

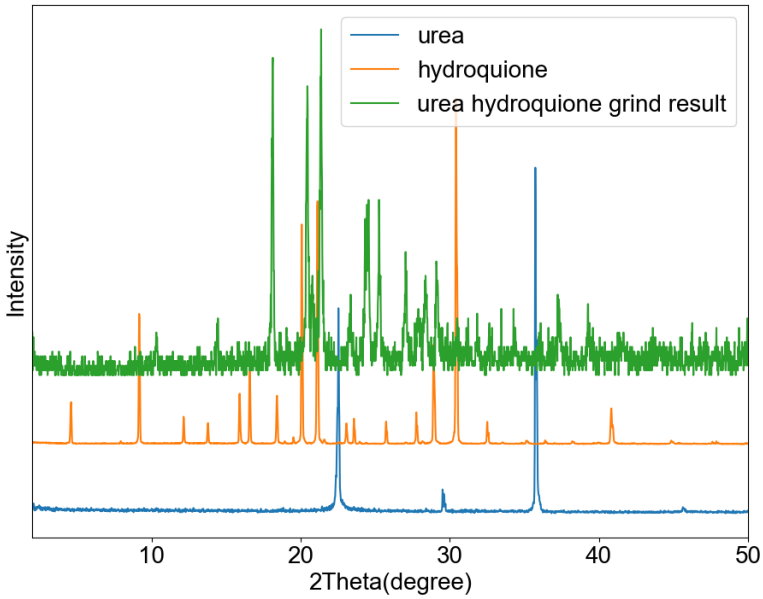

Figure A.1. PXRD profiles of urea, hydroquion, and urea hydroquione cocrystal obtained by grinding

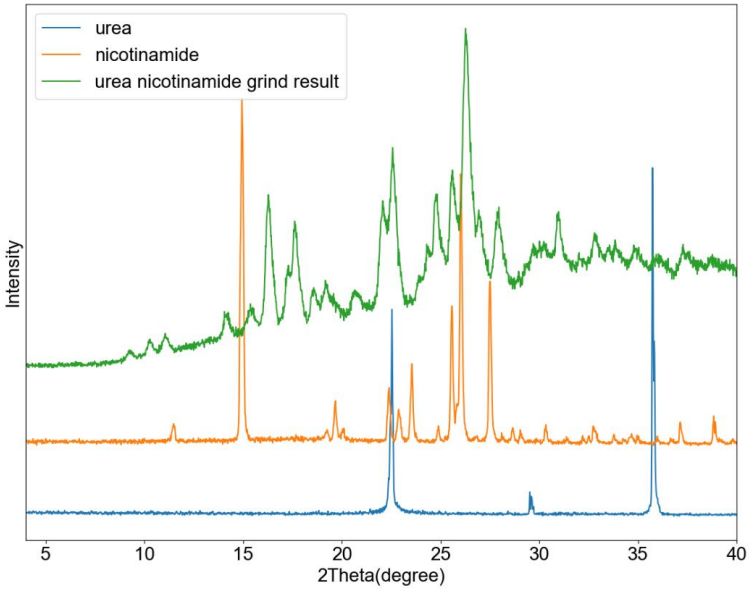

Figure A.2. PXRD profiles of urea, nicotinamide, and urea nicotinamide cocrystal obtained by grinding

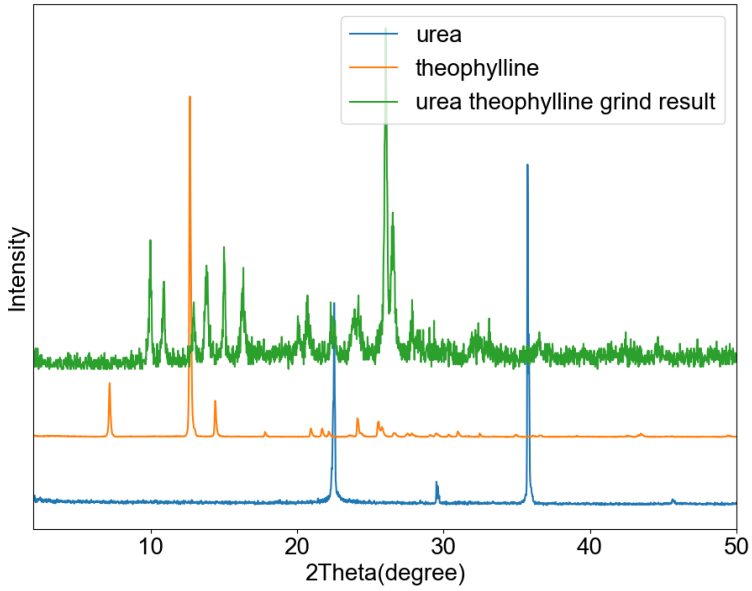

Figure A.3. PXRD profiles of urea, theophylline, and urea theophylline cocrystal obtained by grinding

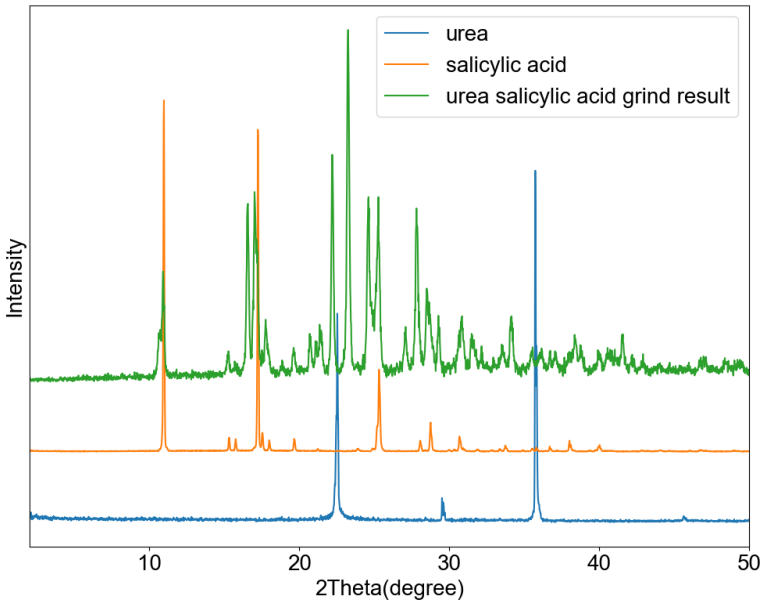

Figure A.4. PXRD profiles of urea, salicylic acid, and urea salicylic acid cocrystal obtained by grinding

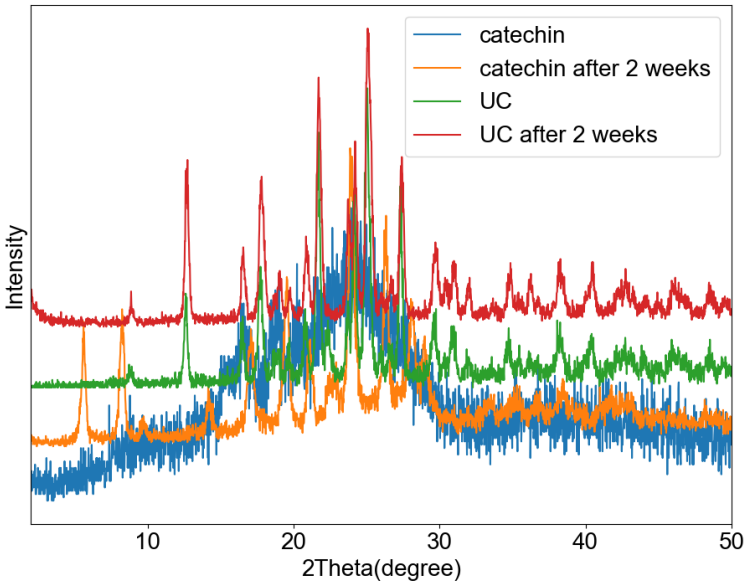

Figure A.5. PXRD profiles of catechin and UC before and after storage at 25 ℃ and 75% relative humidity for two weeks.

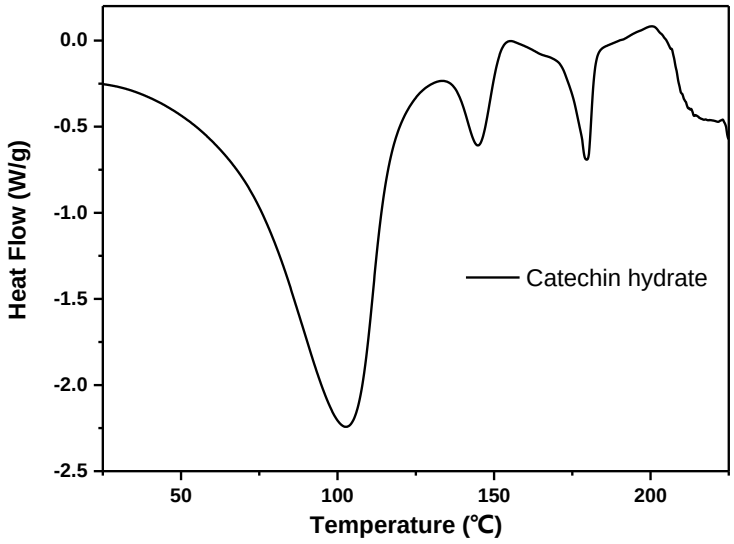

Figure A.6. DSC curve of catechin hydrate

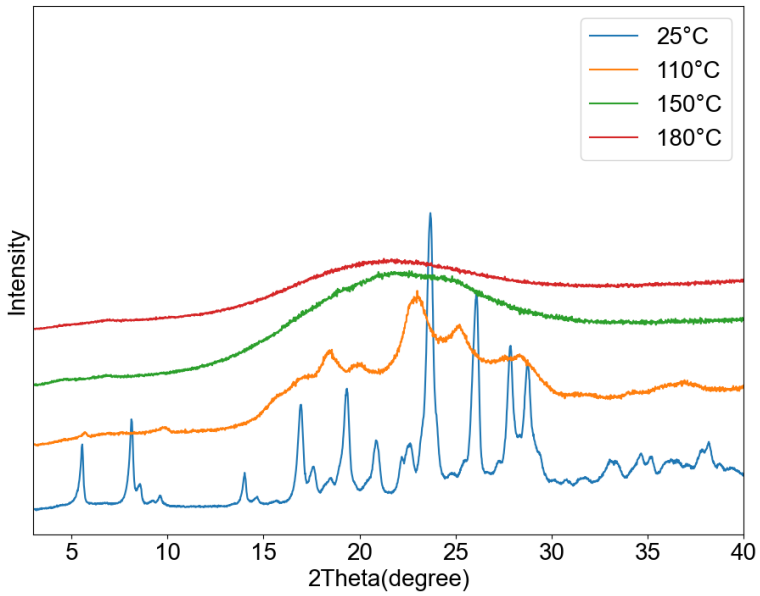

Figure A.7. VT-PXRD profile of catechin hydrate.

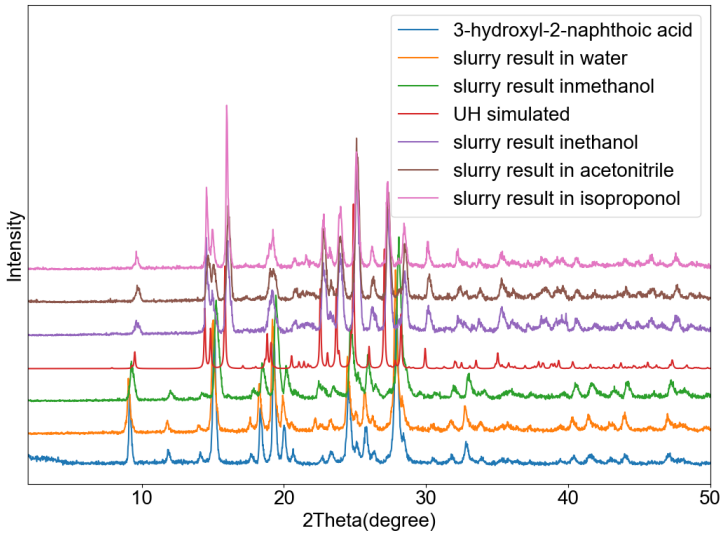

Figure A.8. PXRD of UH congruency experiments in different solvents

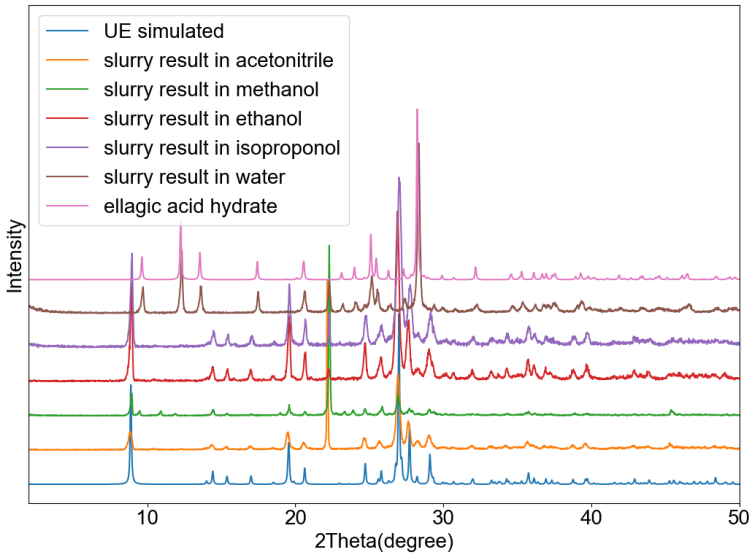

Figure A.9. PXRD of UE congruency experiments in different solvents.

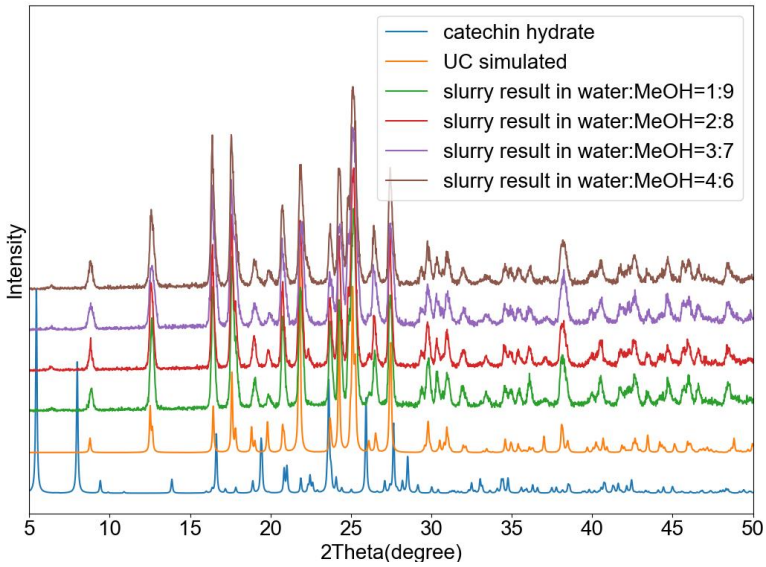

Figure A.10. PXRD of congruency experiments of UC in water/methanol mixed solvents (from 1:9 to 4:6)

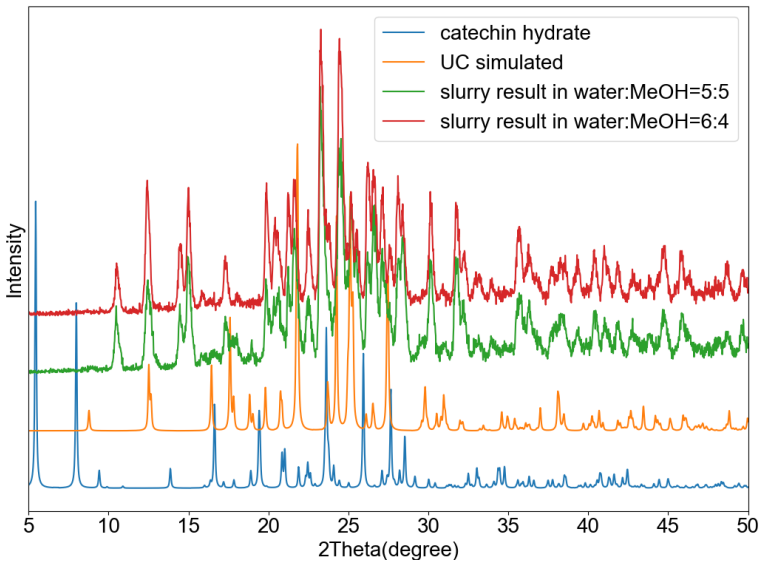

Figure A.11. PXRD of congruency experiments of UC in water/methanol mixed solvent (from 5:5 to 6:4)

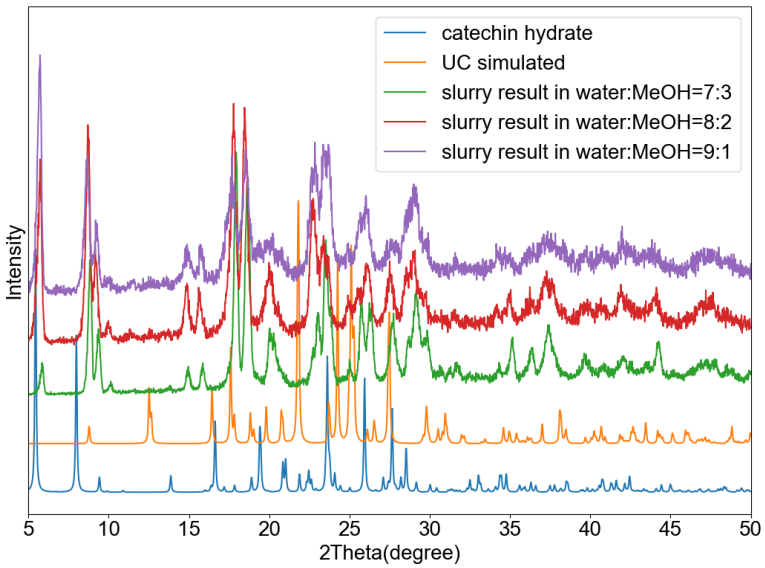

Figure A.12. PXRD of congruency experiments of UC in water/methanol mixed solvent (from 7:3 to 9:1)

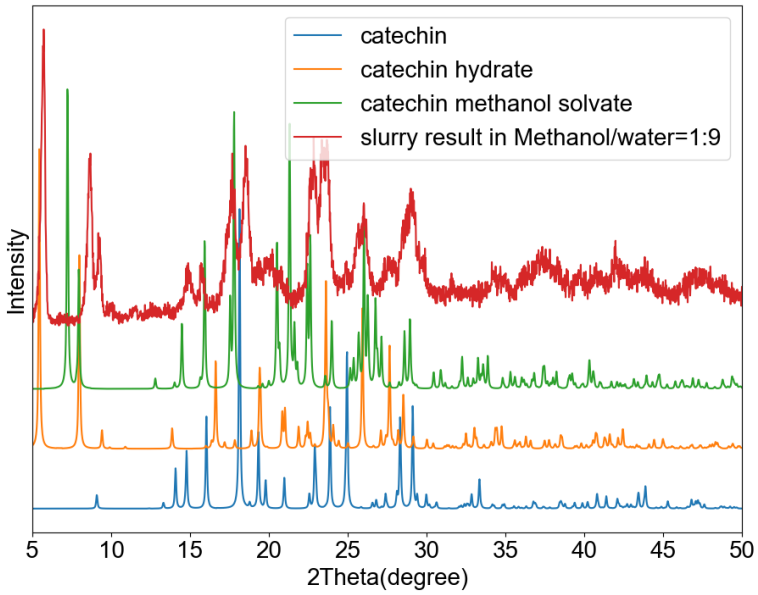

Figure A.13. PXRD profiles of the new catechin solvate obtained from slurrying urea and catechin in mixed solvent of methanol and water (1:9), and reported catechin polymorph or solvate

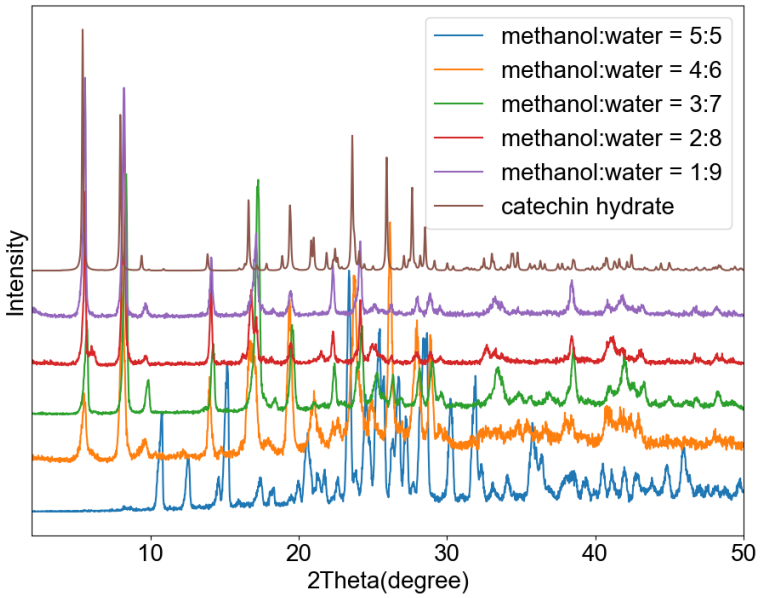

Figure A.14. PXRD profiles of catechin slurry result in methanol/water mixed solvent

Appendix B

B. Supporting information for Chapter 3.1

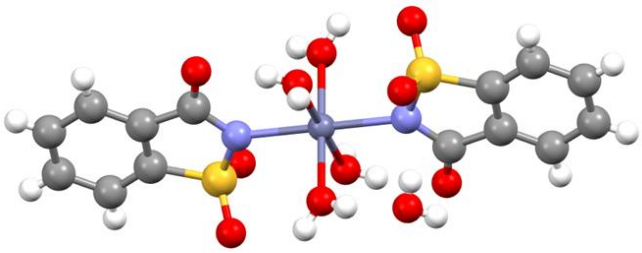

Figure B.1. Chemical structure of zinc saccharinate (Refcode: BEPSAQ01)

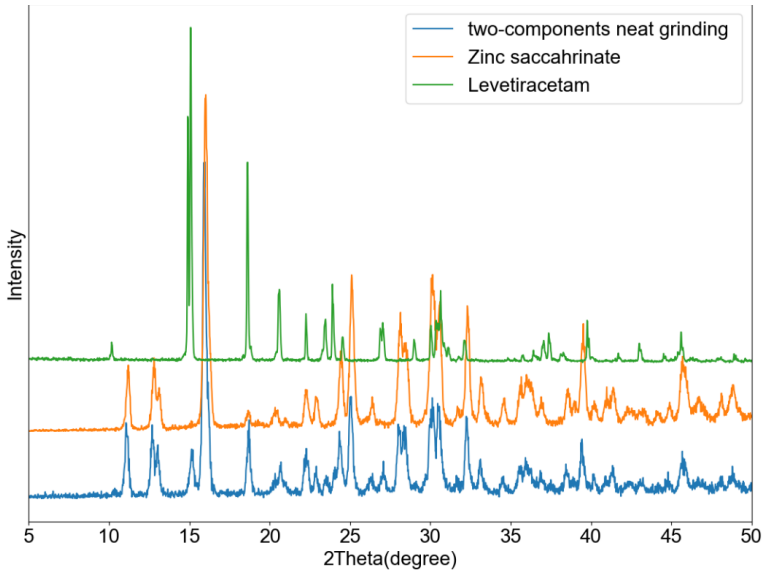

Figure B.2. PXRD overlay of levetiracetam, zinc saccharinate, and neat two-component grinding result between zinc saccharinate and levetiracetam

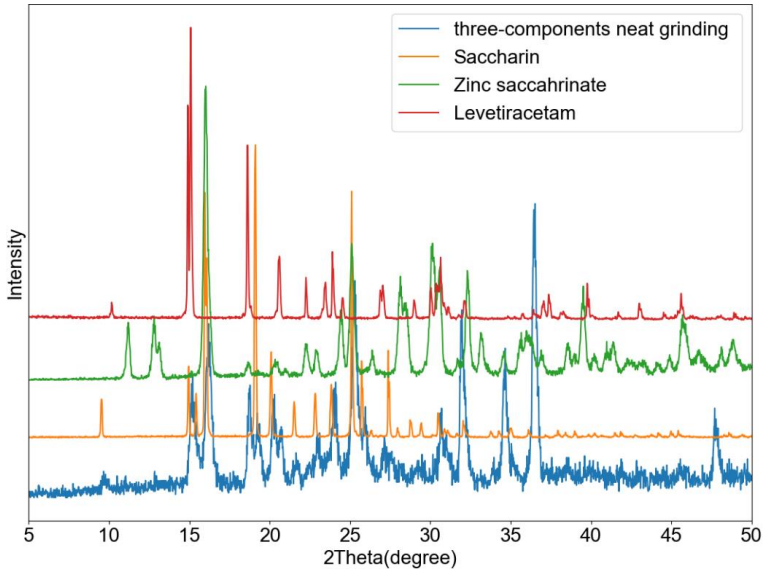

Figure B.3. PXRD overlay of saccharin, levetiracetam, zinc saccharinate, and neat three-component grinding result among saccharin, zinc oxide and levetiracetam

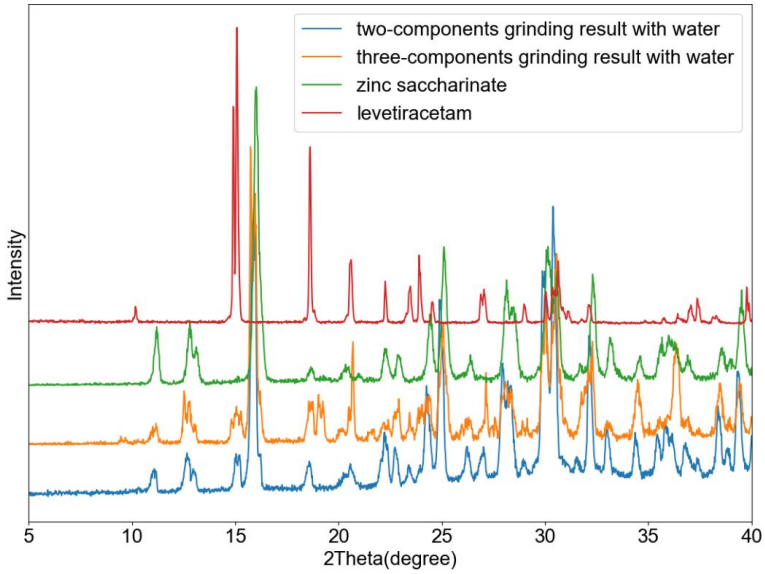

Figure B.4. PXRD overlay of levetiracetam, zinc saccharinate, and product obtained from two-component and three-component grinding with water.

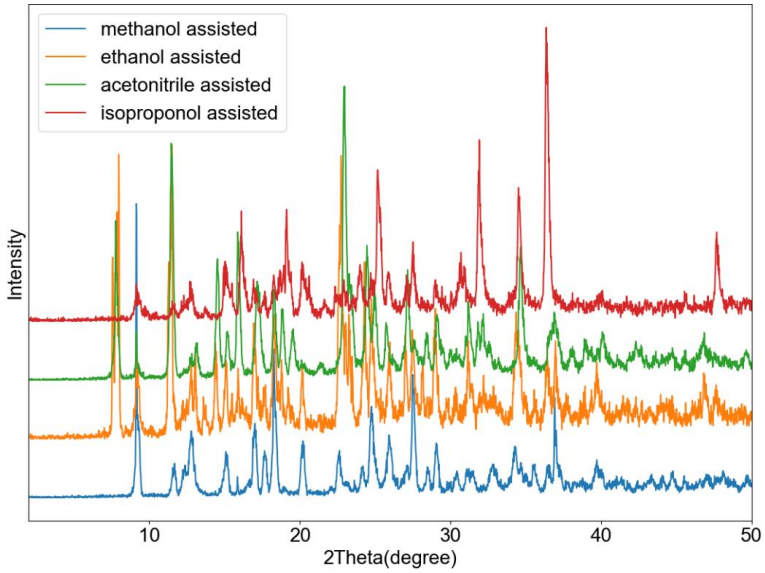

Figure B.5. Three-component grinding result using saccharin, zinc oxide and levetiracetam with the assistance of different organic solvents.

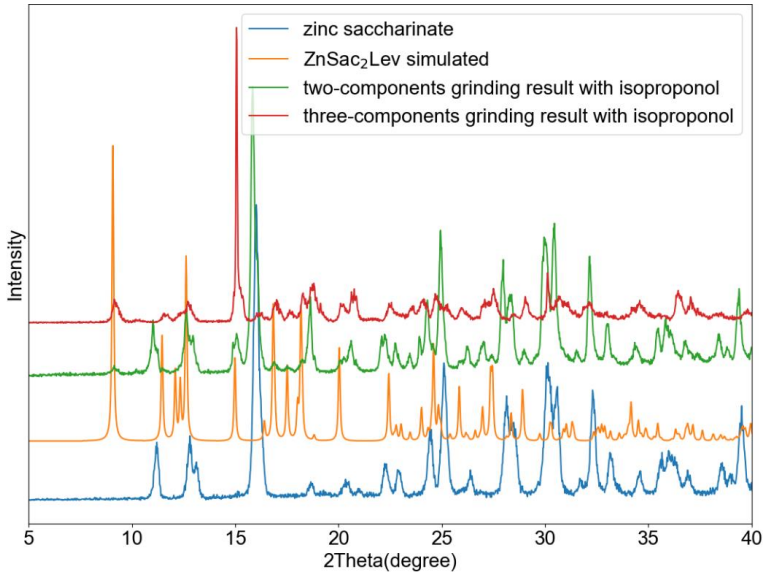

Figure B.6. PXRD overlay of zinc saccharinate, product obtained from two-component and three-component grinding with isopropanol as a solvent and simulated pattern of Sac_2ZnLev.

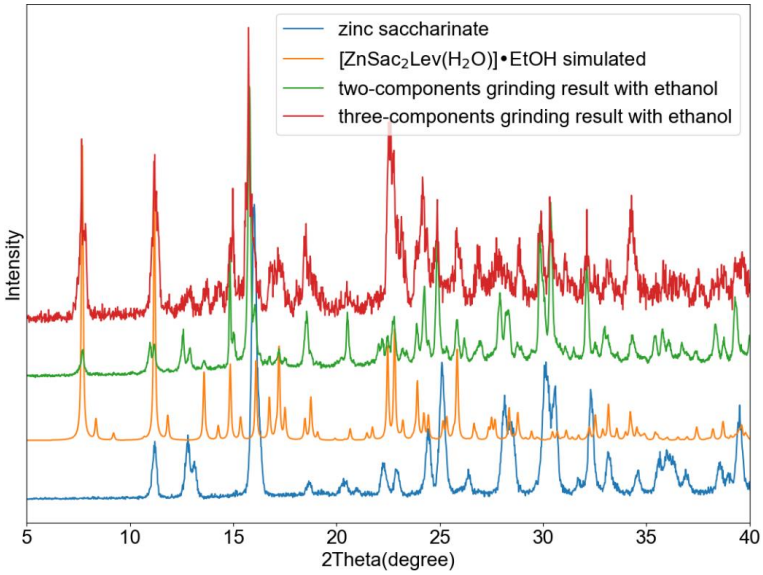

Figure B.7. PXRD overlay of zinc saccharinate, product obtained from two-component and three-component grinding with ethanol as solvent and simulated pattern of [$Sac_2ZnLev(H_2O)$]•EtOH.

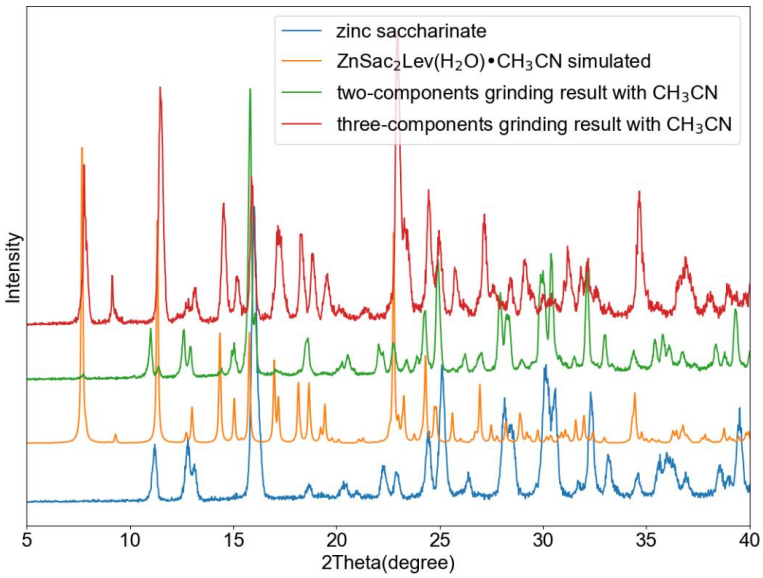

Figure B.8. PXRD overlay of zinc saccharinate, product obtained from two-component and three-component grinding with acetonitrile as solvent and simulated pattern of [$Sac_2ZnLev(H_2O)$]•CH_3CN.

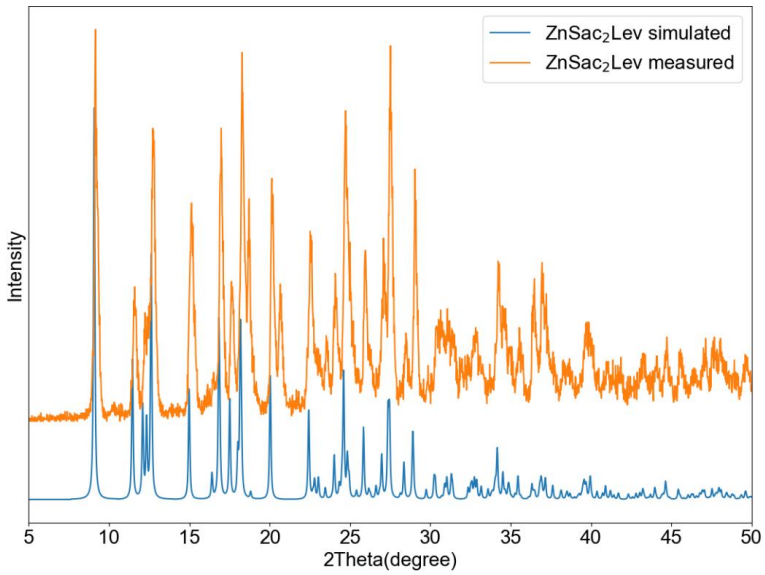

Figure B.9. PXRD overlay of $ZnSac_2Lev$ obtained by three-component grinding with methanol, and the simulated pattern of $ZnSac_2Lev$.

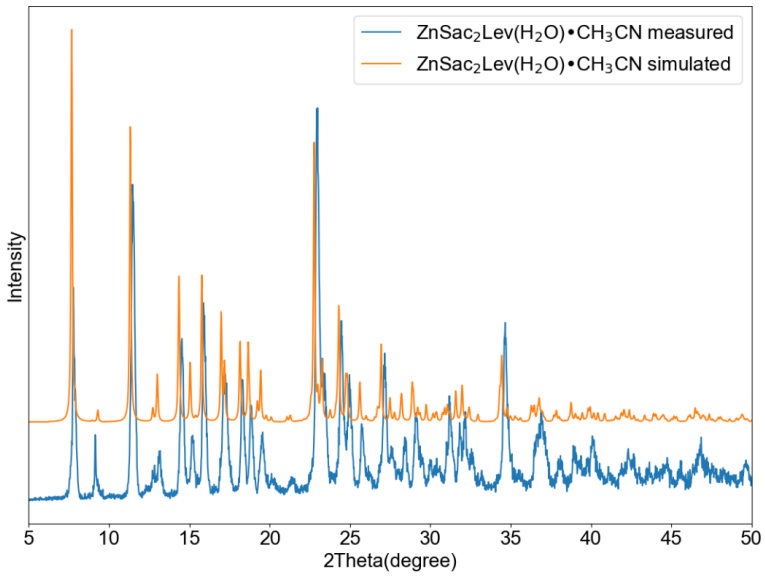

Figure B.10. PXRD overlay of $[ZnSac_2Lev(H_2O)]•CH_3CN$ obtained by three-component grinding with acetonitrile, and the simulated pattern of $[ZnSac_2Lev(H_2O)]•CH_3CN$.

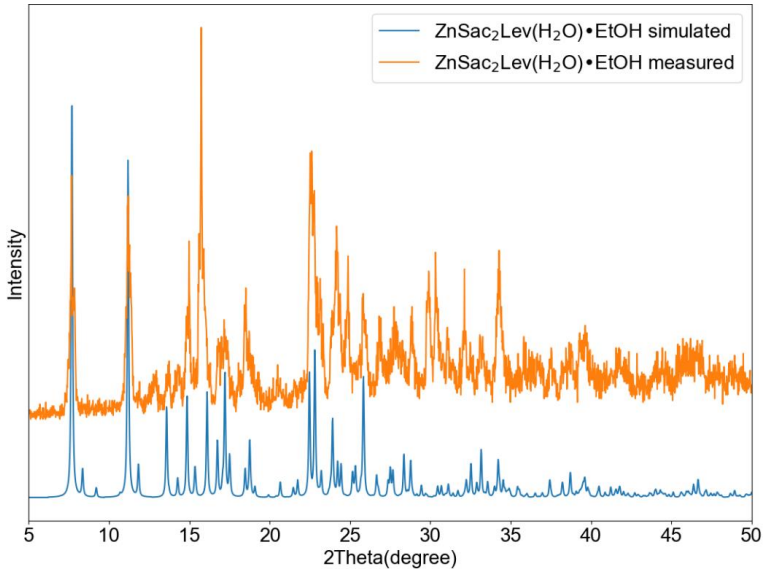

Figure B.11. PXRD overlay of [$ZnSac_2Lev(H_2O)$]•EtOH obtained by three-component grinding with ethanol, and the simulated pattern of [$ZnSac_2Lev(H_2O)$]•EtOH.

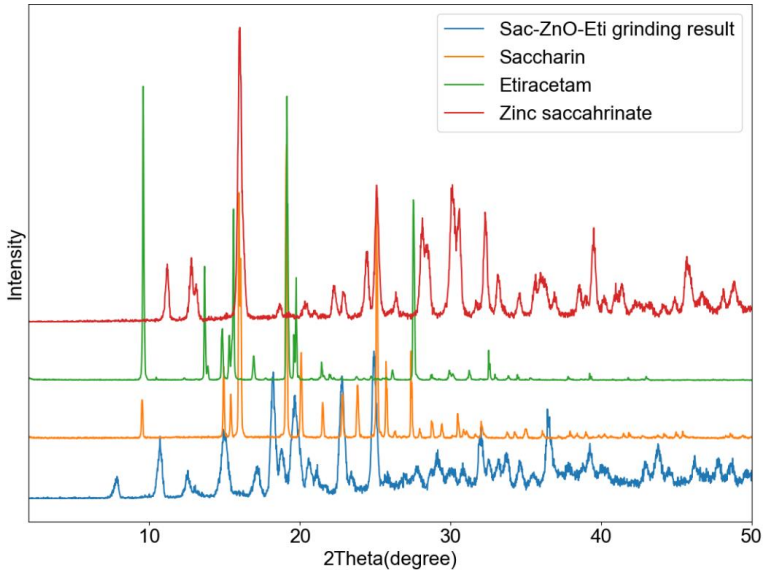

Figure B.12. PXRD overlay of saccharin, etiracetam, zinc saccharinate and three-component grinding result using zinc oxide, etiracetam and saccharin in a 1:1:2 ratio with methanol as solvent.

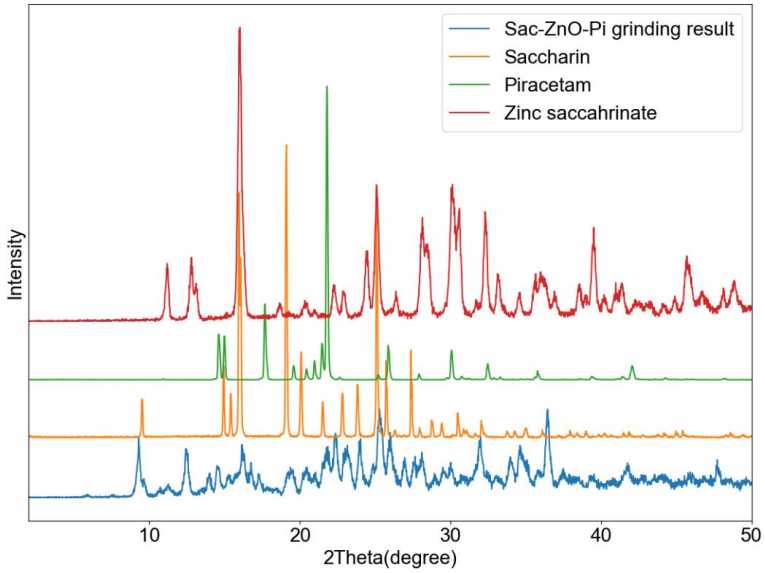

Figure B.13. PXRD overlay of saccharin, piracetam, zinc saccharinate and three-component grinding result using zinc oxide, saccharin and piracetam in a 1:2:1 ratio with acetonitrile as solvent.

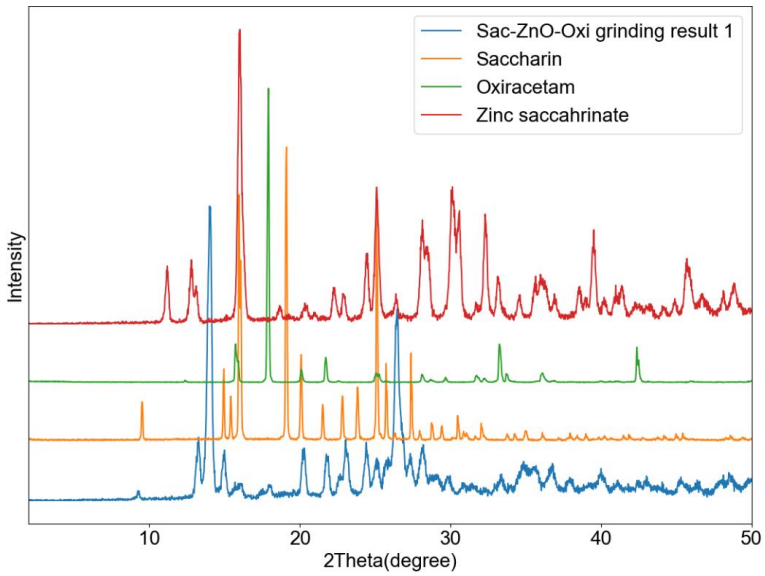

Figure B.14. PXRD overlay of saccharin, oxiracetam, zinc saccharinate and three-component grinding result using zinc oxide, saccharin and oxiracetam in a 1:2:1 ratio with acetonitrile as solvent.

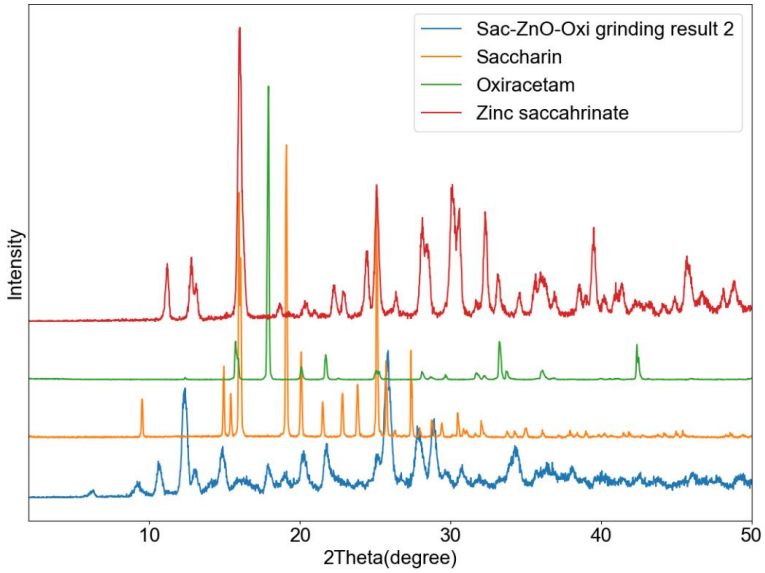

Figure B.15. PXRD overlay of saccharin, oxiracetam, zinc saccharinate and three-component grinding result among zinc oxide, saccharin and oxiracetam in a 1:2:1 ratio with isopropanol as solvent.

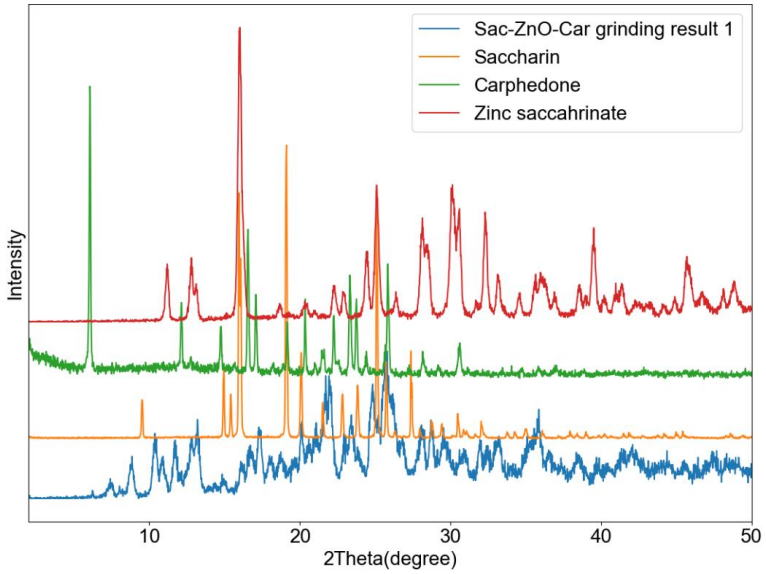

Figure B.16. PXRD overlay of saccharin, carphedon, zinc saccharinate and three-component grinding result using zinc oxide, saccharin and carphedon in a 1:2:1 ratio with ethanol as solvent.

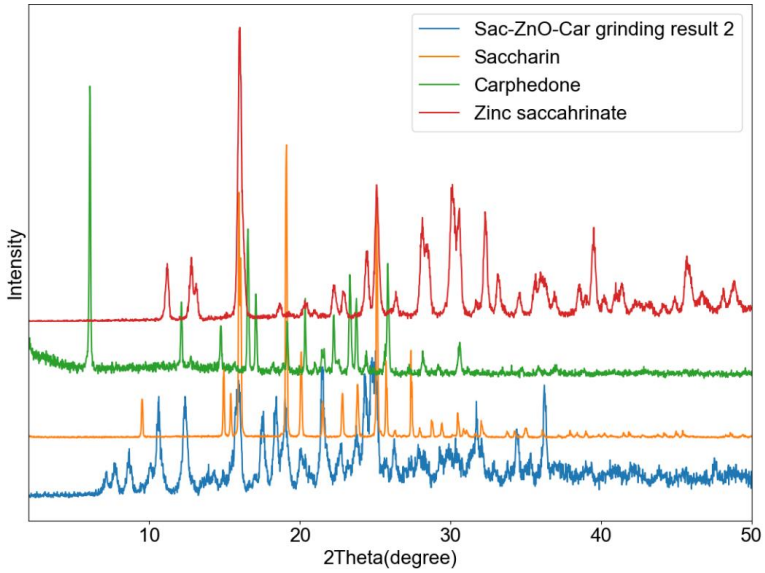

Figure B.17. PXRD overlay of saccharin, carphedon, zinc saccharinate and three-component grinding result using zinc oxide, saccharin and carphedon in a 1:2:1 ratio with acetonitrile as solvent.

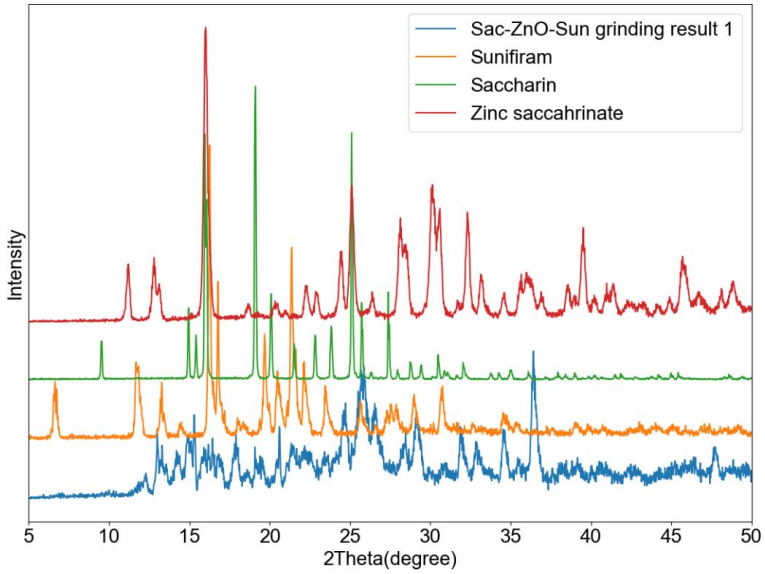

Figure B.18. PXRD overlay of saccharin, sunifiram, zinc saccharinate and three-component grinding result using zinc oxide, saccharin and sunifiram in a 1:2:1 ratio with methanol as solvent.

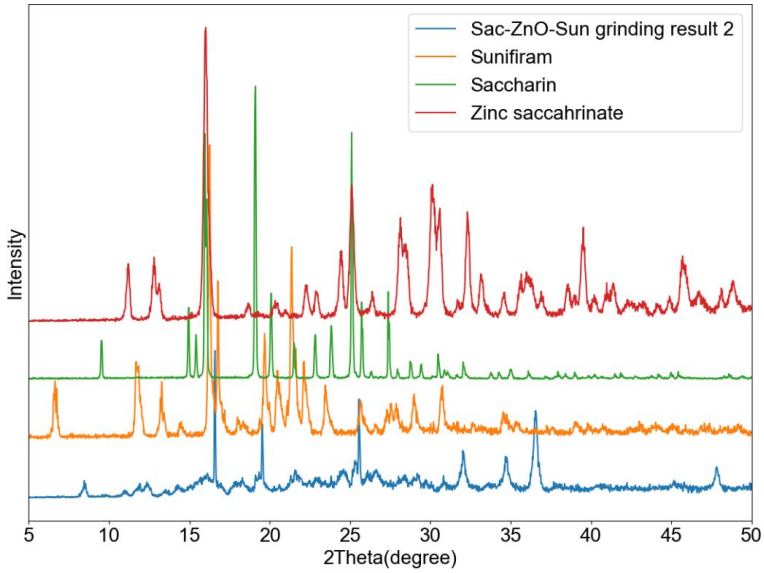

Figure B.19. PXRD overlay of saccharin, sunifiram, zinc saccharinate and three-component grinding result using zinc oxide, saccharin and sunifiram in a 1:2:1 ratio with ethanol as solvent.

Table B.1. Crystallographic data of $ZnSac_2$ solvates

Crystal name	$ZnSac_2$ acetonitrile solvate	$ZnSac_2$ ethanol solvate	$ZnSac_2$ methanol solvate	$ZnSac_2$ isopropanol solvate
Empirical formula	$C_{16}H_{12}N_3O_7S_2Zn$	$C_{18}H_{20}N_2O_8S_2Zn$	$C_{16}H_{16}N_2O_8S_2Zn$	$C_{17}H_{18}N_2O_8S_2Zn$
Formula weight	487.78	521.85	493.8	507.82
Crystal system	monoclinic	Monoclinic	monoclinic	Monoclinic
Space group	P21/m	P21/c	P21/c	P2/n
a/Å	7.0251(5)	15.3270(12)	14.4073(7)	17.3569(15)
b/Å	19.6400(10)	13.5994(7)	13.3347(7)	6.9074(4)
c/Å	7.3901(5)	10.6368(7)	10.4660(6)	18.1440(18)
α/°	90	90	90	90
β/°	113.155(8)	107.473(8)	108.427(6)	110.995(11)
γ/°	90	90	90	90
Volume/Å3	937.50(12)	2114.8(3)	1907.60(19)	2030.9(3)
Z	2	4	4	4
ρcalcg/cm3	1.728	1.639	1.719	1.661
μ/mm 1	1.579	1.408	1.555	1.463
F(000)	494	1072	1008	1040
Radiation	MoKα (λ = 0.71073)	MoKα (λ = 0.71073)	MoKα (λ = 0.71073)	MoKα (λ = 0.71073)
F(000)	494	1072	1008	1040
Independent reflections	1912 (Twining)	Independent reflections	1912 (Twining)	Independent reflections
Data/restraints/parameters	1912/0/141	4168/16/296	3789/0/270	4052/1/280
GOOF	1.08	1.039	1.084	1.042
Final R indexes [I>=2σ (I)]	R1 = 0.0483, wR2 = 0.1357	R1 = 0.0271, wR2 = 0.0729	R1 = 0.0416, wR2 = 0.1134	R1 = 0.0304, wR2 = 0.0702
Final R indexes [all data]	R1 = 0.0510, wR2 = 0.1375	R1 = 0.0294, wR2 = 0.0743	R1 = 0.0469, wR2 = 0.1174	R1 = 0.0380, wR2 = 0.0730

Table B.2 Crystallographic data of $Zn_3Sac_6Pi_2(H_2O)_4$, $ZnSac_2Lev$, $[ZnSac_2Lev(H_2O)]$•EtOH and $[ZnSac_2Lev(H_2O)]$•CH_3CN

Identification code	$ZnSac_2Lev$	$[ZnSac_2Lev(H_2O)]$ •EtOH	$[ZnSac_2Lev(H_2O)]$•CH_3CN
Empirical formula	$C_{22}H_{22}N_4O_8S_2Zn$	$C_{24}H_{30}N_4O_{10}S_2Zn$	$C_{23.42}H_{26.12}N_{4.71}O9S_2Zn$
Formula weight	599.92	664.01	647.01
Temperature/K	293(2)	293(2)	293(2)
Crystal system	Triclinic	orthorhombic	monoclinic
Space group	P1	P212121	I2
a/Å	7.8639(18)	10.5584(2)	11.9169(16)
b/Å	8.0633(3)	11.9100(2)	10.4325(10)
c/Å	10.648(2)	22.9554(5)	23.307(3)
α/°	102.180(11)	90	90
β/°	108.414(18)	90	99.147(12)
γ/°	96.518(12)	90	90
Volume/$Å^3$	614.24(19)	2886.65(10)	2860.7(6)
Z	1	4	4
ρcalcg/cm3	1.622	1.528	1.502
μ/mm^{-1}	1.226	1.056	1.062
F(000)	308	1376	1334
Crystal size/mm^3	0.15 × 0.06 × 0.06	0.2 × 0.15 × 0.15	0.45× 0.4 × 0.3
Radiation	MoKα	MoKα	MoKα
Reflections collected	8697	20545	17573
Independent reflections	4443 Rint =0.0428	5754 Rint = 0.0236	5665 Rint =0.0482
Data/restraints/parameters	4443/3/335	5754/3/377	5665/39/383
GOOF	1.068	1.036	1.029
Final R indexes [I>=2σ (I)]	R1 =0.0299, wR2=0.0767	R1 = 0.0261, wR2 = 0.0746	R1 = 0.0303, wR2 = 0.0713
Final R indexes [all data]	R1 =0.0313, wR2 = 0.0782	R1 = 0.0273, wR2 = 0.0756	R1 = 0.0348, wR2 = 0.0731

Table B.3 Crystallographic data for [$ZnSac_2Pi$]•CH_3CN, [$ZnSac_2Oxi$]•CH_3CN, [Sac_2ZnSun]•CH_3CN and Sac_2ZnCar

Identification code	[$ZnSac_2Pi$]•CH3CN	[$ZnSac_2Oxi$]•CH_3CN	[$ZnSac_2Sun$]•CH_3CN	$ZnSac_2Car$
Empirical formula	$C_{44}H_{42}N_{10}O_{16}S_4Zn_2$	$C_{44}H_{42}N_{10}O_{18}S_4Zn_2$	$C_{30}H_{29}N_5O_8S_2Zn$	$C_{52}H_{44}N_8O_{16}S_4Zn_2$
Formula weight	1225.85	1257.9	717.07	1295.9
Temperature/K	293(2)	293(2)	293(2)	293(2)
Crystal system	triclinic	triclinic	orthorhombic	triclinic
Space group	*P-1*	*P-1*	*Pbca*	*P-1*
a/Å	9.2864(11)	9.1442(14)	15.5050(3)	9.6957(16)
b/Å	10.8927(13)	11.3806(5)	20.2029(5)	12.3009(17)
c/Å	13.7978(9)	13.719(2)	20.6271(4)	13.382(2)
α/°	109.504(9)	108.738(10)	90	105.940(13)
β/°	98.068(8)	98.936(13)	90	97.551(13)
γ/°	96.639(10)	97.535(9)	90	105.898(14)
Volume/$Å^3$	1282.7(2)	1310.3(3)	6461.4(2)	1438.6(4)
Z	1	1	8	1
ρcalcg/cm^3	1.587	1.594	1.474	1.496
μ/mm 1	1.177	1.157	0.947	1.053
F(000)	628.0	644	2960	664
Crystal size/mm^3	0.23 × 0.05 × 0.05	0.2 × 0.1 × 0.09	0.17 × 0.1 × 0.05	0.2 × 0.12 × 0.07
Radiation	MoKα	MoKα	MoKα	MoKα
Reflections collected	17977	17033	44367	17736
Independent reflections	5051 Rint= 0.0600	5219 Rint = 0.0331	6457 Rint = 0.0558	5331 Rint=0.050
Data/restraints/parameters	5051/39/373	5219/92/460	6457/41/503	5331/278/537
GOOF	1.034	1.066	1.043	1.093
Final R indexes [I>=2σ (I)]	R1=0.0363, wR2=0.0908	R1=0.0309, wR2 =0.0791	R1=0.0346, wR2=0.0818	R1=0.0589, wR2=0.164
Final R indexes [all data]	R1=0.0439, wR2=0.0952	R1 = 0.0353, wR2=0.0813	R1=0.0478, wR2 =0.0878	R1=0.0683, wR2=0.1711

Table B.4 Crystallographic data for $[ZnSac_2(H_2O)_2]$•Car•EtOH•H_2O, $Zn_3Sac_6Pi_2(H_2O)_4$ and $ZnSac_2Eti_2$

Identification code	$Zn_3Sac_6Pi_2(H_2O)_4$	$[ZnSac_2(H_2O)_2]$•Car•EtOH•H_2O	$ZnSac_2Eti_2$
Empirical formula	$C_{54}H_{52}N_{10}O_{26}S_6Zn_3$	$C_{28}H_{34}N_4O_{12}S_2Zn$	$C_{30}H_{36}N_6O_{10}S_2Zn$
Formula weight	1645.5	748.08	770.14
Temperature/K	293(2)	293(2)	293(2)
Crystal system	triclinic	Triclinic	monoclinic
Space group	P-1	*P-1*	P21/c
a/Å	8.7413(4)	8.7039(4)	7.7870(5)
b/Å	12.5383(18)	12.8956(16)	23.6027(13)
c/Å	15.550(2)	15.1304(14)	9.8017(7)
α/°	91.435(11)	97.836(9)	90
β/°	92.734(8)	95.581(6)	111.169(8)
γ/°	105.720(9)	106.939(8)	90
Volume/$Å^3$	1637.4(3)	1592.5(3)	1679.9(2)
Z	1	2	2
ρcalcg/cm^3	1.669	1.56	1.522
μ/mm 1	1.372	0.971	0.921
F(000)	840	776	800
Crystal size/mm^3	0.12 × 0.08 × 0.06	0.32 × 0.2 × 0.12	0.35 × 0.04 × 0.03
Radiation	MoKα	MoKα	MoKα
Reflections collected	23267	21949	13002
Independent reflections	6554	6337 Rint = 0.0262	3301 Rint =0.0709
Data/restraints/parameters	Rint =0.0389	6337/24/441	3301/4/231
GOOF	6554/0/454	1.032	1.054
Final R indexes [I>=2σ (I)]	1.054	R1 = 0.0401, wR2 = 0.1026	R1 =0.0414, wR2 =0.102
Final R indexes [all data]	R1 = 0.0343, wR2 = 0.0778	R1 = 0.0433, wR2 = 0.1047	R1=0.0527, wR2=0.1088

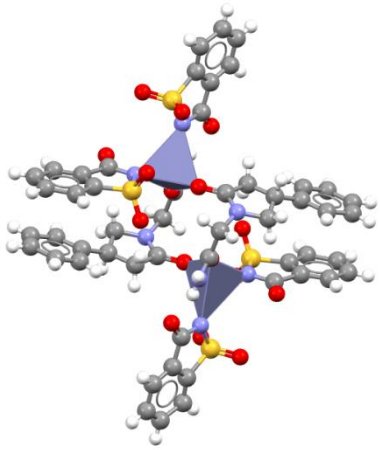

Figure B.20. Crystal structure of $ZnSac_2Car$

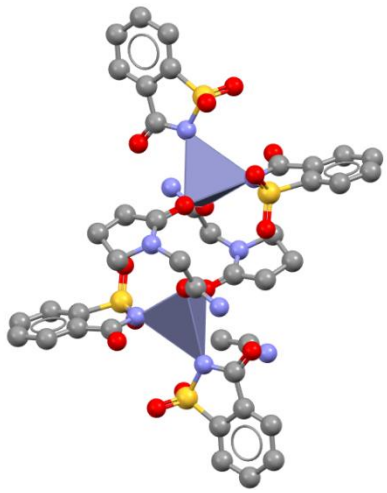

Figure B.21. Crystal structure of $[ZnSac_2Oxi]•CH_3CN$. Hydrogen atoms are omitted for clarity

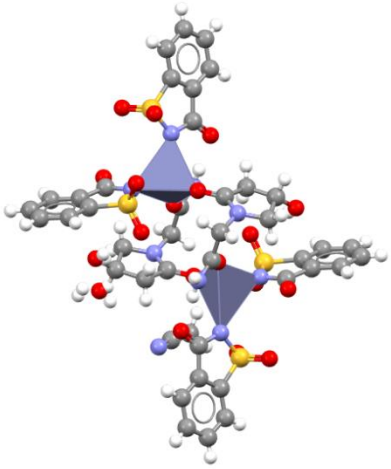

Figure B.22. Crystal structure of [$ZnSac_2Oxi$]•CH_3CN

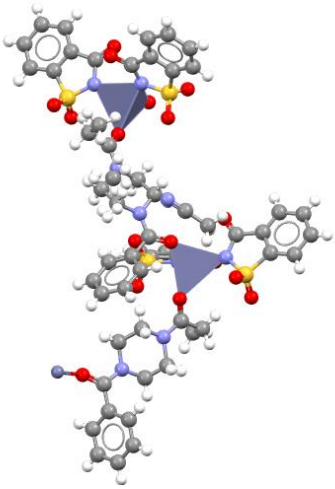

Figure B.23. Crystal structure of [$ZnSac_2Sun$]•CH_3CN

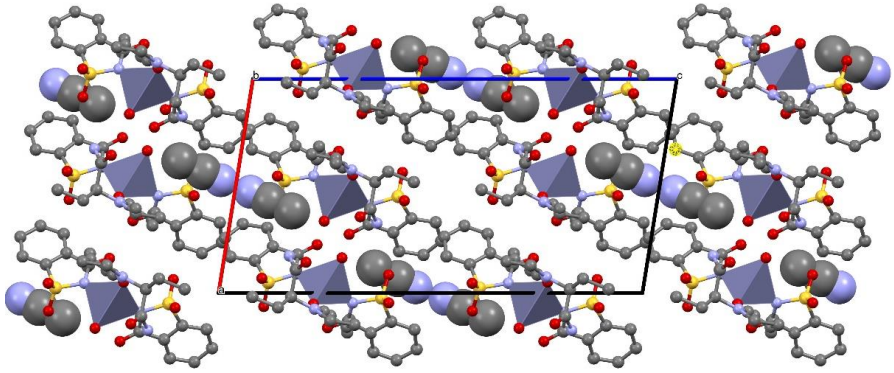

Figure B.24 Crystal structure of [$ZnSac_2Lev(H_2O)$]•CH_3CN

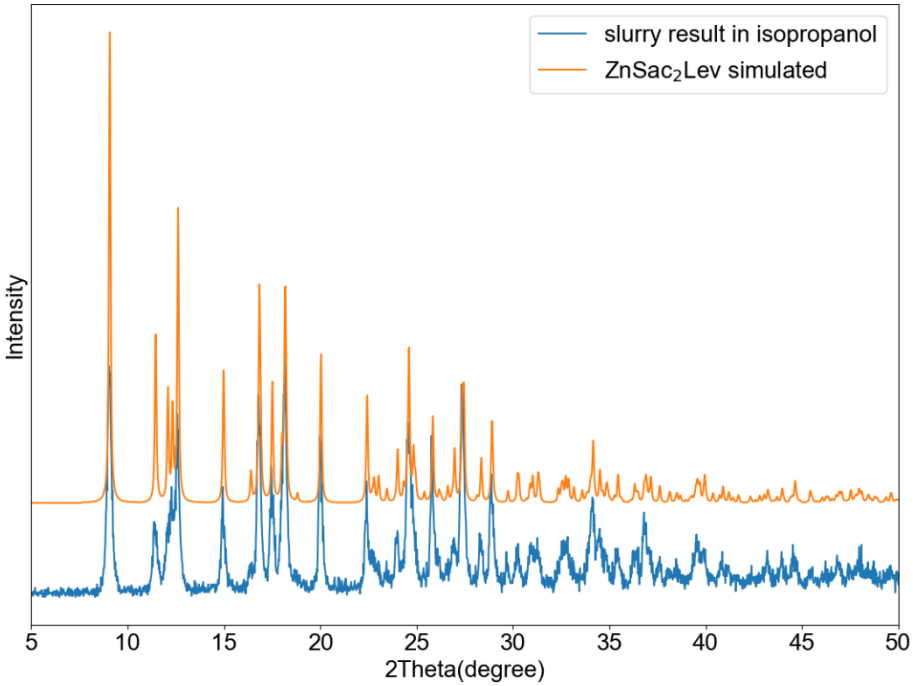

Figure B.25 PXRD overlay of levetiracetam, zinc saccharinate, slurrying result in isopropanol with the ratio of 1.2:1 and simulated profile of $ZnSac_2Lev$.

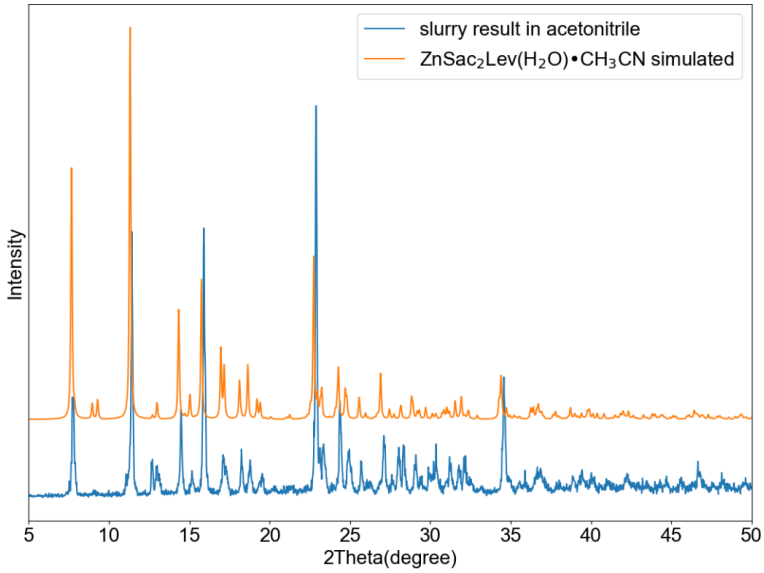

Figure B.26 PXRD overlay of slurrying result of a stoichiometric mixture of levetiracetam-zinc saccharinate in acetonitrile and simulated profile of $[ZnSac_2Lev(H_2O)]•CH_3CN$.

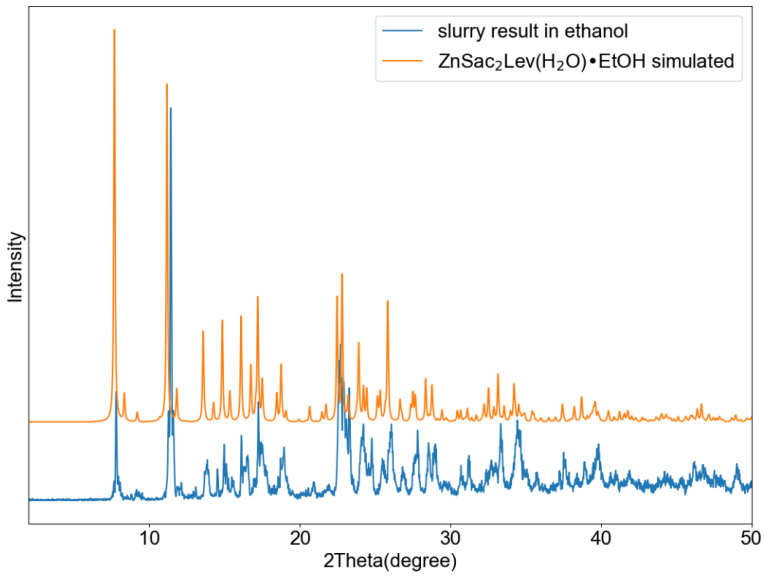

Figure B.27 PXRD overlay of slurrying result of a stoichiometric ratio of levetiracetam-zinc saccharinate in ethanol and simulated pattern of $[ZnSac_2Lev(H_2O)]•EtOH$.

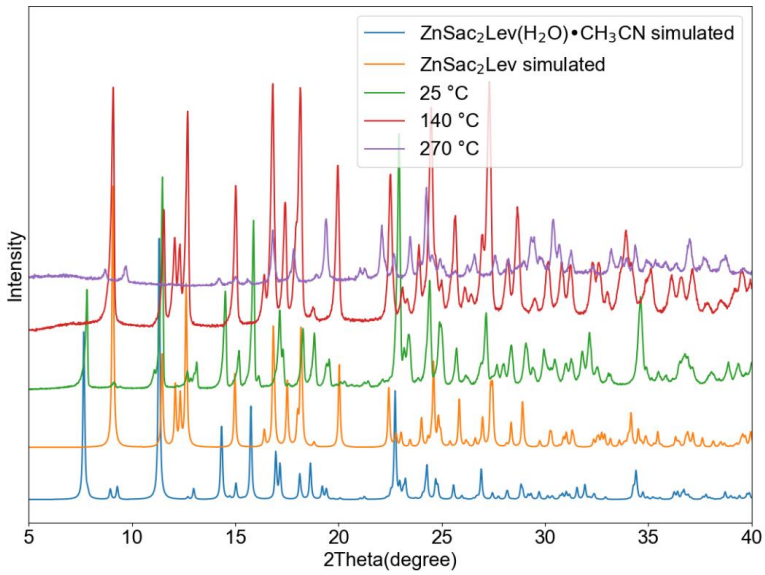

Figure B.28 PXRD overlay showing simulated pattern of $[ZnSac_2Lev(H_2O)]•CH_3CN$, simulated pattern of $ZnSac_2Lev$, and VT-PXRD result of $[ZnSac_2Lev(H_2O)]•CH_3CN$ at 25°C, 140°C, 270°C.

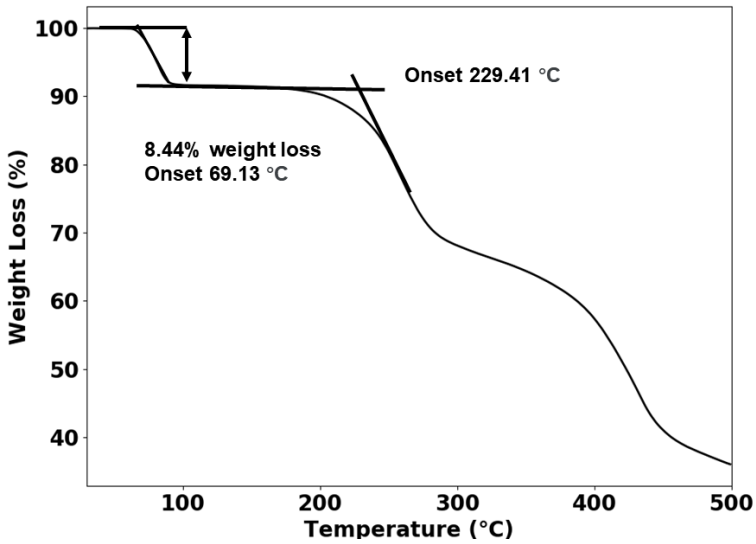

Figure B.29 TGA curve of $[ZnSac_2Lev(H_2O)]•EtOH$

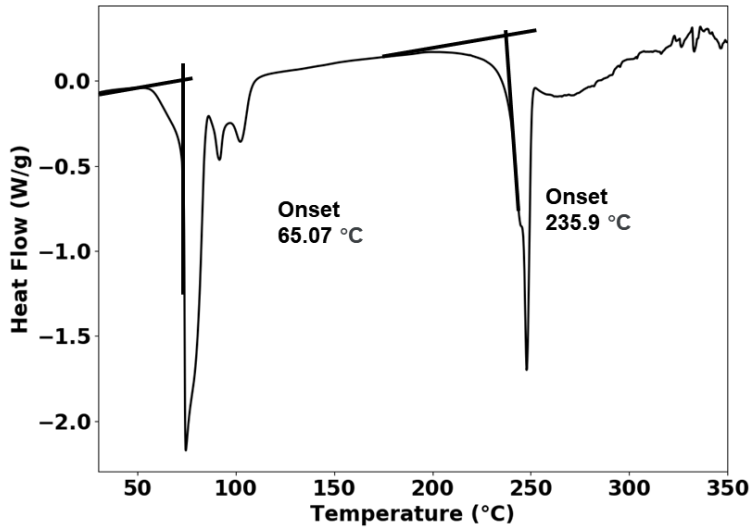

Figure B.30 DSC curve of [$ZnSac_2Lev(H_2O)$]•EtOH

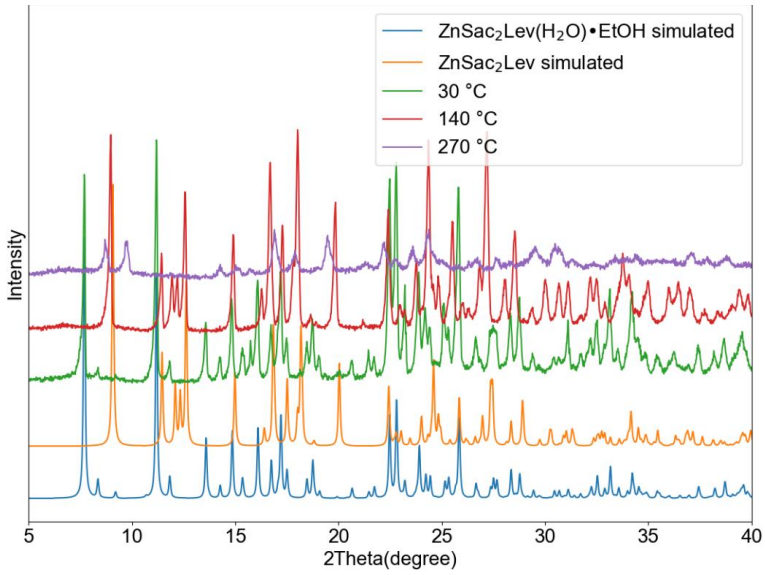

Figure B.31 PXRD overlay of simulated pattern of [$ZnSac_2Lev(H_2O)$]•EtOH, simulated pattern of $ZnSac_2Lev$, and VT-XRD result of [$ZnSac_2Lev(H_2O)$]•EtOH at 25°C, 140°C, 270°C.

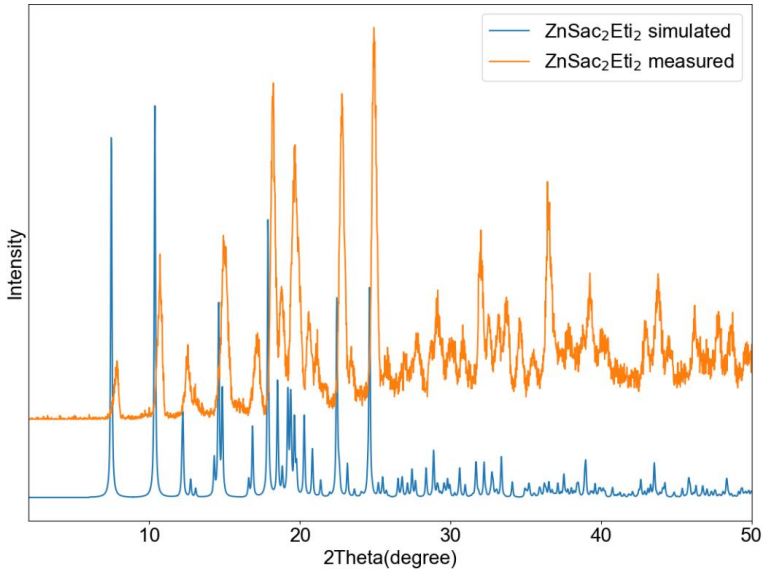

Figure B.32 PXRD profiles of $ZnSacEti_2$ obtained by grinding with an organic solvent, and the simulated pattern of $ZnSacEti_2$.

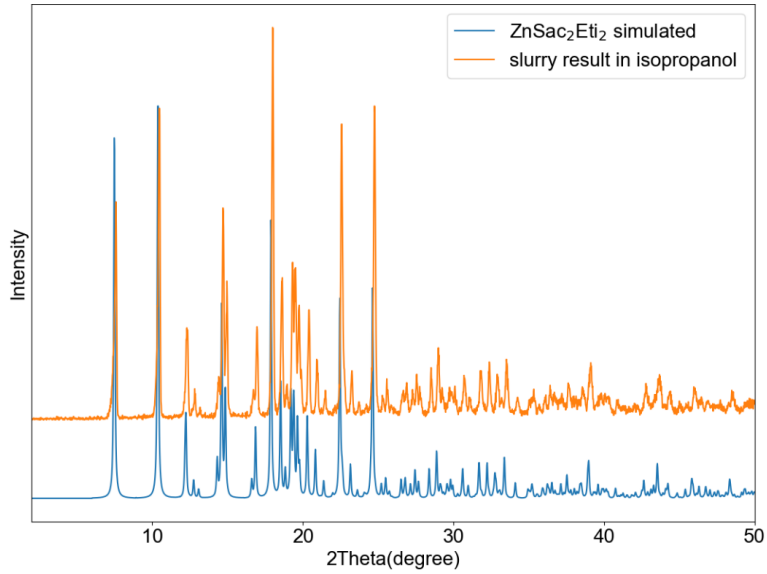

Figure B.33. PXRD of congruency experiments between etiracetam and zinc saccharinate in ethanol and isopropanol.

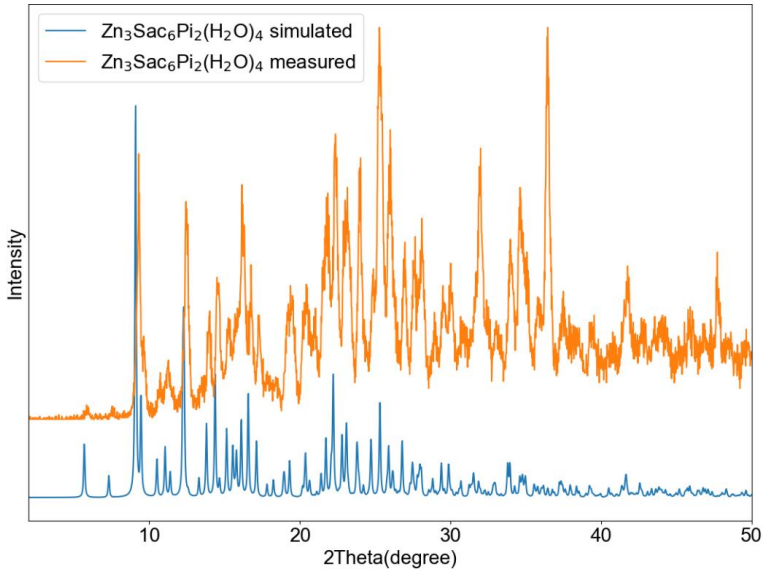

Figure B.34. PXRD of $Zn_3Sac_6Pi_2(H_2O)_4$ obtained by grinding, and the simulated pattern of $Zn_3Sac_6Pi_2(H_2O)_4$.

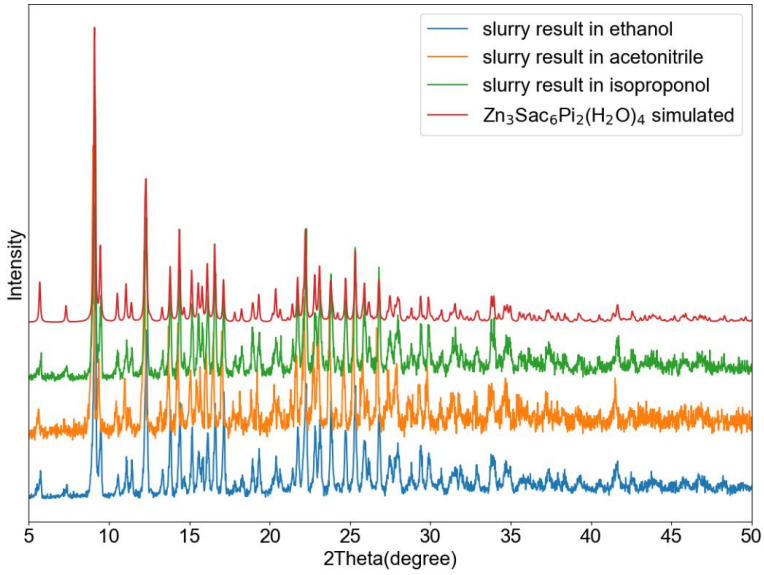

Figure B.35. PXRD of congruency experiments between piracetam and zinc saccharinate in different solvents.

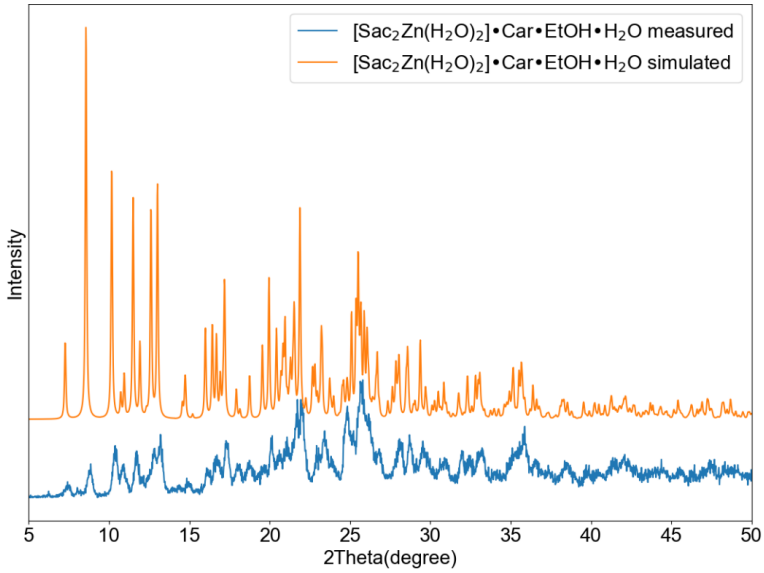

Figure B.36. PXRD of $[Sac_2Zn(H_2O)_2]$•Car•EtOH•H_2O obtained by LAG with ethanol, and the simulated pattern of $[Sac_2Zn(H_2O)_2]$•Car•EtOH•H_2O.

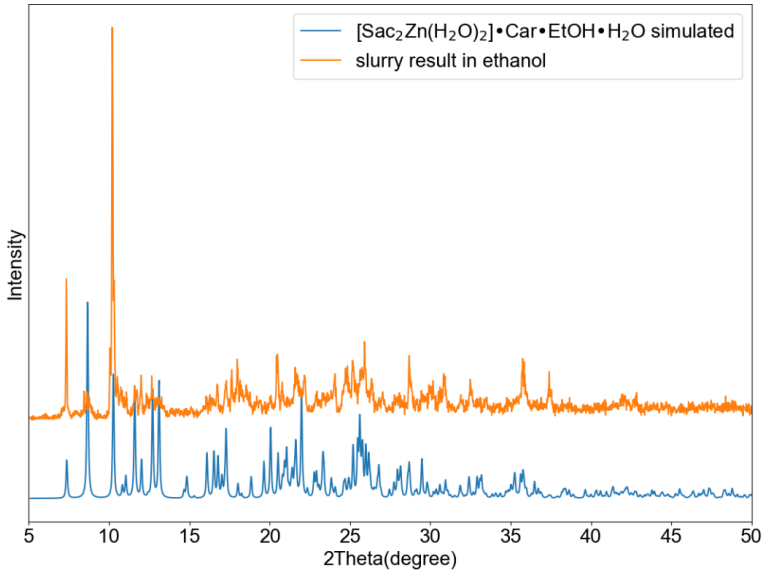

Figure B.37. PXRD of congruency experiments between carphedon and zinc saccharinate in ethanol.

Appendix B

Appendix C

C. Supporting information for Chapter 3.2

Crystallographic data.

Table C1a~C1d. Crystal data and structure refinement for the investigated structures. CCDC 2194913-2194925 contain the supplementary crystallographic data for this paper. These data can be obtained free of charge from The Cambridge Crystallographic Data Centre via www.ccdc.cam.ac.uk/structures.

Table C.1a. Crystal data and structure refinement for the investigated structures.

Identification code	$Zn(IBU)_2(NC)$	$Zn(IBU)_2(INC)_2(H_2O)_2$	$Zn(IBU)_2(INZ)$
Empirical formula	$C_{64}H_{80}N_4O_{10}Zn_2$	$C_{38}H_{50}N_4O_8Zn$	$C_{32}H_{42}N_3O_5Zn$
Formula weight	1196.06	756.19	614.05
Temperature (K)	297(2)	297(2)	297(2)
Wavelength (Å)	0.71073	0.71073	0.71073
Crystal system	Triclinic	Triclinic	Monoclinic
Space group	*P*-1	*P*-1	$P2_1/c$
A	10.8461(8)	5.5047(5)	5.49695(15)
B	11.1730(14)	10.9599(6)	15.4850(5)
C	15.667(2)	16.9517(16)	36.8845(9)
A	109.991(12)	72.152(7)	90
B	95.467(9)	86.676(8)	89.950(3)
Γ	111.284(10)	89.379(6)	90
Volume ($Å^3$)	1609.5(4)	971.83(14)	3139.61(15)
Z	1	1	4
F(000)	632	400	1300
Theta range for data collection (°)	3.280 to 25.255	3.639 to 25.246	3.059 to 25.254
Reflections collected	19056	14375	5682
Independent reflections	5803 [R(int) =0.0682]	3521 [R(int) = 0.0633]	5682
Completeness	99.7	99.8	99.6
Data / restr / param	5803 / 317 / 548	3521 / 127 / 278	5682 / 52 / 407
GooF	1.095	1.058	1.059
Final R indices [I>2s(I)]	R1 = 0.0636, wR2 = 0.1546	R1 = 0.0552, wR2 = 0.1423	R1 = 0.0359, wR2 = 0.1003
R indices (all data)	R1 = 0.0815, wR2 = 0.1645	R1 = 0.0639, wR2 = 0.1494	R1 = 0.0392, wR2 = 0.1028
$\Delta\rho$(max,min)($e.Å^{-3}$)	1.113, -0.562	1.319, -0.434	0.338, -0.325

Table C.1b. Crystal data and structure refinement for the investigated structures.

Identification code	$Zn(IBU)_2(INC)$	$Zn(PABA)_2(AMI)_2$	$Zn_2(ASP)_4(INC)_2$
Empirical formula	$C_{38}H_{46}N_4O_6Zn$	$C_{62}H_{82}N_6O_8Zn_2$	$C_{30}H_{26}N_4O_{10}Zn$
Formula weight	720.16	1170.07	667.92
Temperature (K)	297(2)	297(2)	297(2)
Wavelength (Å)	0.71073	0.71073	0.71073
Crystal system	Monoclinic	Triclinic	Monoclinic
Space group	*I*2/*a*	*P*-1	$P2_1/c$
a	20.7691(13)	10.7578(13)	19.2090(10)
b	5.4155(3)	11.2000(9)	8.4481(6)
c	33.352(2)	14.613(2)	19.0056(12)
α	90	84.364(10)	90
β	105.757(6)	75.219(12)	94.578(5)
γ	90	65.014(11)	90
Volume ($Å^3$)	3610.3(4)	1543.0(4)	3074.4(3)
Z	4	1	4
F(000)	1520	620	1376
Theta range for data collection (°)	2.538 to 26.034	3.255 to 25.514	2.640 to 25.417
Reflections collected	12341	18613	5552
Independent reflections	3559 [R(int) = 0.0480]	5740 [R(int) = 0.0560]	5552 R(int) = 0*
Completeness	99.8	99.7	99.8
Data / restr / param	3559 / 46 / 255	5740 / 197 / 450	5552 / 0 / 410
GooF	1.038	1.033	1.097
Final R indices [I>2s(I)]	R1 = 0.0439, wR2 = 0.0986	R1 = 0.0559, wR2 = 0.1429	R1 = 0.0640, wR2 = 0.1686
R indices (all data)	R1 = 0.0611, wR2 = 0.1055	R1 = 0.0699, wR2 = 0.1520	R1 = 0.0732, wR2 = 0.1753
Δρ(max,min)($e.Å^{-3}$)	0.375, -0.325	0.865, -0.817	1.101, -0.488

*****this structure is refined against HKLF5 formatted data, which impose R(int)=0

Table C.1c. Crystal data and structure refinement for the investigated structures

Identification code	$Zn(IBU)_2(AMI)$	$Zn(PABA)_2(NIC)_2$	$Zn(PABA)(Ac)(MN)_2 \cdot H_2O$
Empirical formula	$C_{62}H_{82}N_6O_8Zn_2$	$C_{26}H_{24}N_6O_6Zn$	$C_{32}H_{32}N_4O_{12}Zn_2$
Formula weight	1170.07	581.88	795.35
Temperature (K)	297(2)	297(2)	297(2)
Wavelength (Å)	0.71073	0.71073	0.71073
Crystal system	Triclinic	Monoclinic	Monoclinic
Space group	*P*-1	*C*2/*c*	$P2_1/n$
a	10.7578(13)	27.119(2)	10.5805(10)
b	11.2000(9)	5.8028(5)	12.6078(14)
c	14.613(2)	16.6168(15)	13.0496(15)
α	84.364(10)	90	90
β	75.219(12)	97.624(8)	107.058(12)
ψ	65.014(11)	90	90
Volume ($Å^3$)	1543.0(4)	2591.8(4)	1664.2(3)
Z	1	4	2
F(000)	620	1200	816
Theta range for data collection	3.255 to 25.514	3.068 to 26.195	2.721 to 26.206
Reflections collected	18613	8735	9950
Independent reflections	5740 [R(int)=0.0560]	2582 [R(int) = 0.0448]	3308 [R(int) = 0.0271]
Completeness	99.7	99.7	99.6
Data / restr / param	5740 / 197 / 450	2582 / 0 / 177	3308 / 0 / 231
GooF	1.033	1.072	1.034
Final R indices [I>2s(I)]	R1 = 0.0559, wR2 = 0.1429	R1 = 0.0350, wR2 = 0.0826	R1 = 0.0290, wR2 = 0.0759
R indices (all data)	R1 = 0.0699, wR2 = 0.1520	R1 = 0.0420, wR2 = 0.0857	R1 = 0.0326, wR2 = 0.0781
$\Delta\rho$(max,min)($e.Å^{-3}$)	0.865, -0.817	0.284, -0.181	0.338, -0.244

Table C.1d. Crystal data and structure refinement for the investigated structures.

Identification code	$Zn(PABA)_2(MN)_2 \cdot H_2O$	$Zn(PABA)_2(INZ) \cdot CH_3OH$	$Zn(PABA)_2(AMI)_2$	$Zn(PABA)_2(INC)_2 \cdot (H_2O)_{0.5}$
Empirical formula	$C_{28}H_{28}N_4O_9Zn$	$C_{21}H_{23}N_5O_6Zn$	$C_{24}H_{26}N_8O_4Zn$	$C_{52}H_{50}N_{12}O_{13}Zn_2$
Formula weight	629.91	506.81	555.90	1181.78
Temperature (K)	297(2)	297(2)	297(2)	297(2)
Wavelength (Å)	0.71073	0.71073	0.71073	0.71073
Crystal system	Monoclinic	Triclinic	Monoclinic	Monoclinic
Space group	$P2_1/c$	P-1	$P2_1/c$	$I2/a$
a	15.2611(14)	9.6899(17)	10.0747(10)	22.7349(13)
b	16.2486(11)	10.4485(7)	19.0081(18)	11.6737(6)
c	11.2437(7)	12.2345(16)	13.0252(13)	20.3594(11)
α	90	70.702(10)	90	90
β	103.123(8)	88.709(12)	103.795(11)	90.019(5)
γ	90	73.166(11)	90	90
Volume ($Å^3$)	2715.3(4)	1115.3(3)	2422.4(4)	5403.4(5)
Z	4	2	4	4
F(000)	1304	524	1152	2440
Theta range (°)	2.398 to 25.772	2.586 to 26.185	2.681 to 26.324	3.205 to 26.148
Reflections collected	7886	15465	15722	17451
Independent reflections	7886 R(int) = 0*	4324 Rint=0.0269	4878 Rint=0.0371]	5357 Rint=0.0415
Completeness	99.7	97.7	99.7	99.6
Data / restr / param	7886 / 0 / 385	4324 / 0 / 300	4878 / 0 / 334	5357 / 1 / 360
GooF	1.050	1.046	1.026	1.051
Final R indices [I>2s(I)]	R1 = 0.0602, wR2 =0.1538	R1 = 0.0370, wR2=0.1020	R1 = 0.0405, wR2 =0.0989	R1 = 0.0368, wR2=0.0959
R indices (all data)	R1 =0.0750, wR2 =0.1608	R1 = 0.0385, wR2=0.1034	R1 = 0.0504, wR2 =0.1049	R1 = 0.0454, wR2=0.1011
$\Delta\rho$(max,min) ($e.Å^{-3}$)	0.623,-0.585	0.750,-0.532	0.461,-0.411	0.481, 0.238

***** this structure is refined against HKLF5 formatted data, which impose R(int) = 0

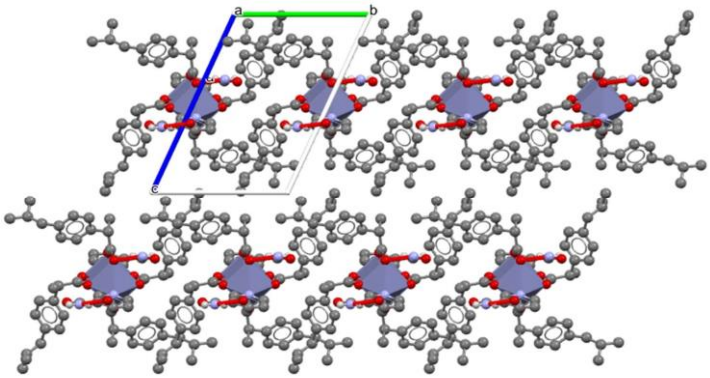

Figure C.1. Crystal packing of Zn(IBU)2(NC); view along crystallographic a-axis. H_{CH} are omitted for clarity.

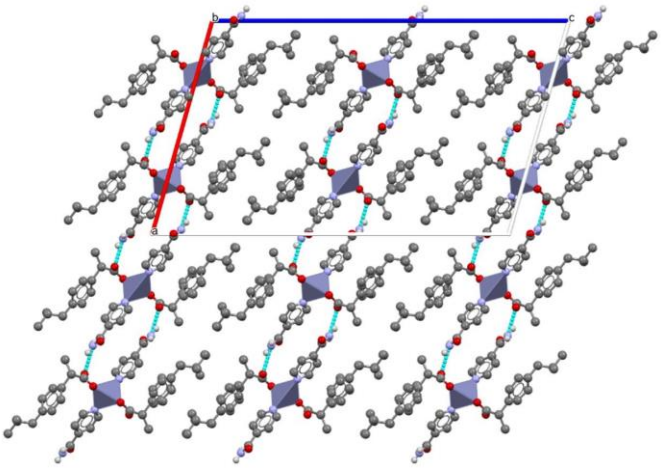

Figure C.2. Crystal packing of Zn(IBU)2(INC)2; view along crystallographic b-axis. HCH are omitted for clarity.

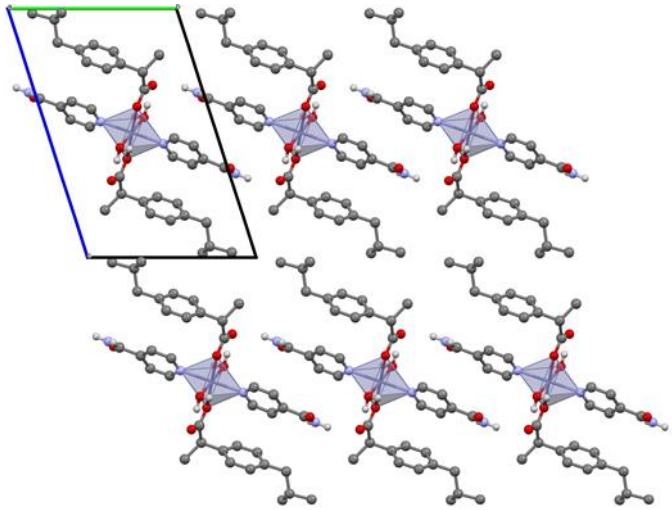

Figure C.3. Crystal packing of $Zn(IBU)_2(INC)_2(H_2O)_2$; view along crystallographic b-axis. H_{CH} omitted for clarity.

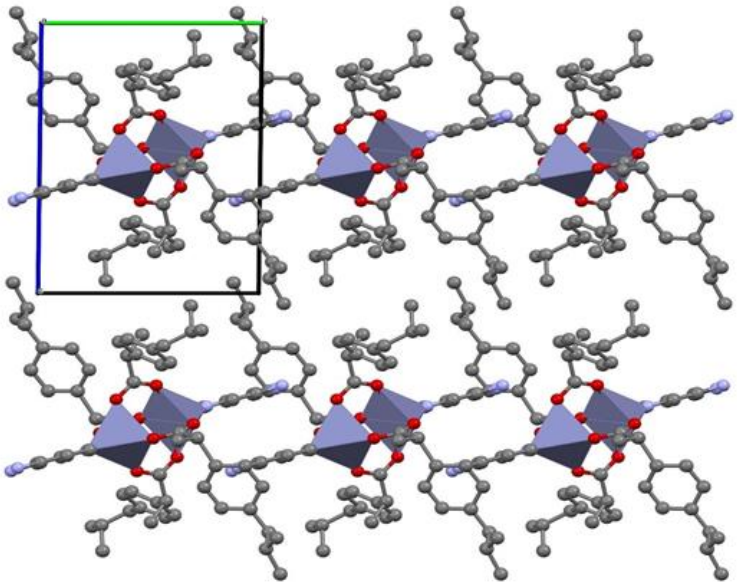

Figure C.4. Crystal packing of $Zn(IBU)_2(AMI)$; view down crystallographic a-axis. Hydrogen atoms omitted for clarity.

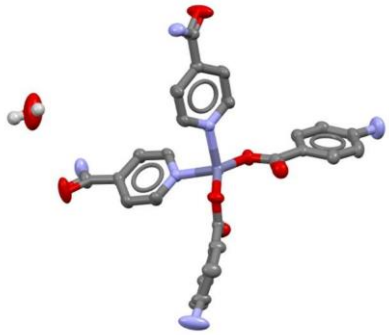

Figure C.5. Tetragonal coordination structure in $Zn(PABA)_2(INC)_2 \cdot 0.5H_2O$. Hydrogen atoms are omitted for clarity.

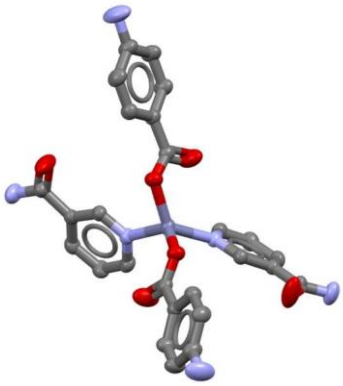

Figure C.6. Tetragonal coordination structure in Zn(PABA)2(NC)2. Hydrogen atoms are omitted for clarity.

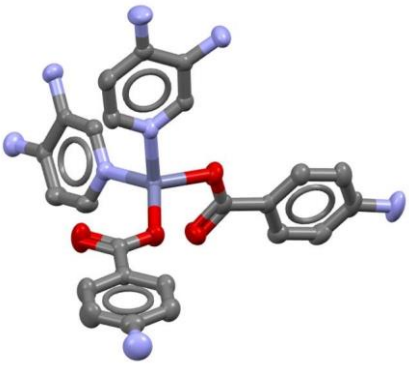

Figure C.7. Tetragonal coordination structure in Zn(PABA)2(AMI)2. Hydrogen atoms are omitted for clarity.

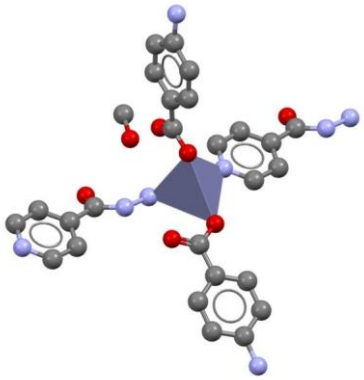

Figure C.8. Tetragonal coordination structure in Zn(PABA)2(INZ)·CH3OH. Hydrogen atoms omitted for clarity.

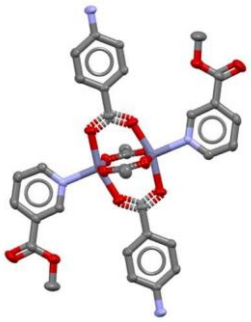

Figure C.9. Paddle-wheel coordination structure in Zn(PABA)(Ac)(MN)·H2O. Hydrogen atoms are omitted for clarity.

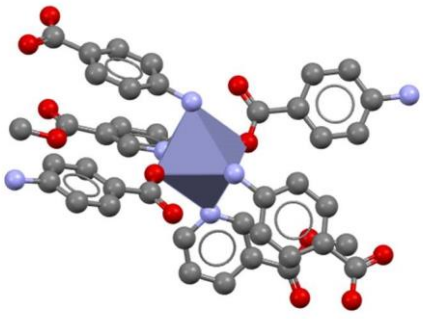

Figure C.10. Octahedral coordination structure in Zn(PABA)2(MN)2·H2O. Hydrogen atoms omitted for clarity.

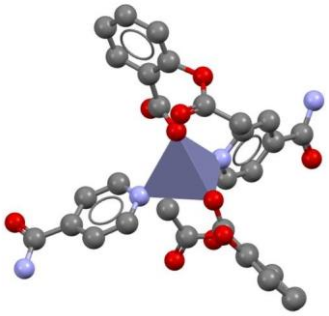

Figure C.11. tetragonal coordination structure in Zn (ASP)2(INC)2. Hydrogen atoms omitted for clarity.

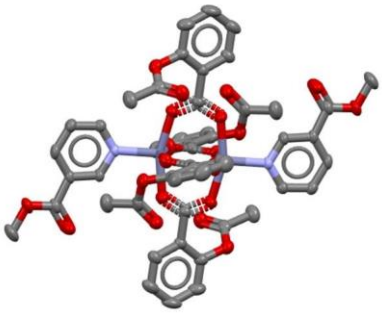

Figure C.12. Paddle-wheel coordination structure in Zn(ASP)2(MN). Hydrogen atoms omitted for clarity.

Thermal analyses.

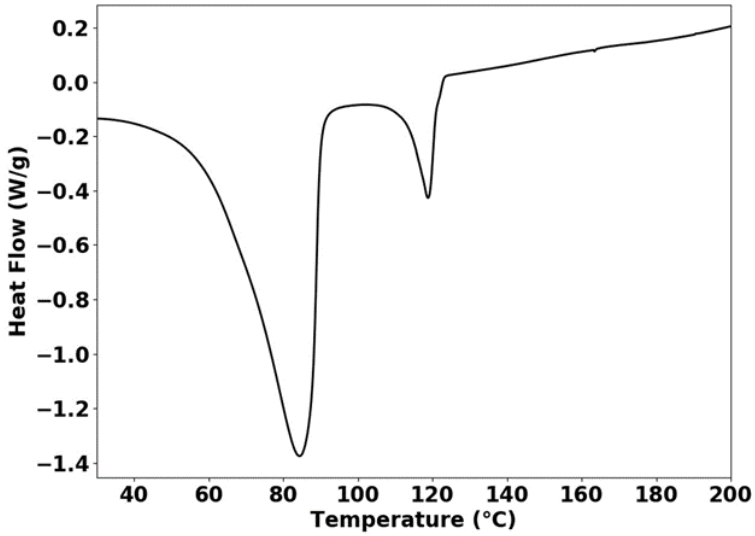

Figure C.13. DSC thermogram of $Zn(IBU)_2(H_2O)_2$.

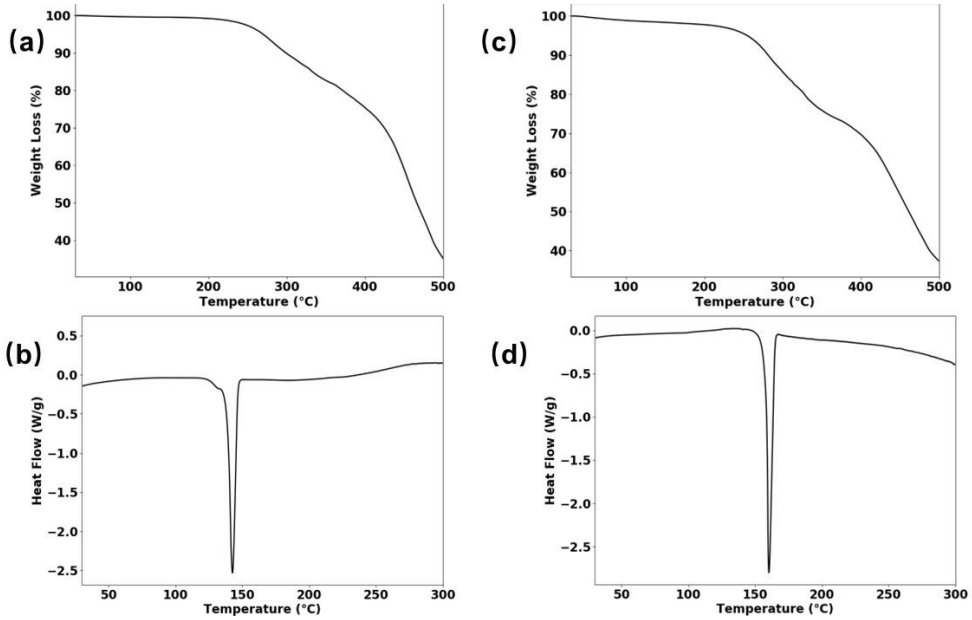

Figure C.14 TGA and DSC thermograms of $Zn(IBU)_2(AMI)$ (a and b) and of $Zn(IBU)_2(AMI)_2$ (c and d)**.**

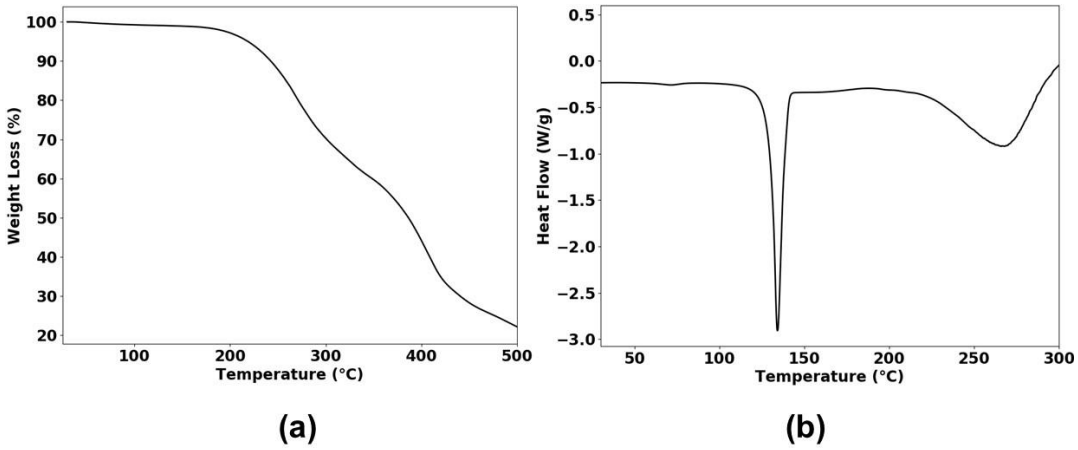

Figure C.15. TGA (a) and DSC (b) thermograms of $Zn(IBU)_2(NC)$**.**

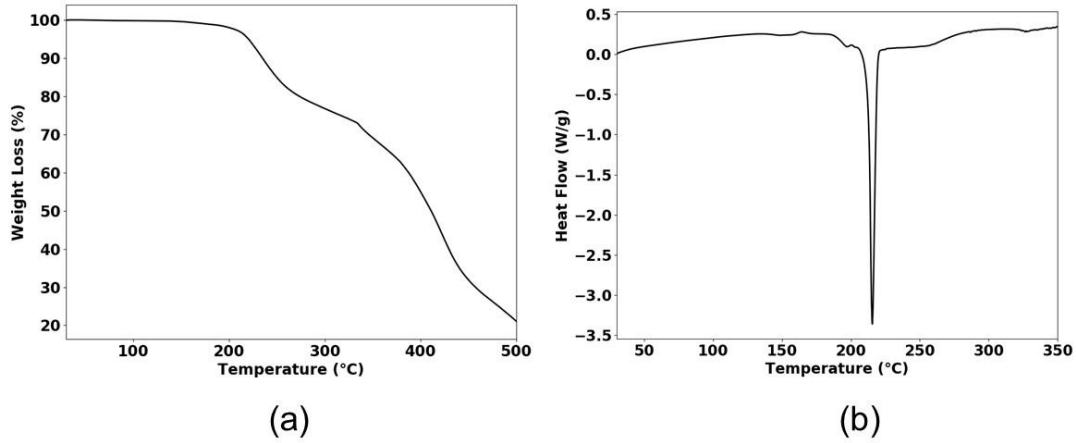

Figure C.16. TGA (a) and DSC (b) thermograms of $Zn(IBU)_2(INZ)$.

The comparison of experimental and simulated PXRD patterns of Zn(IBU)2-PD complexes.

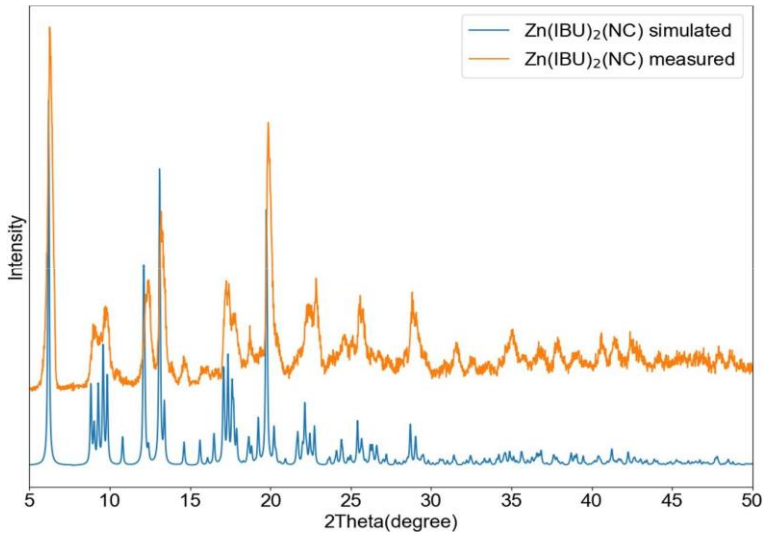

Figure C.17. Comparison between the experimental (obtained by slurry in acetonitrile) and calculated PXRD patterns for Zn(IBU)2(NC).

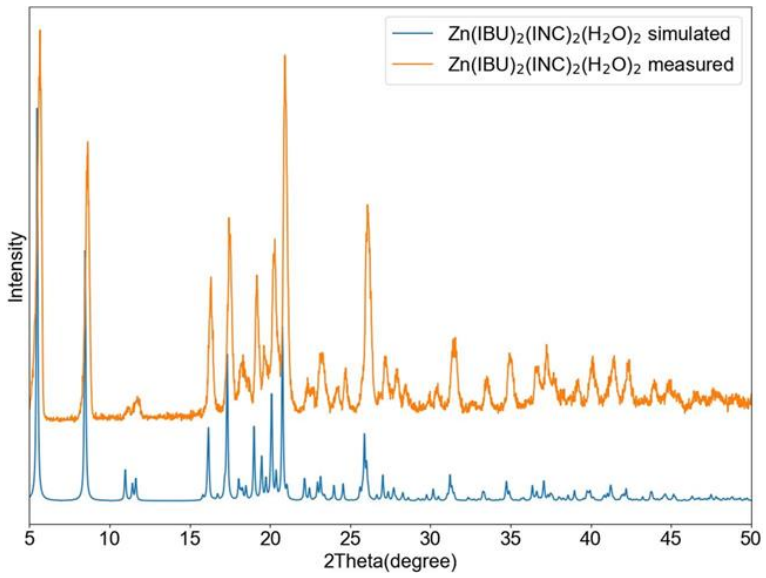

Figure C.18. Comparison between the experimental (obtained by slurry in H_2O) and calculated PXRD patterns for $Zn(IBU)_2(INC)_2(H_2O)_2$.

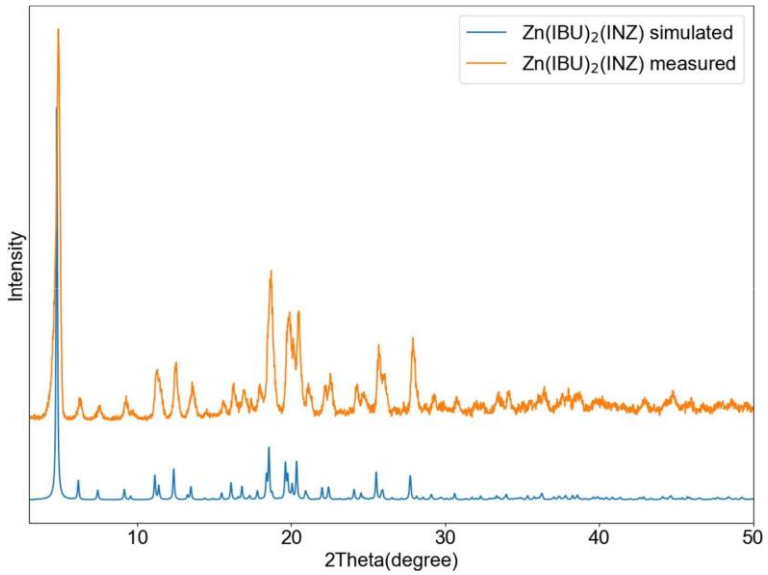

Figure C.19. Comparison between the experimental (obtained by slurry in H_2O) and calculated PXRD patterns for $Zn(IBU)_2(INZ)$.

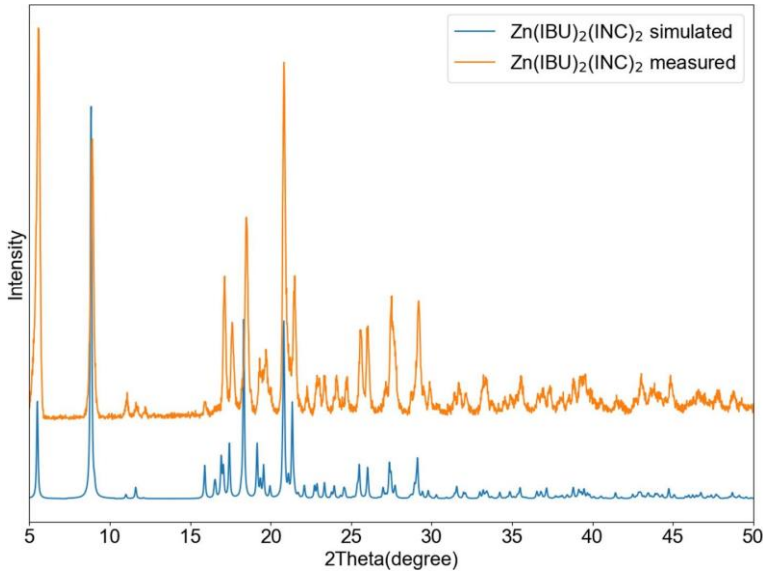

Figure C.20. Comparison between the experimental (obtained by slurry in H_2O) and simulated PXRD patterns for $Zn(IBU)_2(INC)_2$.

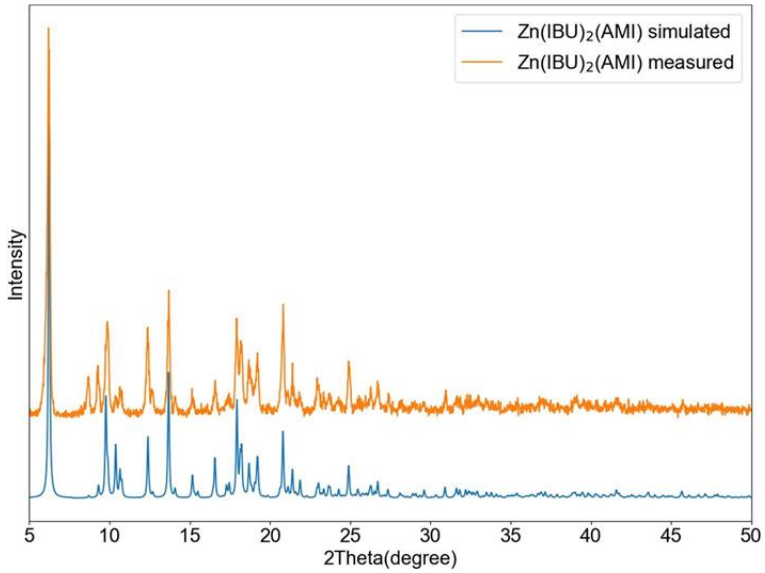

Figure C.21. Comparison between the experimental (obtained by slurry in H_2O) and simulated PXRD patterns for $Zn(IBU)_2(AMI)$.

Mechanochemical screening results

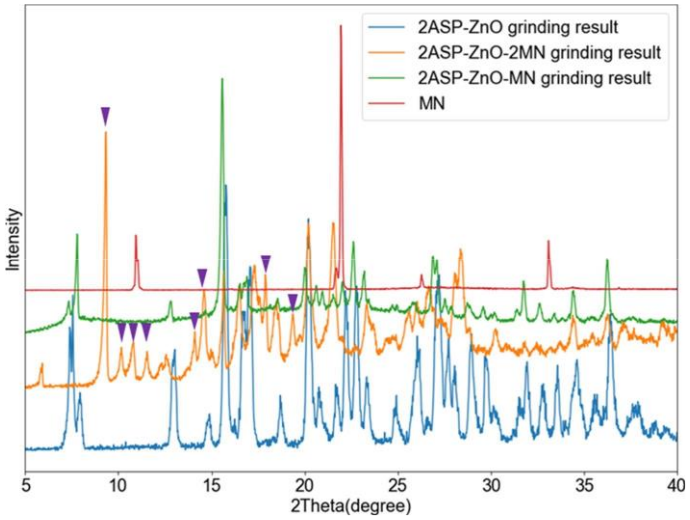

Figure C.22. Comparison of PXRD patterns for MN (red), ASP-ZnO grinding result in 2:1 (blue) as well as ASP-ZnO-MN three-component grinding results in 2:1:1 (green) and 2:1:2 (orange) ratios.

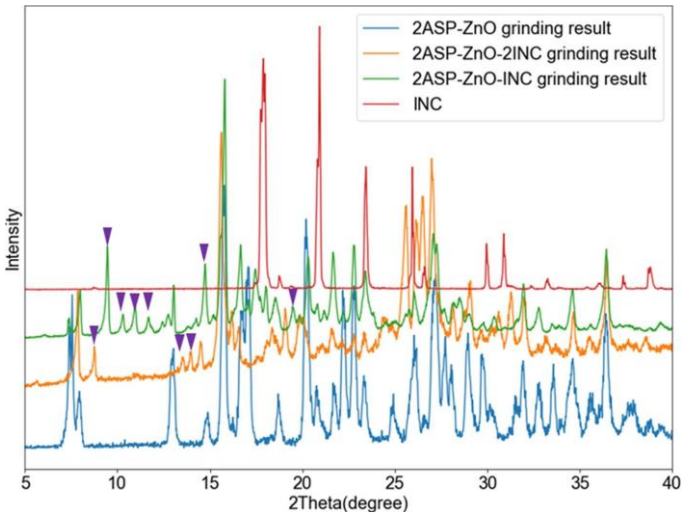

Figure C.23. Comparison of PXRD patterns for INC (red), ASP-ZnO grinding result in 2:1 (blue) as well as ASP-ZnO-INC three-component grinding results in 2:1:1 (green) and 2:1:2 (orange) ratios.

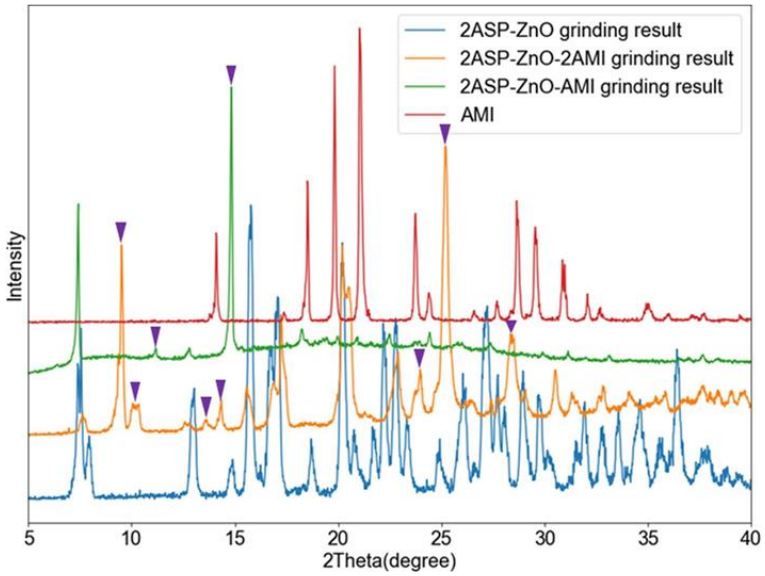

Figure C.24. Comparison of PXRD patterns for AMI (red), ASP-ZnO grinding result in 2:1 (blue) and ASP-ZnO-AMI three-component grinding results in 2:1:1 (green) and 2:1:2 (orange) ratios.

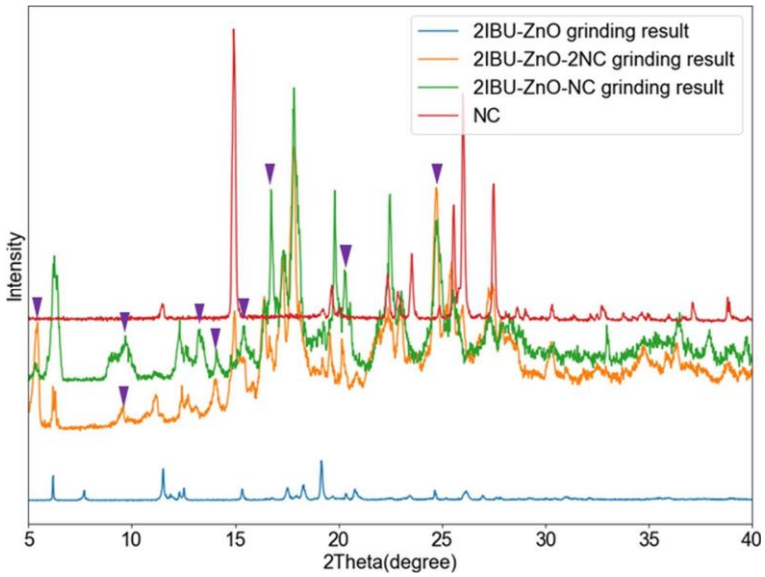

Figure C.25. Comparison of PXRD patterns for NC (red), IBU-ZnO grinding result in 2:1 (blue) and IBU-ZnO-NC three-component grinding results in 2:1:1 (green) and 2:1:2 (orange) ratios.

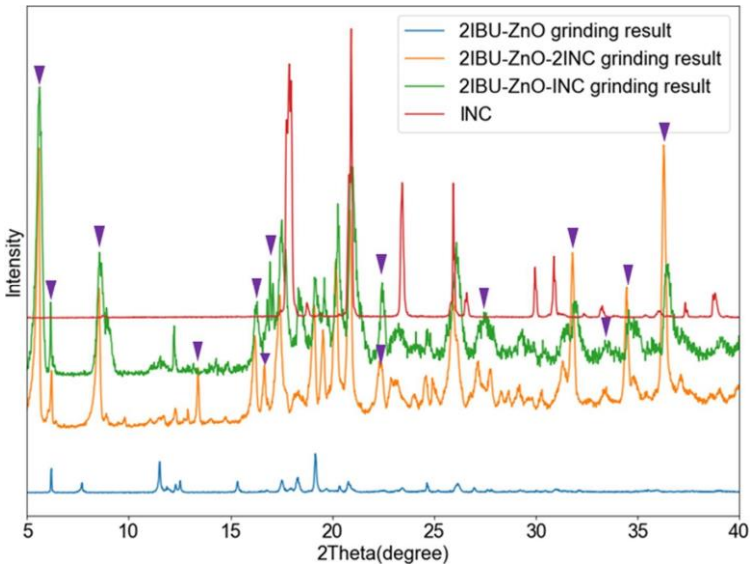

Figure C.26. Comparison of PXRD patterns for INC (red), IBU-ZnO grinding result in 2:1 (blue) and IBU-ZnO-INC three-component grinding results in 2:1:1 (green) and 2:1:2 (orange) ratios.

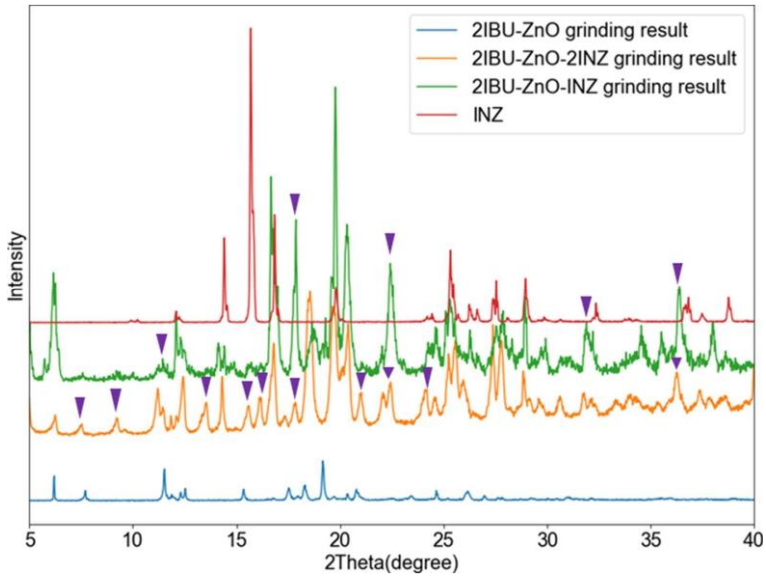

Figure C.27. Comparison of PXRD patterns for INZ (red), IBU-ZnO grinding result in 2:1 (blue) and IBU-ZnO-INZ three-component grinding results in 2:1:1 (green) and 2:1:2 (orange) ratios.

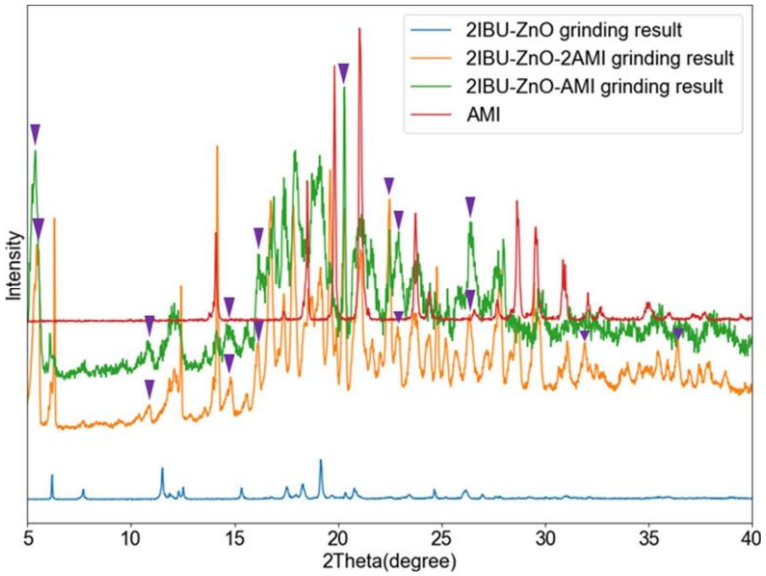

Figure C.28. Comparison of PXRD patterns for AMI (red), IBU-ZnO grinding result in 2:1 (blue) and IBU-ZnO-AMI three-component grinding results in 2:1:1 (green) and 2:1:2 (orange) ratios.

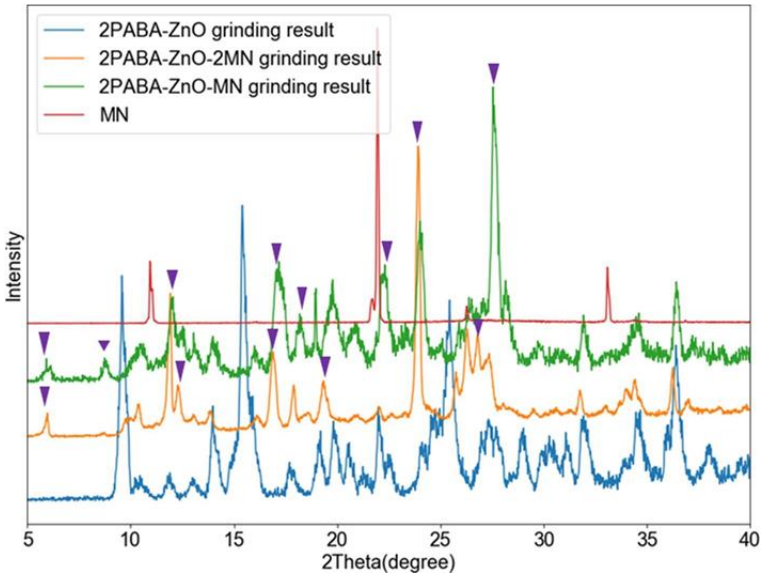

Figure C.29. Comparison of PXRD patterns for MN (red), PABA-ZnO grinding result in 2:1 (blue) and PABA-ZnO-MN three-component grinding results in 2:1:1 (green) and 2:1:2 (orange) ratios.

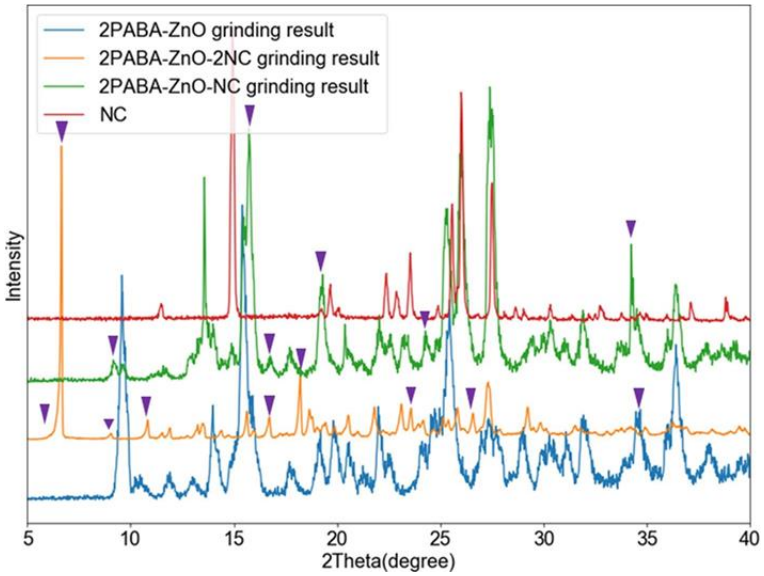

Figure C.30. Comparison of PXRD patterns for NC (red), PABA-ZnO grinding result in 2:1 (blue) as well as PABA-ZnO-NC three-component grinding results in 2:1:1 (green) and 2:1:2 (orange) ratios.

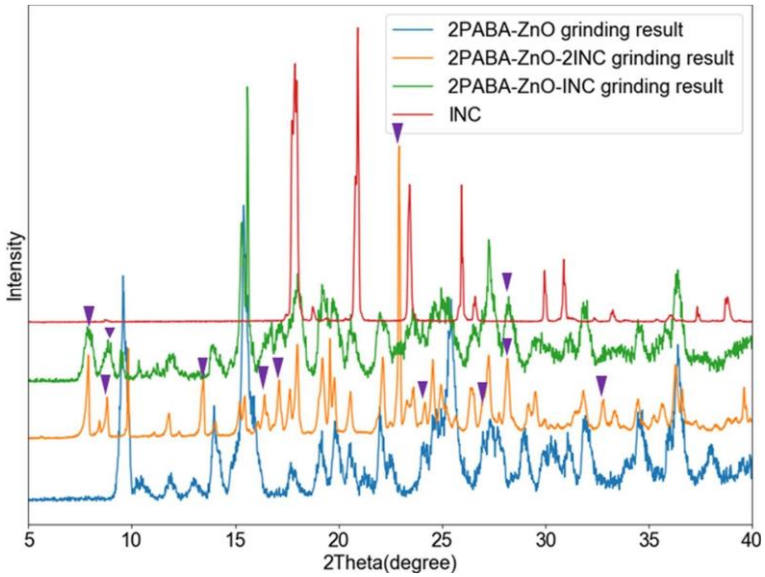

Figure C.31. Comparison of PXRD patterns for INC (red), PABA-ZnO grinding result in 2:1 (blue) as well as PABA-ZnO-INC three-component grinding results in 2:1:1 (green) and 2:1:2 (orange) ratios.

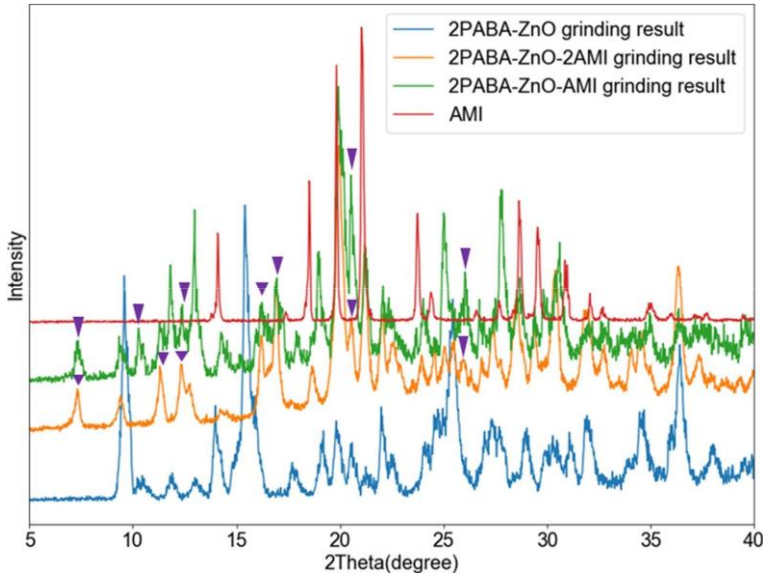

Figure C.32. Comparison of PXRD patterns for AMI (red), PABA-ZnO grinding result in 2:1 (blue) as well as PABA-ZnO-AMI three-component grinding results in 2:1:1 (green) and 2:1:2 (orange) ratios.

VT-PXRD

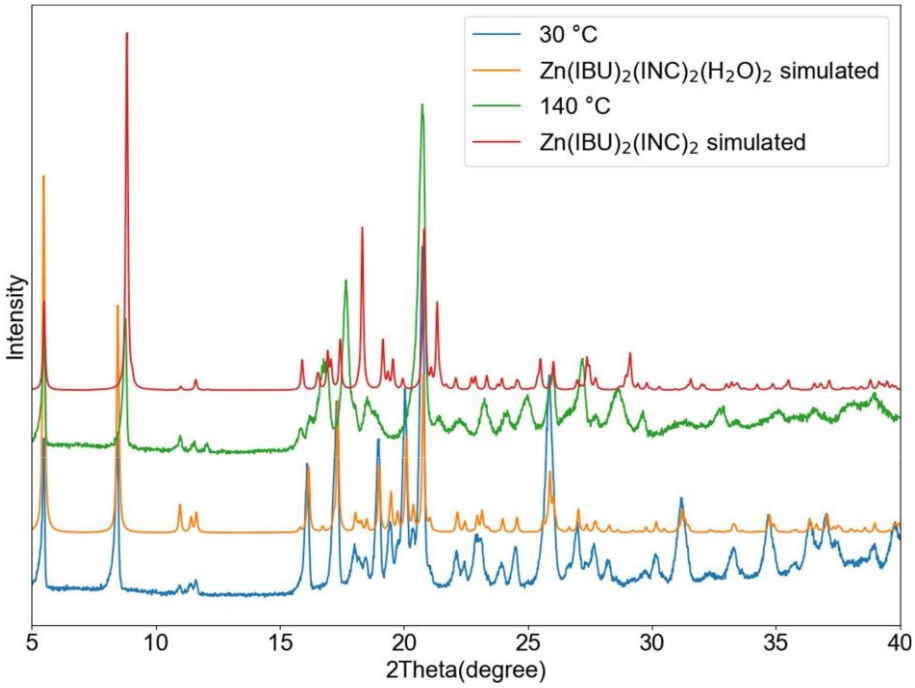

Figure C.33. VT-PXRD analyses of Zn(IBU)2(INC)2(H2O)2 taken at 30 °C (blue) and 140 (green). The simulated PXRD patterns of the hydrated (orange) and the anhydrous (red) complexes are given for comparison.

Binary cocrystal screen

A binary cocrystal screen was performed between the organic compounds through methanol LAG. Most binary combinations also lead to cocrystal formation. However, this is not the case for eg. Aspirin-methylnocotinate.

Table C.2: Binary screening result between carboxylic acid and pyridine containing drug compounds used.

	Aspirin (ASP)	Ibuprofen (IBU)	4-aminobenzoic acid
Methylnicotinate (MN)	Liquid	Liquid	Yes
Nicotinamide (NC)	Yes	Yes	Yes
Isonicotinamide (INC)	Yes	yes	Yes
Isoniazid (INZ)	yes	no	yes
Amifampridine (AMI)	Salt	Liquid	yes